Flow over complex terrain. The secrets of Bolund

Lange, Julia

Publication date:
2016

Document Version
Publisher's PDF, also known as Version of record

Flow over complex terrain

The secrets of Bolund

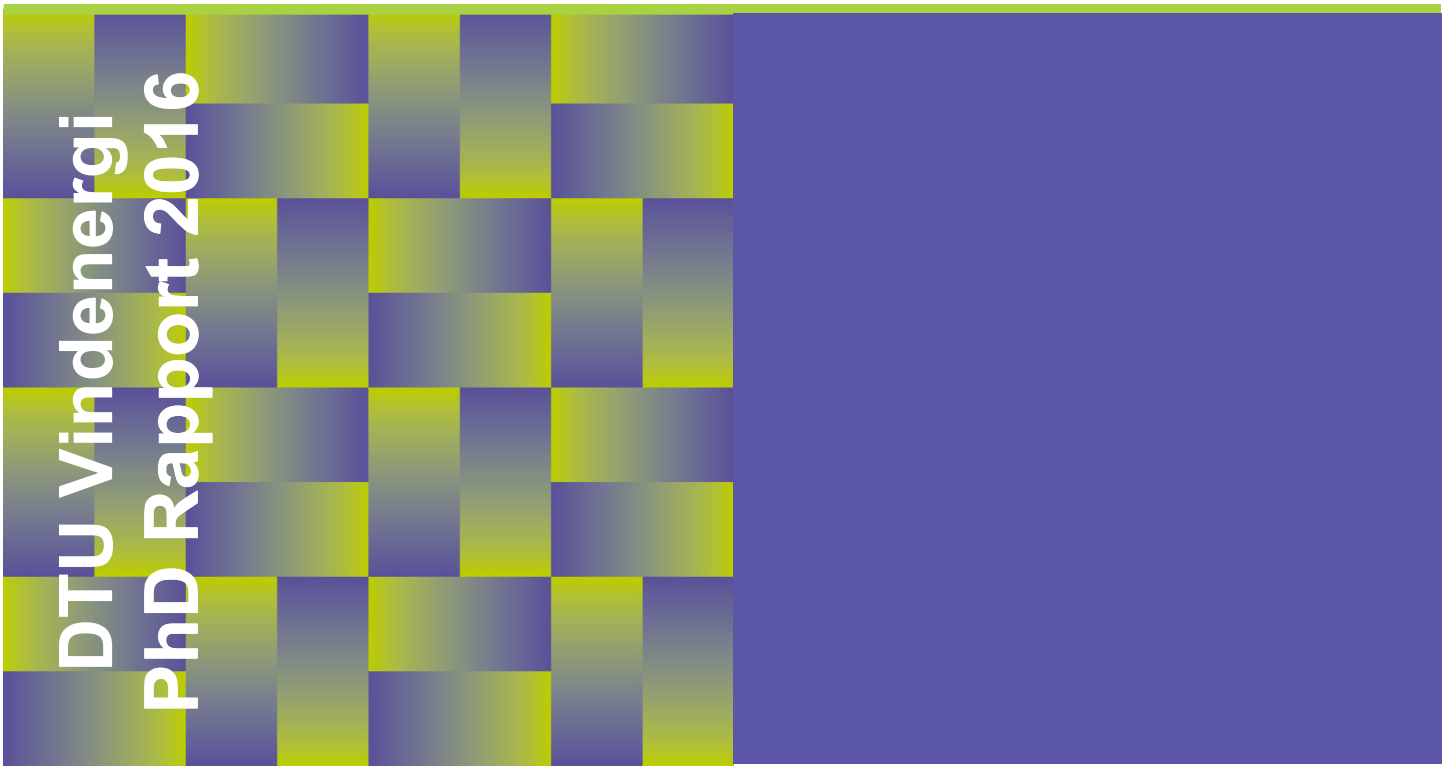

Julia Lange

DTU Wind Energy PhD-0060(EN)

05 2016

DTU Vindenergi
Institut for Vindenergi

Author: Julia Lange

Titel: The secrets of Bolund

Institut: DTU Wind Energy

DTU Wind Energy PhD-0060(EN)

Summary:

Since the Bolund field campaign in 2007, the Bolund peninsula in the Roskilde Fjord in Denmark is a well-known reference case for numerical and physical modelling for wind modelling and wind turbine siting. Its well-described characteristics and boundary conditions makes it ideal for the analysis and the understanding of flow over complex terrain.

The work presented in this thesis contains two diverse approaches to help under- stand the flow behavior over a complex terrain site, in this case the Bolund peninsula. The first approach investigates the wake and recirculation zone downstream of the Bolund escarpment with the help of a continuous-wave Doppler lidar (light detection and ranging). The instrument measures the line-of-sight wind-speed 390 times per second in highly resolved 7-m tall profiles by rapidly changing the focus distance and beam direction. The profiles reveal a detailed and rapidly changing structure of the recirculation zone induced by the Bolund escarpment. This wake grows with distance from the escarpment, with the wake height depending strongly on the wind direction, such that the minimum height appears when the flow is perpendicular to the escarpment.

Although the presented full-scale experiments around the Bolund escarpment has been performed with great success, experiments in controlled environments such as wind tunnels provide the opportunity to study problems systematically in greater detail. Such a controlled experiment was realized at the WindEEE Dome, a wind-tunnel facility of the Western University, London, Ontario, Canada and presents the second approach of this thesis. This large-scale wind laboratory investigation of the flow field over a large-scale model of the Bolund peninsula shows that the mean wind, wind shear and turbulence level are extremely sensitive to the exact details of the terrain. A modification of the escarpment of the Bolund model to give a sharper edge has dramatic consequences for a wind turbine positioned close to the edge. Additionally the wind-tunnel investigations show only a modest Reynolds number dependence of the flow, while it is more sensitive to the details of the inflow wind profile.

The thesis is submitted to the Danish Technical University in partial fulfillment of the requirements for the PhD degree.

ISBN:
978-87-93278-83-7

Vejledere:
Jakob Mann
Jacob Berg

Bemærkninger:
[Tekst]

Kontrakt nr.:
[Tekst]

Projektnr.:
[Tekst]

Sponsorship:
Center for Computational Wind Turbine Aerodynamics and Atmospheric Turbulence funded by the Danish Council for Strategic Research, grant number 09-067216

Sider: [Tekst]
Tabeller: 2
Referencer: 39

Danmarks Tekniske Universitet
DTU Vindenergi
Nils Koppels Allé
Bygning 403
2800 Kgs. Lyngby
Telefon

www.vindenergi.dtu.dk

Ph.D. Thesis

Flow over complex terrain

The secrets of Bolund

Julia Lange

Risø Campus, 2016

DTU Wind Energy
Department of Wind Energy

DTU

DTU Wind Energy
Department of Wind Energy
Technical University of Denmark

DTU Wind Energy
DTU Risø Campus
Frederiksborgvej 399
DK-4000 Roskilde
http://www.vindenergi.dtu.dk

Summary

Since the Bolund field campaign in 2007, the Bolund peninsula in the Roskilde Fjord in Denmark is a well-known reference case for numerical and physical modeling for wind modeling and wind-turbine siting. Its well-described characteristics and boundary conditions makes it ideal for the analysis and the understanding of flow over complex terrain.

The work presented in this thesis contains two diverse approaches to help understand the flow behavior over a complex terrain site, in this case the Bolund peninsula. The first approach investigates the wake and recirculation zone downstream of the Bolund escarpment with the help of a continuous-wave Doppler lidar (light detection and ranging). The instrument measures the line-of-sight wind-speed 390 times per second in highly resolved 7-m tall profiles by rapidly changing the focus distance and beam direction. The profiles reveal a detailed and rapidly changing structure of the recirculation zone induced by the Bolund escarpment. This wake grows with distance from the escarpment, with the wake height depending strongly on the wind direction, such that the minimum height appears when the flow is perpendicular to the escarpment.

Although the presented full-scale experiments around the Bolund escarpment has been performed with great success, experiments in controlled environments such as wind tunnels provide the opportunity to study problems systematically in greater detail. Such a controlled experiment was realized at the WindEEE Dome, a wind-tunnel facility of the Western University, London, Ontario, Canada and presents the second approach of this thesis. This large-scale wind laboratory investigation of the flow field over a large-scale model of the Bolund peninsula shows that the mean wind, wind shear and turbulence level are extremely sensitive to the exact details of the terrain. A modification of the escarpment of the Bolund model to give a sharper edge has dramatic consequences for a wind turbine positioned close to the edge. Additionally the wind-tunnel investigations show only a modest Reynolds number dependence of the flow, while it is more sensitive to the details of the inflow wind profile.

Dansk sammendrag

Halvøen Bolund ved Roskilde Fjord var i 2007-2008 genstand for et velkendt reference felteksperiment for vindmodeller, både numeriske samt fysiske, som beskriver middelstrømning og turbulens over terræn til brug for placering af vindmøller. Siden eksperimentet fandt sted er det blevet brugt flittigt til dette formål. Eksperimentets velbeskrevne grænsebetingelser gør det ideelt til analyse og forståelse af strømning over komplekst terræn.

Arbejdet indeholdt i denne afhandling omhandler to forskellige tilgange til at forståstrømningen over komplekst terræn, i dette tilfælde Bolund. Den første metode undersøger "kølvandet" og recirkulationszonen nedstrøms for den næsten lodrette skrænt ved hjælp af en continuous-wave Doppler lidar (light detection and ranging). Instrumentet måler komposanten af strømningen i laserstrålens retning 390 gange i sekundet i højt opløste og syv meter høje profiler ved lynhurtigt at ændre fokusafstanden samt retningen af laserstrålen. Profilerne viser i detaljer den hurtigt varierende struktur af recirkulationszonen forårsaget af Bolund skrænten. Højden af denne meget turbulente zone vokser med afstanden til skrænten og den afhænger kraftigt af retningen af indstrømningen, således at den mindste højde fås når strømningen er vinkelret påskrænten.

Selvom felteksperimenterne omkring Bolund var vellykkede, sågiver eksperimenter under mere kontrollerede omstændigheder såsom for eksempel i en vindtunnel adgang til mere detaljerede undersøgelser. Sådan et kontrolleret forsøg blev udført i den såkaldte WindEEE Dome, en ny vindfacilitet ved Western University i London, Ontario i Canada, og dette udgør den anden metode i denne afhandling. Denne undersøgelse i med en model af Bolund i meget stor skala viser at middelstrømningen, vindændringer og turbulens over halvøen er ekstremt følsomme overfor den eksakte udformning af modellen. En lille ændring, hvor toppen af skrænten gøres skarpere, ville have dramatiske konsekvenser for ydelsen af en (skaleret) vindmølle anbragt tæt påskrænten. Vindtunnelundersøgelserne viser ogsåat strømningens afhængighed af Reynolds-tallet kun er moderat, mens den udviser en større følsomhed overfor ændringer i indstrømningsprofilet.

Zusammenfassung

Die Halbinsel Bolund im Roskilde Fjord in Dänemark ist ein namenhaftes Referenz-Experiment für numerische and physische Modellierungen von Windströmungen und für die Standortwahl von Windkraftanlagen. Die sehr gut vorhandenen und beschriebenen Randbedingungen haben zur Folge, dass Bolund ideal für die Analyse und das Verstehen von Windströmungen über komplexen Terrain ist.

Die vorliegende Arbeit beinhaltet zwei unterschiedliche Ansätze um das Strömungsverhalten über komplexen Gelände, in diesem Fall anhand des Beispiels der Bolund Halbinsel, zu verstehen. Der erste Ansatz untersucht die Wirbel- und Rezirkulationszone hinter dem Bolund Kliff, mit Hilfe eines continuous-wave Doppler Lidar (Abkürzung für engl. light detection and ranging). Dieses Instrument misst die Windgeschwindigkeit 390 mal pro Sekunde in hoch aufgelösten, sieben meter hohen Profilen, indem ein ständiger und schneller Wechsel von Fokusabstand und Läserstrahlrichtung erfolgt. Die Profile zeigen ein detailliertes Bild der sich ständig ändernden Struktur der Rezirkulationszone, die durch das Bolund Kliff entsteht. Diese Wirbelströmung wächst mit Abstand zur Klippe und ihre Größe ist stark abhängig von der Windrichtung.

Obwohl die ausgeführten Meßkampagnen auf Bolund sehr erfolgreich waren, ermöglichen Experimente in einem kontrollierten Umfeld, zum Beispiel in Windkanälen, einzelne Parameter systematischer und detaillierter zu untersuchen. Solch ein Experiment wurde im WindEEE Dome, eine neue Windforschungseinrichtung der Western University in London, Ontario, Kanada, realisiert und stellt in dieser Arbeit den zweiten Ansatz dar. Die Untersuchung der Strömungsverhältnisse über einem großskaligem Bolund-Modell in diesem großskaliger Windkanal zeigt, dass die Durchschnittswindgeschwindigkeiten, das Windprofil und die Turbulenzen über der Halbinsel sehr abhängig von der Modellform sind. Eine kleine Änderung der Kliffform, um einen steileren Zustand zu erhalten, bewirkt dramatische Konsequenzen für die Standortwahl von Windkraftanlagen. Zusätzlich dokumentiert das Windkanal Experiment, dass die Strömung nur mäßig anhängig von der Reynolds-Zahl ist, sich aber deutlich mit einer Veränderung der Anströmverhältnisse ändert.

Acknowledgements

I would like to express my gratitude to my supervisors Jakob Mann and Jacob Berg. Jakob, thank you for your endless patience, encouragement, advice and for the amount of time you have dedicated to me. Thank you for always having an open ear for personal matters and problems and simply for supporting and believing in me. Jacob, thank you for being the opposite of Jakob and for pushing and demanding, but at the same time being positive and supporting. I am glad to not only call you my supervisors, but also my friends.

A special thanks to my lovely colleagues from the former MET section. Thank you Andrea for being so welcoming and making my start at Risø so pleasant. Thank you Xiaoli, Ebba and Alfredo for your friendship. Thanks to all of my office mates and fellow PhD students, especially to Jesper, Bjarke and Ásta for making the day at work even more enjoyable. I have to thank Nikolas not only for all his efforts trying to explain the WindScanner to me, but also for simply being there and being a very good friend.

I also greatly appreciate that I had the possibility to carry out the experiment at the WindEEE research institute. I am grateful to all people that I met there, especially for the great working spirit and teamwork during the successful experiment execution.

Last but not least I would like to thank Max. Thank you for all the amazing travels and for being on my side throughout the years. Finally I would like to thank my parents for their endless love and trust.

Contents

CHAPTER 1

Introduction

Onshore wind energy is one of the cheapest forms of electrical generation available according to the International Renewable Energy Agency (IRENA) (IRENAb 2015). The forecast for 2020 by the U.S. Energy Information Administration indicates that it will remain cheaper than most conventional power sources including coal and gas and all significant renewable energies including hydro and solar photovoltaic (EIA 2015). By the end of 2014 361 GW of onshore wind energy was installed worldwide contributing 20% of all renewable energy sources (IRENAa 2015). However, the cost range of wind power generation ($\approx 0.03 - 0.16$ USD/kWh) is wider than that of fossil fuel ($\approx 0.04 - 0.14$ USD/kWh), and the local wind climate is a large contributor to this variation (IRENAb 2015). The wind energy industry is continuously challenged by wind farm projects showing large negative discrepancies between predicted and actual power production. This is often the case when the wind farm is placed on complex terrain, where wind turbines exploit the strong speed-up present around highly irregular terrain features, such as ridges or escarpments. The flow in such situations can, on the other hand, be quite complex and associated with high levels of turbulence and strong shear layers, which stresses the construction of the turbines and make reliable power predictions difficult. Uncertainty in the estimation of the wind-energy potential, the level of wind shear and turbulence has obvious implications of the financial feasibility of wind energy projects and it must be reduced in order to lower the cost of electricity. To reduce stress on the turbines, it is required to construct them in a way that the lower part of the rotor is almost always above a turbulent zone caused by complex terrain.

During the last four decades various experimental studies have been performed, with the aim of characterising complex flow over hills. Studies over hills with gentle slopes have been performed by Sacré 1979, Baskaran et al. 1987 and Walmsley and Taylor 1996, in which the growth of the internal boundary layer and the influences of roughness changes are described. Jensen and Peterson 1978 investigated roughness changes along the Risø peninsula. The flow over several escarpments, including vertical profiles and turbulence structures in New Zealand have been studied by Bowen 1979. A more complex field experiment, the Hjardemål experiment, was analyzed by Emeis et al. 1995, where mean flow profiles, turbulent power spectra and momentum flux were investigated.

Even though full-scale experiments of wind flow around hills and escarpments have been performed with great success, for example by Taylor et al. 1987 and Berg et al.

2011, they are often considered as time consuming and costly. Therefore engineers and atmospheric scientists, engaged in modeling and assessing wind loads on buildings and siting of wind turbines in complex terrain, often resort to numerical and physical models of varying fidelity to achieve insight into complex flow fields. On one hand these experiments in a more controlled environments like numerical-simulation tools and wind tunnels provide us with the opportunity to study isolated problems in greater detail, but on the other hand the validation and eventually the improvement of those models often relies heavily on comparisons with suitable high-quality wind and turbulence field measurements.

One of the best known reference cases is the Askervein Hill experiment described by Taylor et al. 1987. The results of the Askervein Hill experiment have been used for many comparison studies with numerical models (Jackson and Hunt 1975; Hunt et al. 1988; Castro et al. 2003; Silva Lopes et al. 2007; Chow F.K. and Street 2009) and wind-tunnel studies (Teunissen et al. 1987). One of the most famous reference cases today is the Bolund peninsula in the Roskilde Fjord, Denmark. Bolund is about 12 m high, 150 m long and 75 m wide. It is surrounded by water and connected to land at low tide. The shape of the peninsula is characterized by a west-facing, mostly vertical escarpment that causes a recirculation zone in front of the cliff and a detachment of the flow above the edge for westerly winds. The flow reattaches on the long, flat hill top, before the terrain slopes down towards the east (Yeow et al. 2013). These flow patterns make the prediction and modeling of the flow around Bolund challenging, but also well-defined through well-known boundary conditions and especially through the 7-km long upstream water fetch on the west site, which is also the predominant wind direction.

Despite the fact that the Bolund peninsula is only 12 m high, its isolated location and the absence of significant Coriolis and thermal effects provide the potential for up-scaling in neutral stratification. In situations with neutral atmospheric stratification and mean wind speeds larger than 8-10 m/s, i.e. above the cut-in wind speed of modern wind turbines, Bolund can be up-scaled 10-30 times. The area thus resembles a full-scale table mountain such as those found in the US Midwest with wind turbines positioned close to the edges (Berg et al. 2011). Bolund's rise to fame began in winter 2007-2008 when DTU Wind Energy carried out a field experiment on Bolund, in order to make a test case for flow modeling in complex terrain (Bechmann et al. 2009). The three-month long intensive measurement campaign produced a unique dataset of 23 sonic and 12 cup anemometer measurements at various heights for selected locations on the Bolund peninsula. Vertical lidar wind profiles complement the dataset (Bechmann et al. 2009; Berg et al. 2011; Dellwik et al. 2010). The combination of the flow patterns observed, the well-defined boundary conditions and long upstream fetch, made Bolund ideal for being a reference case for numerical and physical models. Since then Bolund has been widely used for this purpose and today the dataset of the Bolund experiment serves as a baseline reference for various studies with respect to numerical and physical modeling.

Initially the Bolund dataset was used for a blind comparison of different micro-scale flow models, including simple linear models such as the BZ model of WAsP,

non-linear models such as Reynolds averaged Navier-Stokes (RANS) models and large-eddy simulation (LES) models, as well as physical models using wind-tunnel and water-channel facilities (Bechmann et al. 2009). Every participant was given the same information about topography, roughness and inflow conditions. The blind comparison revealed significant scatter for both wind speed and turbulence levels among the different models, indicating that numerical models still have to develop in order to successfully model flow over real complex terrain.

Following the blind comparison, Bolund has been used to verify the quality of a steady state RANS solver with a two-equation turbulence model (Prospathopoulos et al. 2012). Furthermore Diebold et al. 2013 tried to reproduce the flow around Bolund with the immersed boundary condition method using an LES model with some success.

Bolund was not only used to verify numerical models, it has also been used to prove the applicability of wind tunnels for atmospheric flow modeling. Yeow et al. 2013 conducted a wind-tunnel study to reproduce the wind flow around Bolund on a scale of 1:115, where they focused on the main flow patterns that occur with the flow over a hill. A similar experiment was carried out by Conan 2012, with a model scale of 1/500. Although, he was able to reproduce the inlet conditions closer to the real inflow than Yeow et al., his results of the flow evolution on top of Bolund showed similar deviations from the real scale.

A comparison study of wind tunnel and LES on Bolund was carried out Conan et al. 2016. They compared Bolund as a 2D model in a LES and a Bolund 3D model in a wind tunnel. They find that the maximum speed-up in the 2D case is higher than in the 3D wind-tunnel case. They also describe that in the LES simulation a recirculation zone is present, while the averaged wind-tunnel flow field does not show such a flow pattern. Nonetheless both cases show an increased turbulent kinetic energy (TKE). Hereby there results are in agreement with Yeow et al. 2013.

Various studies conduct wind-tunnel modeling on forward facing steps (FFS) as a first-pass approximation to characterize the flow in the vicinity of the step. Pioneering work in this field was carried out by Bowen and Lindley 1977 and Kiya and Sasaki 1983. Already Bowen and Lindley motivate their work by describing how the power generation of wind turbines can be enhanced through a precise positioning in complex terrain and an improved load calculation through a better knowledge of the flow pattern. More recent work deals with wall pressure fluctuations (Largeau and Moriniere 2006). Largeau and Morine understand mechanisms of formation of separated flows over three FFS heights. They focused on measuring the surface pressure field and the visualization of the flow field, which leads to additional knowledge of the organization of a flow over a FFS. In more detail they describe the average reattachment length of the flow. Sherry et al. 2010 pick up the motivation by Bowen and Lindley 1977 and emphasize the importance of the characterization of the flow pattern (separation and reattachment) behind a step to ensure estimated power production of a wind turbine. Therefore they investigate the structure of the recirculation zone downstream of the FFS over a range of different Reynolds numbers. They find that the reattachment length depends on the ratio of boundary-layer thickness and step height. They could

distinguish between two regimes. The first, where the reattachment length is dependent on the Reynolds number and secondly, at high Reynolds number greater than 8500, where the reattachment length is independent. Here the Reynolds number is based on the FFS height h. Another study using FFS to optimize the siting of wind turbines near cliffs is published by Rowcroft et al. 2015. More specifically, they characterize the flow pattern downstream of the FFS with regard to a varying yaw angle of 0°, 20°, 30° and 40°. They find that if the yaw angle increases, the maximum speed-up decreases. Additionally they show that the turbulence intensity is two to three times higher behind the FFS crest than the inflow turbulence. This wake profile extends up to 10 step heights of the FFS downstream. In general they find high veer and turbulence intensity as well as lower wind speeds and shear in the recirculation zone independent of the yaw angle.

The following work is mainly based on the published and submitted literature and structured in the following way:

This thesis starts with a paper published in *Boundary-Layer Meteorology* about a scanning lidar campaign on the Bolund peninsula. The following chapter covers the description of the set-up as well as the analysis of a large-scale wind-tunnel experiment of flow over a 1/25 scale model of the Bolund peninsula. The forth chapter presents the results of the experiment and comparisons with literature. The thesis is summarized in a conclusion, which also gives an outlook to new possible research questions.

CHAPTER 2

Wake height over the Bolund escarpment

Since many modeling results show problems to reproduce the Bolund mast campaign values in the vicinity of the Bolund escarpment, DTU Wind Energy decided to investigate this area further by carrying out a lidar scanning campaign. By scanning seven 7 m-tall profiles close to the escarpment along the 270° line, DTU expanded the Bolund mast-campaign data-set, which lead to a more in depth understanding of the flow pattern over Bolund. The following study (Lange et al. 2016) published in *Boundary-Layer Meteorology* describes the behavior of the wake that develops downstream of the escarpment and the variation of the wake height with wind direction deviating from west.

Boundary-Layer Meteorol
DOI 10.1007/s10546-015-0107-8

ARTICLE

Variations of the Wake Height over the Bolund Escarpment Measured by a Scanning Lidar

Julia Lange[1] · Jakob Mann[1] · Nikolas Angelou[1] · Jacob Berg[1] · Mikael Sjöholm[1] · Torben Mikkelsen[1]

Received: 20 February 2015 / Accepted: 27 October 2015

Abstract The wake zone behind the escarpment of the Bolund peninsula in the Roskilde Fjord, Denmark, has been investigated with the help of a continuous-wave Doppler lidar. The instrument measures the line-of-sight wind speed 390 times per second in highly resolved 7-m tall profiles by rapidly changing the focus distance and beam direction. The profiles reveal the detailed and rapidly changing structure of the wake induced by the Bolund escarpment. The wake grows with distance from the escarpment, with the wake height depending strongly on the wind direction, such that the minimum height appears when the flow is perpendicular to the escarpment. The wake increases by 10–70 % when the wind direction deviates $\pm 15°$ from perpendicular depending on the distance to the edge and to a lesser degree on the method by which the wake height is determined. This finding is supported by a comparison with in situ measurements acquired on the Bolund peninsula.

Keywords Bolund · Complex flow · Wake height · WindScanner

1 Introduction

Complex terrain creates complex atmospheric flow. Complex terrain, which is characterized by a high variance in the surface characteristics such as roughness and elevation, causes the growth of local turbulent structures that are hard to predict. Such turbulent structures are far from fully understood and are typically found in wake regions in the immediate rear of solid bodies. Over steep hills these wake areas consist of complex turbulent structures and time varying processes that so far defy reliable prediction through numerical modelling.

The knowledge of these turbulent structures in the wake region is important for assessment of the impact of wind and turbulence on buildings, constructions and especially wind turbines. For wind turbines in particular the wake height on top of escarpments is important.

✉ Julia Lange
jull@dtu.dk

[1] DTU Wind Energy, Technical University of Denmark, Risø Campus, 4000 Roskilde, Denmark

Published online: 07 November 2015

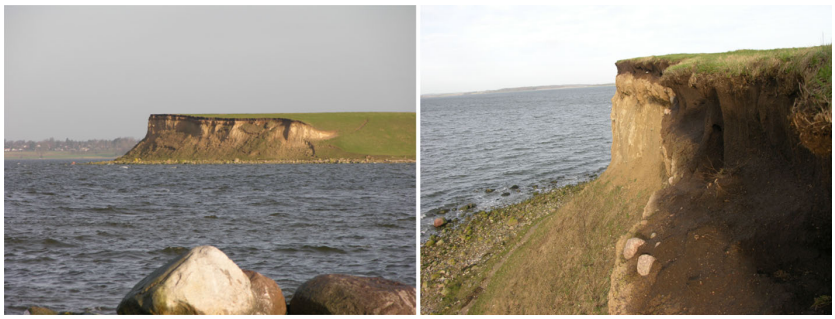

Fig. 1 *Left* Photo of Bolund, taken south of the peninsula. *Right* Photo of the Bolund escarpment edge

To reduce stress on the turbines, it is required to construct them in a way that the lower part of the rotor is almost always above the turbulence caused by the escarpment. Because atmospheric experiments are often time consuming and costly, engineers and atmospheric scientists, engaged in modelling and assessing wind loads on buildings and siting of wind turbines in complex terrain, often resort to numerical models of varying fidelity to achieve insight into complex flow fields. The validation and eventually the improvement of those models often relies heavily on comparisons with suitable high-quality wind and turbulence field measurements.

During the last four decades various experimental studies have been performed, with the aim of characterizing complex flow over hills. Studies over hills with gentle slopes have been performed by Sacré (1979), Baskaran et al. (1987) and Walmsley and Taylor (1996) in which the growth of the internal boundary layer and the influences of roughness changes are described. Jensen and Peterson (1978) investigated roughness changes along the Risø peninsula. The flow over several escarpments, including vertical profiles and turbulence structures in New Zealand have been studied by Bowen (1979). A more complex field experiment, the Hjardemål experiment, was analyzed by Emeis et al. (1995), where mean flow profiles, turbulent power spectra and momentum flux were investigated.

One of the best known hill experiments, is the Askervein Hill experiment described by Taylor and Teunissen (1985). The results of the Askervein Hill experiment have been used for many comparison studies with numerical models (Jackson and Hunt 1975; Hunt et al. 1988; Castro et al. 2003; Silva Lopes et al. 2007; Chow and Street 2009) and wind-tunnel studies (Teunissen et al. 1987).

This more recent field experiment builds on previous studies and examines the flow over the Bolund peninsula. Bolund is an isolated flat-topped hill with steep sides in the Roskilde Fjord, Denmark, that is connected to land at low tide with an isthmus on the east side. The hill extends 150 m in the west–east direction, is 75 m wide on the north–south axis and is about 12 m high. A contour plot is available in Berg et al. (2011). The shape of the peninsula includes a west facing, mostly vertical escarpment (Fig. 1) that is accountable for a recirculation zone in front of the cliff and a detachment of the flow above the edge for westerly winds. The flow reattaches on the long, flat hill top, before the terrain slopes down towards the east (Yeow et al. 2013). These flow patterns make the prediction and modelling of the flow around Bolund challenging, but also well defined through well-known boundary conditions and especially through the 7-km long upstream water fetch on the west site.

DTU Wind Energy performed an atmospheric experiment at the Bolund peninsula during winter 2007-2008 in order to make a test case for flow modelling in complex terrain (Bechmann et al. 2011; Berg et al. 2011). The two-month long intensive measurement campaign produced a unique dataset of sonic and cup anemometer measurements at various heights for selected locations on the Bolund peninsula. Vertical lidar wind profiles complement the dataset (Bechmann et al. 2009, 2011; Berg et al. 2011). Today the dataset of the Bolund experiment serves as a baseline reference for various studies with respect to numerical and physical modelling.

Initially the Bolund dataset was used for a blind comparison of different microscale flow models, including simple linear models such as WAsP, non-linear models such as Reynolds-averaged Navier–Stokes (RANS) models and large-eddy simulation (LES), as well as physical models using wind-tunnel and water-channel facilities (Bechmann et al. 2011). Every participant was given the same information about topography, roughness and inflow conditions. There was significant scatter for both wind speed and turbulence levels among the different models, indicating that numerical models still have to develop in order to successfully model flow over real complex terrain.

An additional RANS solver verification was carried out by Prospathopoulos et al. (2012). The Bolund experimental dataset was used to verify the quality of a steady state RANS solver with a two-equation turbulence model. Difficulties with the modelling of the sharp escarpment lead to deviations between the predictions and the observed values downstream of the cliff. The deviation decreased with height. It was also stated that the predictions of the main flow are reliable, but that it was not possible to reproduce the turbulent behaviour of the flow with the applied method. The usage of a more advanced method, like LES, to improve the results for such complex terrain was suggested.

Furthermore Diebold et al. (2013) reproduced the flow around Bolund with the immersed boundary condition method using an LES model. Although close agreement was found with the field measurements, problems occurred in modelling locations close to the escarpment and close to the ground. The increased deviations from the field measurements are explained by insufficient information about the surface roughnesses and by a too coarse model grid.

The Bolund experiment was not only used to verify numerical models, it has also been used to prove the applicability of wind tunnels for atmospheric flow modelling. Yeow et al. (2013) conducted a wind-tunnel study to reproduce the wind flow around Bolund, where they focused on the main flow patterns that occur with the flow over a hill.

Yeow et al. (2013) reproduced the Bolund experiment on a scale of 1:115 in a neutral boundary-layer wind tunnel for two different Reynolds numbers. Particle image velocimetry (PIV) and a three-component hot-wire probe were used to obtain results along the 270° axis. The wind-tunnel measurements are in close agreement with the Bolund field measurements. However, vertical scans in the wind tunnel showed that the Bolund escarpment represents a critical point in the flow, indicating an over-prediction of the speed-up downstream of the escarpment at 2 m height. This deviation is not present at 5 m above the terrain. One possible explanation for the deviation is that Yeow et al. (2013) are not able to reproduce the inflow profile from the Bolund experiment. A second potential cause for the discrepancies is given by the fact that the ratio between the atmospheric boundary-layer height and the height of the peninsula in the wind tunnel is smaller than at full scale. These circumstances subsequently influence the flow perturbation caused by the peninsula and the resulting flow pattern evolution.

A similar experiment is carried out by Conan (2012), with a model scale of 1/500. Although he is able to reproduce the inlet conditions closer to the real inflow than Yeow et al. (2013), his results of the flow evolution on top of Bolund show similar deviations from the real scale.

Recently, Rowcroft et al. (2014) conducted extensive wind-tunnel tests on a forward-facing step with varying wind direction. They found a small increase of the reattachment length with increasing deviation from perpendicular flow. Unfortunately, they did not report on the wake height induced by the forward-facing step, making direct comparison with this study difficult.

Many of the mentioned studies state that their comparisons would improve with more detailed information about the flow. Especially the detachment and the wake area behind the edge of the escarpment have been the most problematic regions to model. To obtain a more comprehensive understanding of the flow pattern over the Bolund peninsula, especially close to the surface, a second field campaign deploying a scanning wind lidar was conducted in October 2011 by DTU Wind Energy. A preliminary investigation of this measurement campaign was carried out by Mann et al. (2014).

In the following section the set-up and procedure of the field campaign is explained, including a description of the scanning Doppler lidar. The lidar measurements are presented in the results section and followed by an investigation of the measured line-of-sight wind speeds. Subsequently, an analysis of the wake-height growth over Bolund show a large dependence on the upstream approaching wind direction. A conclusion summarizes the study and gives suggestions for future field measurement campaigns.

2 The Experiment

To gain insight into the recirculation zone downstream of the escarpment a complementary field experiment on the Bolund peninsula was conducted. In October 2011 a laser anemometer, in the following called WindScanner, was placed on the peninsula 20 m inland from the westward facing escarpment. The WindScanner, aligned on the 270° axis, was operated during westerly wind conditions to scan the area downstream of the Bolund edge. This experimental set-up stayed fixed during the whole experiment. The atmospheric inflow was measured in seven, 7-m high, vertical profiles with distances of 8, 10.75, 14, 16, 18, 20, 31 m from the scanning lidar as shown in Fig. 2. Figure 2 shows that the first six profiles are located above the peninsula, while the seventh profile is measured upstream, above the water. In addition to the seven vertical profiles a horizontal arc extending ±60° was scanned 120 m away from the instrument, at a height 13 m above the fjord in front of the peninsula (not shown in Fig. 2). Consecutive scans of all eight profiles is defined as one full-scan cycle. Each individual vertical profile consists of approximately 300 single vertical scans, while each vertical scan is constructed from measurements at 40 different heights distributed over the 7-m tall profiles. The eighth profile consists of 60 horizontal scans, while each individual horizontal scan comprises of 390 measurement points along the arc. While westerly wind directions prevailed, lidar measurements were recorded continuously during an almost 24-h long measurement period.

The line-of-sight wind speeds of the eighth profile were used to determine the undisturbed inflow wind speed and wind direction.

Due to the small distances involved in the experiment a short-range WindScanner was used, an instrument developed in the Wind Energy department of the Danish Technical University in collaboration with the lidar manufacturer ZephIR, UK. The lidar is a continuous-wave, coherent Doppler lidar first described in Karlsson et al. (2000). Its two main components are a modified directional sensing version of a commercial ZephIR Z150 wind lidar (Kindler et al. 2007; Smith et al. 2006) and a fast-scanning scanner head (Mikkelsen et al. 2011).

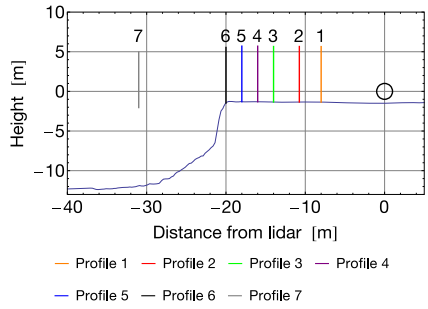

Fig. 2 The position and height of the seven vertical profiles scanned by the lidar relative to the Bolund escarpment. The position of the WindScanner itself is indicated by the *circle*. Not shown is the horizontal arc scan, profile 8, which is located 120 m from the instrument at a height of 13 m above the water

The scanner head consists of two independently controlled top-mounted rotating prisms, each with a 30° deflection angle that steers the lidar's line-of-sight within a scanning cone with a full opening angle of 120°. The design of the focusing mechanism allows a minimum focusing distance of approximately 8 m. The instrument has been calibrated in order to achieve a pointing accuracy of 0.1° during scanning. The design of the control system of the scanner head helps provide feedback of the actual position of each of the prisms, which is used to determine the direction of the line-of-sight of the short-range WindScanner. Uncertainties in the position of the measurements will originate mainly from the synchronization of the one radial wind-speed measurement with the corresponding line-of-sight direction defined by the data acquired from the scanner. The synchronization of these two has an uncertainty of ±1.7 ms. Therefore a radial wind speed may be displaced by (1.7 ms × 7 m)/(0.1 s) = 0.119 m when measuring a 7-m tall profile during 0.1 s. It is confirmed by investigating the position of the wake top during consecutive up and down sweeps that the estimate of the height uncertainty due to synchronization uncertainty is indeed conservative. A more detailed description of the WindScanner measurement technique is found in Sjöholm et al. (2014).

The probe length is defined by the width of the line-of-sight intensity profile of the focused laser-light energy around the focus point, which peaks around the lidar's adjustable focus point. To a good approximation, the line-of-sight intensity profile of a continuous wave lidar, follows a Lorentzian distribution weighting function (Sonnenschein and Horrigan 1971).

The theoretically expected probe lengths have been calculated based on the properties of the optical components of the instrument and have also been experimentally evaluated using hard target return. The probe lengths are represented in Fig. 3, in which highlighted areas correspond to the focus distances used in each of the seven vertical profiles. As far as it concerns the focus distance, the estimated uncertainty will result in an error of determining the point of focus, which will increase along with the distance. For example, at the first profile this is 0.007 m and at profile 7 it is 0.12 m. The produced laser Doppler spectra contain information about the average wind speed projected to the line-of-sight of the instrument over the probe length (Angelou et al. 2012).

During this experimental set-up 500 laser Doppler spectra were averaged in real time resulting in an effective data-streaming rate of approximately 390 line-of-sight wind-speed samples per second, which corresponds to 40 height measurements per sweep and to approximately 300 vertical profile measurements per profile location. Prior to the post processing of the spectra they are averaged to reduce the noise. More information about the data filtering and processing is described in Angelou et al. (2012). The resulting spectra offer the possibility of measuring radial wind speeds between 0.3 m s^{-1} and 18 m s^{-1} with a Doppler spectral speed resolution of 0.15 m s^{-1}. Furthermore the opto-electronic design of the instrument,

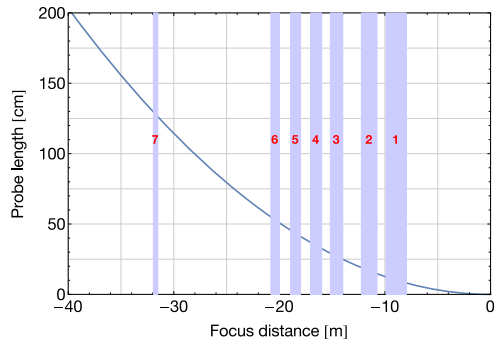

Fig. 3 The probe length of the short-range WindScanner measurements as a function of focus distance. The *highlighted areas* correspond to the vertical planes scanned during this experiment. Not shown on the figure is profile 8, which has a focus distance of 120 m and a probe length of 1.8 m

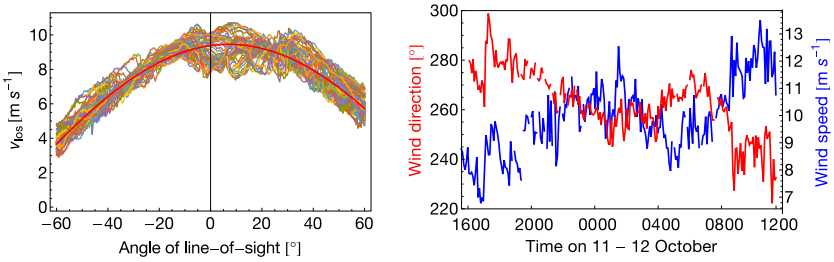

Fig. 4 *Left* Angle of the wind vector of each measurement relative to the instrument coordinates for one scan cycle of profile 8. The sinusoidal fit is displayed by the *red solid line*. *Right* Development of the undisturbed inflow wind speed and direction over the whole measurement period calculated from profile 8

which includes an optical acoustic modulator, allows for the distinction of the sign of the wind-speed component, not only the absolute value.

The measurement of the line-of-sight wind speed is limited by close to ground and close zero speed measurements (Abari et al. 2015). Due to the lidar's lower wind-speed detection limit (0.3 m s^{-1}), 14 scan cycles (equal to 70 min of measurement time) that had more than 1000 consecutive below-limit measurements were filtered out.

The upstream scan of the horizontal plane (profile 8, 120 m away from the instrument) was used to determine the undisturbed inflow. A RANS simulation (not shown here) shows that the wind direction changes by less than 1/10 degree and that the wind speed reduces by less than 3 % within the upstream distance of 100 m. The measurements of the horizontal profile were used to calculate the angle of the horizontal wind vector of each measurement relative to the instrument's westerly orientation coordinates. A sinusoidal fit was applied to the calculated angle to solve for two unknown parameters, wind speed and wind direction (Fig. 4). The wind direction ranged from 220° to 300° and the wind speed increased from 7 to 13 m s^{-1} throughout the measurement period. The average wind speed was 9.3 m s^{-1}.

3 Results

Figure 5 shows the line-of-sight wind speed over a 30-s period at profile 2. Fluctuations in positive and negative line-of-sight wind speeds close to the ground and increasing wind speeds with height visualize the dynamics of the unsteady atmospheric flow.

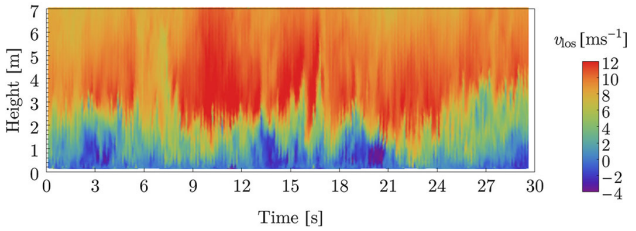

Fig. 5 The line-of-sight wind-speed scan at profile 2, 10.75 m from the WindScanner over 30 s. 296 consecutive vertical profiles are plotted

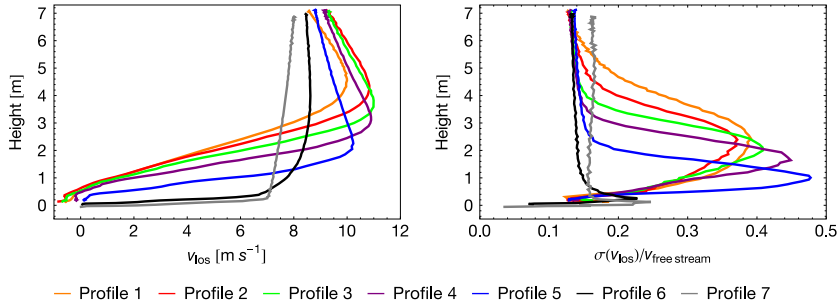

Fig. 6 *Left* Time-averaged wind-speed profiles with an inflow wind direction of 270° ± 5° of all seven vertical profiles. Some profiles show reversed mean flow close to the ground. *Right* Corresponding profiles of the normalized standard deviation (turbulence intensity) of the line-of-sight wind speed

The time average of the line-of-sight wind speed (approximately 4.5 h) at wind directions 270° ± 5° for each profile leads to the vertical profiles shown in the left panel of Fig. 6. Negative mean line-of-sight wind speeds indicate reversed mean winds close to the ground for profiles 1–4. Already at the position of the escarpment (profile 6) we see a velocity deficit in the lowest 1–2 m (Fig. 6, left) and enhanced turbulence in the lowest 1 m (Fig. 6, right). We hypothesize that this is created by the stony beach and the rough slope of the escarpment. Profile 6 may also be influenced by moving grass on the edge and therefore the data may be erroneous. The normalized standard deviation of the line-of-sight wind speed (normalized by the freestream wind speed at 7-m height of every profile location) in the right panel of Fig. 6, reaches its maximum at heights between 1 and 2 m, indicating a high degree of variation. Turbulence intensities show values up to 50 % at these heights. The turbulence profile of profile 7 (located 11 m upstream of the escarpment) differs from the other six profiles at the upper heights. A different measurement height of 12–19 m above ground and a different air mass below alters the shape of profile 7. The 1-h mean profile of the standard deviation of the line-of-sight velocity in (Mann et al. 2014, Fig. 6) shows that the deviation of profile 7 can be smaller.

Both figures (Fig. 6, left, right) show a turbulent layer that grows with the distance from the edge.

3.1 Wake Height–Wind Direction Dependence

The characteristic of the escarpment-induced wake height is further investigated by identifying the boundary between the turbulent wake layer and the freestream flow above. Due to the

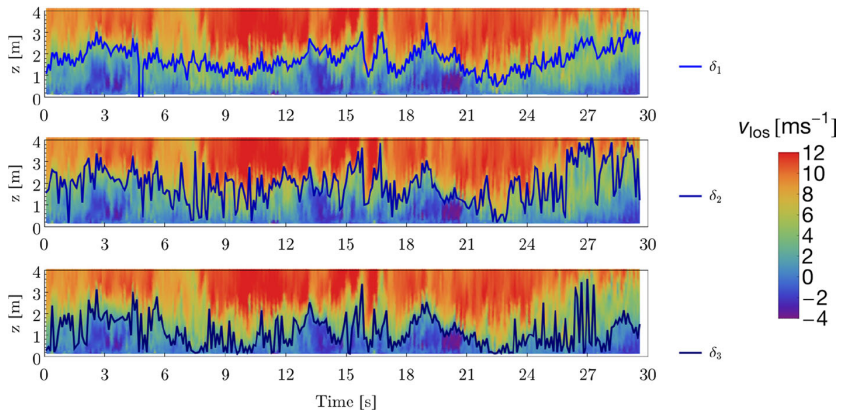

Fig. 7 The line-of-sight projected wind speed of profile 3, 12 m away from the WindScanner lasting for 30 s with the defined wake heights using three different methods

high measurement-sampling rate a precise determination of the interface between the two distinctly different layers is possible. We determine the wake height δ using three different methods.

1. The first approach determines the displacement thickness, δ_1, that is defined as the distance that the boundary layer is displaced to compensate for the reduction in flow rate on account of the wake formation, where $u(z)$ is the line-of-sight wind speed at height z, z_{top} is the top of the profile, and u_0 is the freestream velocity (Hinze 1975, pp. 593–597)

$$\delta_1 = \int_0^{z_{\text{top}}} \left(1 - \frac{u(z)}{u_0}\right) \mathrm{d}z. \tag{1}$$

2. The second approach identifies the height of the maximum, $\arg\max_z$, gradient of the line-of-sight wind speed, δ_2, of each vertical scan (Emeis et al. 2008, Sect. 2.2.2)

$$\delta_2 = \arg\max_z \left[\frac{\mathrm{d}u(z)}{\mathrm{d}z}\right]. \tag{2}$$

3. The third approach identifies the height at which the average between the integral of the two atmospheric layers is the greatest, δ_3, which resembles Davis et al. (2000) and Emeis et al. (2008, Sect. 2.2.3),

$$\delta_3 = \arg\max_z \left[\frac{1}{z_{\text{top}} - z}\int_z^{z_{\text{top}}} u(z)\mathrm{d}z - \frac{1}{z}\int_0^z u(z)\mathrm{d}z\right]. \tag{3}$$

The results of the wake-height identifications of all three methods are presented in Fig. 7. All three methods manage to identify a wake height, although the actual height differs between the methods. Method 1 gives the highest value of the wake heights.

The calculated wake height for each profile location can be placed in relation to the undisturbed wind direction and speed. The dependence of the wake height, obtained with method 1, on the wind direction is presented in Fig. 8. With increasing distance from the

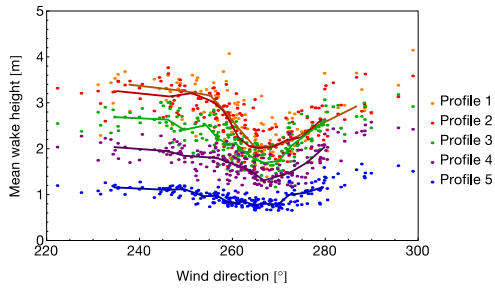

Fig. 8 Dependence of the determined wake height with method 1 on the wind direction. The *solid lines* depict the average wake height

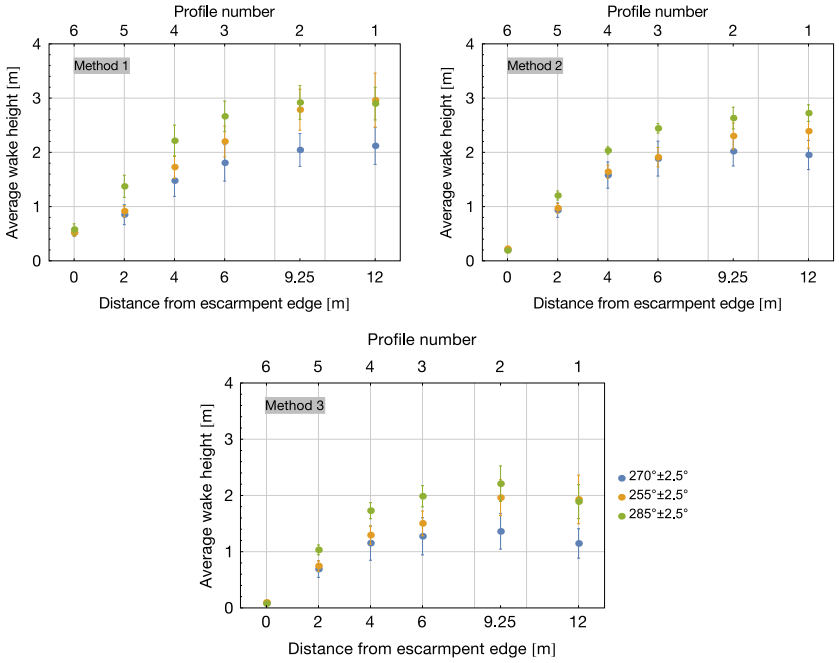

Fig. 9 Averaged wake height for wind-direction bins 270° ± 2.5°, 255° ± 2.5° and 285° ± 2.5° for six profiles downstream of the edge. The *error bars* display the corresponding standard deviation of the wake height

escarpment, the wake heights show a stronger dependence on the wind direction. The lowest wake heights of every profile is located at a wind direction of 270° (Fig. 8). At larger direction deviations the height is near constant. Profile 6 is located over the edge, where no wake develops and is therefore omitted from the plots.

To support the relation between wake height and wind direction we show in Fig. 9 the calculated mean and standard deviation of the wake height, determined with all three methods mentioned above, for three wind-direction bins (270° ± 2.5°, 255° ± 2.5° and 285° ± 2.5°) at every profile. It is seen that the wake height grows with distance to the escarpment, which is also supported by Fig. 6, left panel. Depending on the distance from the escarpment the

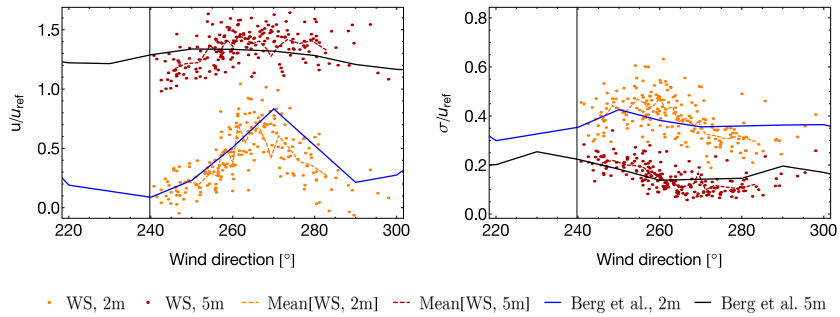

Fig. 10 *Left* Comparison of the line-of-sight wind speed at profile 2 at 2 and 5 m with values at M6 from the Bolund experiment (Berg et al. 2011). The reference values u_{ref} were interpolated logarithmically from $z = 13\,\mathrm{m}$ and $z_0 = 0.0006\,\mathrm{m}$ to 5-m height. *Right* Comparison of the normalized turbulence at profile 2 at 2 and 5 m with values at M6 from the Bolund experiment (Berg et al. 2011)

wake height increases between 10 and 70 % when the wind direction deviates from west, either to the north or the south ±15°. The standard deviation shows values between 3 % and 20 % of the mean wake-height value. The comparison of the three different methods shows that the direction dependence is not an artefact of the wake-height determination method.

It has also been verified that the wake height is independent of the incoming wind speed (not shown here). The atmospheric stability has not been measured during this experiment, though results from Berg et al. (2011) show that stability changes have only a small effect on wind speeds on Bolund. This implies that the wake height is mainly influenced by the wind direction and the peninsula itself.

3.2 Comparison of Mast 6 and Profile 2

To strengthen the finding of the direction dependence, the WindScanner data are compared to the original mast-based Bolund experiment. Profile 2 was measured 10.75 m away from the WindScanner, which corresponds to the position where mast 6 (M6) was located during the Bolund experiment (Berg et al. 2011), allowing for a comparison of the datasets. In Fig. 9 of Berg et al. (2011), the relative wind speed and the normalized turbulence at M6 are shown relative to the wind direction measured at mast 0 (M0, upstream mast, 100 m in front of the Bolund peninsula). Berg et al. (2011) used the 5-m high horizontal wind speed at M0 as the reference speed for all cases. For the purpose of this experiment the horizontal speed at M0 at 5-m height was also used as the reference value for the turbulence. These values were calculated for profile 2. As the reference wind speed the calculated wind speed of the horizontal arc scan at 13-m height (100 m in front of the Bolund escarpment, above water) was interpolated logarithmically ($z_0 = 0.0006\,\mathrm{m}$) to 5-m height. Figure 10, left panel, shows the comparison of the horizontal speed and the line-of-sight wind speed at the location of M6 and profile 2 relative to the wind direction. Both datasets show similar patterns in the same data ranges. A speed-up and an even distribution of the relative speed at all wind directions is seen at 5 m. Both cases show nearly zero mean wind speeds at 2 m, with a clear increase of the normalized wind speed at 270°.

The comparison of the normalized turbulence reveals, in the right panel of Fig. 10, higher turbulence at 2 m in both datasets. Both M6 (all heights) and profile 2 at 5-m height show, for wind directions near 270°, a clear decrease in the normalized turbulence. A deviation of

the wind direction from 270°, leads to a turbulence increase. This is in accordance with Figs. 8 and 9, where the wake height is lowest around 270° and increases up to 1 m with a change of wind direction. This agreement supports the relationship between wake height and wind direction.

4 Conclusion

The relationship between the wake height and the wind direction revealed in this study is based on the analysis of high frequency atmospheric measurements with a rapidly scanning continuous-wave Doppler lidar. The measurement technique produces highly resolved images of the rapidly changing wake zone of the Bolund peninsula. Seven vertical profiles, each 7-m high, show the development of the escarpment-induced wake. The wake increases in height with distance from the west-facing escarpment and shows highly turbulent structures. The highly resolved measurements allow for a precise determination of the wake height, which was calculated using three different methods. All three methods show a surprisingly sharp increase of the wake height with deviation of the wind direction from 270°. As the wind direction deviates from west by $\pm 15°$, the height grows between 10 % and 70 % depending on the distance from the edge with the strongest effect farthest from the edge. This behaviour of the wake height can also be seen in the data of the mast-based Bolund experiment (Berg et al. 2011), where this relation has not been emphasized before.

For future campaigns we suggest a longer measurement campaign, which should improve the statistical significance of the quantitative findings, although we have no reason to expect the main qualitative findings to change. Additionally, stability measurements along side the WindScanner measurements would add an extra dimension to the study of the growth of the wake zone, although we believe that due to the low height of Bolund (12 m) stability effects are small. Also a wind vane upstream would allow more frequent wind-direction measurements and serve as a control for the wind-direction determination from the horizontal plane scan. To extend the experiment the usage of three WindScanners would allow the measurement of all three wind components and lead to a more comprehensive picture of the recirculation zone.

Acknowledgments This work is supported by the Center for Computational Wind Turbine Aerodynamics and Atmospheric Turbulence funded by the Danish Council for Strategic Research, grant number 09-067216. The authors gratefully acknowledge the financial support from the Danish Agency for Science, Technology and Innovation through grant number 2136-08-0022, the windscanner.dk project. Finally the authors are thankful to Neil Davis from DTU Wind Energy for providing valuable language feedback.

References

Abari CF, Pedersen AT, Dellwik E, Mann J (2015) Performance evaluation of an all-fiber image-reject homodyne coherent Doppler wind lidar. Atmos Meas Tech 8(4):3729–3752. doi:10.5194/amtd-8-3729-2015

Angelou N, Mann J, Sjöholm M, Courtney M (2012) Direct measurement of the spectral transfer function of a laser based anemometer. Rev Sci Inst 83(3):33,111

Baskaran V, Smits A, Joubert P (1987) A turbulent flow over a curved hill. Part 1. Growth of an internal boundary layer. J Fluid Mech 182:47–83
Bechmann A, Berg J, Courtney M, Jørgensen H, Mann J, Sørensen N (2009) The Bolund experiment: overview and background Risø-R-Report. Tech. Rep., July, Risø-DTU, National Laboratory for Sustainable Energy, Roskilde
Bechmann A, Sørensen NN, Berg J, Mann J, Réthoré PE (2011) The Bolund experiment, Part II: blind comparison of microscale flow models. Boundary-Layer Meteorol 141(2):245–271. doi:10.1007/s10546-011-9637-x
Berg J, Mann J, Bechmann A, Courtney M, Jørgensen H (2011) The Bolund experiment, part I: flow over a steep, three-dimensional hill. Boundary-Layer Meteorol 141(2):219–243
Bowen A (1979) Some effects of escarpments on the atmospheric boundary layer. PhD Dissertation, University of Canterbury
Castro FA, Palma JMLM, Lopes AS (2003) Simulation of the Askervein flow. Part 1: Reynolds averaged Navier–Stokes equations (k–ϵ turbulence model). Boundary-Layer Meteorol 107(3):501–530
Chow FK, Street RL (2009) Evaluation of turbulence closure models for large-eddy simulation over complex terrain: flow over Askervein Hill. J Appl Meteorol Climatol 48(5):1050–1065
Conan B (2012) Wind resource assessment in complex terrain by wind tunnel modelling. PhD Thesis, Karman Institute/Orléans University
Davis KJ, Gamage N, Hagelberg CR, Kiemle C, Lenschow DH, Sullivan PP (2000) An objective method for deriving atmospheric structure from airborne lidar observations. J Atmos Ocean 17(11):1455–1468. doi:10.1175/1520-0426(2000)0171455:AOMFDA2.0.CO;2
Diebold M, Higgins C, Fang J, Bechmann A, Parlange M (2013) Flow over hills: a large-eddy simulation of the Bolund case. Boundary-Layer Meteorol 148(1):177–194
Emeis S, Frank H, Fiedler F (1995) Modification of air flow over an escarpment. Results from the Hjardemål experiment. Boundary-Layer Meteorol 74(1–2):131–161
Emeis S, Schäfer K, Münkel C (2008) Surface-based remote sensing of the mixing-layer height—a review. Meteorol Z 17(5):621–630. doi:10.1127/0941-2948/2008/0312
Hinze J (1975) Turbulence, 2nd edn. McGraw-Hill Book Co, New York, 790 pp
Hunt J, Leibovich S, Richards K (1988) Turbulent shear flows over low hills. Q J R Meteorol Soc 114:1435–1470
Jackson P, Hunt J (1975) Turbulent flow over a low hill. Q J R Meteorol Soc 101:929–955
Jensen N, Peterson E (1978) On the escarpment wind profile. Q J R Meteorol Soc 104(441):719–728
Karlsson C, Olsson FA, Letalick D, Harris M (2000) All-fiber multifunction continuous-wave coherent laser radar at 1.55 μm for range, speed, vibration, and wind measurements. Appl Opt 39(21):3716–3726
Kindler D, Oldroyd A, MacAskill A, Finch D (2007) An eight month test campaign of the Qinetiq ZephIR system: preliminary results. Meteorol Z 16(5):479–489
Mann J, Angelou N, Sjöholm M, Mikkelsen T, Hansen K, Cavar D, Berg J (2014) Laser scanning of a recirculation zone on the Bolund escarpment. J Phys Conf Ser 555. doi:10.1088/1742-6596/555/1/012066
Mikkelsen T, Mann J, Nielsen M (2011) Rotating prism scanning device and method for scanning. Patent No.: WO 2009/155924 A1, 2009
Prospathopoulos J, Politis E, Chaviaropoulos P (2012) Application of a 3D RANS solver on the complex hill of Bolund and assessment of the wind flow predictions. J Wind Eng Ind Aerodyn 107–108:149–159
Rowcroft J, Burton D, Blackburn H, Sheridan J (2014) Surface flow visualisation over forward facing steps with varying yaw angle. J Phys Conf Ser 555. doi:10.1088/1742-6596/555/1/012086
Sacré C (1979) An experimental study of the airflow over a hill in the atmospheric boundary layer. Boundary-Layer Meteorol 17(3):381–401
Silva Lopes A, Palma JMLM, Castro FA (2007) Simulation of the Askervein flow. Part 2: large-eddy simulations. Boundary-Layer Meteorol 125(1):85–108
Sjöholm M, Angelou N, Hansen P, Hansen KH, Mikkelsen T, Haga S, Silgjerd J, Starsmore N (2014) Two-dimensional rotorcraft downwash flow field measurements by lidar-based wind scanners with agile beam steering. J Atmos Ocean 31(4):930–937
Smith DA, Harris M, Coffey AS, Mikkelsen T, Jørgensen HE, Mann J, Danielian R (2006) Wind lidar evaluation at the Danish wind test site in Høvsøre. Wind Energy 9(1–2):87–93
Sonnenschein C, Horrigan FA (1971) Signal-to-noise relationships for coaxial systems that heterodyne backscatter from the atmosphere. Appl Opt 10(7):1600
Taylor P, Teunissen H (1985) The Askervein Hill Project: report on the Sept./Oct. 1983 Main Field Experiment. Tech. Rep. Research Report MSRB-84-6. Meteorological Services Research Branch Atmospheric Environment Service, Toronto

Teunissen HW, Shokr ME, Bowen AJ, Wood CJ, Green DWR (1987) The Askervein Hill Project: wind-tunnel simulations at three length scales. Boundary-Layer Meteorol 40(1–2):1–29. doi:10.1007/BF00140067
Walmsley J, Taylor P (1996) Boundary-layer flow over topography: Impacts of the Askervein study. Boundary-Layer Meteorol 78(3–4):291–320
Yeow T, Cuerva-Tejero A, Perez-Alvarez J (2013) Reproducing the Bolund experiment in wind tunnel. Wind Energy 18(1):153–169. doi:10.1002/we.1688

CHAPTER 3

Bolund in WindEEE

A natural and next consequential step was to investigate the flow behavior over the Bolund peninsula in a controlled environment. Although the presented full-scale experiments around the Bolund escarpment has been performed with great success (see Berg et al. 2011 and chapter 2), experiments in controlled environments such as wind tunnels provide the opportunity to study problems systematically in greater detail, e.g. a wind-tunnel allows to test different scenarios and to modify single variables that influence the flow field. Such a controlled experiment was realized at the WindEEE Dome, a facility of the Western University, London, Ontario, Canada.

3.1 The WindEEE Dome

The Wind Engineering, Energy and Environment (WindEEE) Dome at the Western University, Canada is the world's first three-dimensional wind testing chamber. In the form of a hexagon, this chamber has a diameter of 25 m and a return circuit of the same shape with a larger diameter of 45 m (see Figure 3.1). Using 106 individually controlled fans, high intensity wind systems such as tornadoes, downbursts, and gust fronts can be physically simulated inside the WindEEE test chamber (Hangan 2014). The study of wind effects on large scale building and topography experimental models is facilitated by the unique flow generation capabilities. It is designed to create a wide variety of wind systems at large scales and Reynolds numbers. WindEEE operates in two distinct modes:

- Multi-fan wind-tunnel mode with the 60-fan wall (4 rows $\times$ 15 columns) pushing air inside the chamber and with the air recirculating above the chamber.

- Axisymmetric mode in which 8 fans situated at the base of each of the 6 walls are coupled with the larger 6 fans situated in the upper plenum, above the ceiling of the testing chamber.

The multi-fan mode on the north wall can be used to generate a variety of flows such as boundary-layer flows, sheared flows horizontally, sheared flows vertically and active turbulent flows.

Figure 3.1: *Top:* WindEEE Dome facility of the Western University, Canada. *Bottom:* The test chamber with a diameter of 25 m, as well as the 60-fan wall. Photos taken by Adrian Costache.

3.2 The Experiment

3.2.1 Test Chamber Configuration

The inflow was produced by the 60-fan wall. In order to generate a turbulent flow, 5 spires and a wooden panel were mounted in front of the fan wall (see Figure 3.2). In combination with the usage of a contraction zone with an inflow-outflow area ratio of 3:1 in front of this 60-fan wall, a channeled, accelerated, turbulent boundary-layer flow was created. Furthermore roughness elements were used and raised in and around the contraction zone as displayed in Figure 3.3 as the areas with the blue squares. Section 0, 1, 4, 20 and 23 were permanently raised by 7.5 cm. In order to investigate the influence of the roughness elements closest to the experimental model in sector 3, the height of the roughness elements directly in front of the turn table, was either 0 cm or 7.5 cm. This variation of section 3 is indicated in the experiment-overview Table 3.1, column 5. The different inflow conditions are presented in section 3.2.3.1.

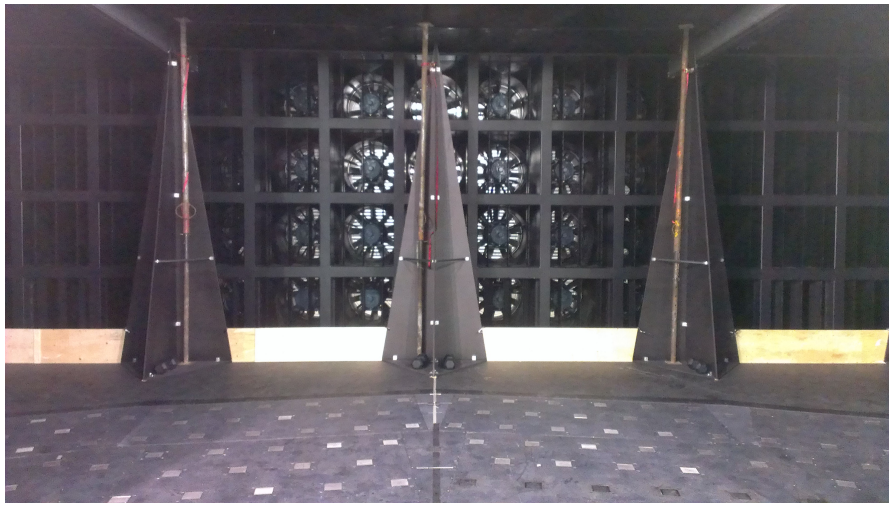

Figure 3.2: Close-up of the 60-fan wall. In front of the wall are spires and a wooden board mounted to produce a turbulent flow.

3.2.2 The Experimental Model

A 1/25 scale model of the Bolund peninsula (Berg et al. 2011; Lange et al. 2016; Yeow et al. 2013; Conan 2012; Diebold et al. 2013; Conan et al. 2016) was constructed. The experimental model was produced by a CNC milling of several large blocks of Expanded Polystyrene (EPS). These blocks were joined together and coated with black latex paint. The resulting Styrofoam Bolund model with the dimensions of 0.48 m height, 3 m width and 4 m length was placed on the turntable. Thereby the model escarpment was located in the middle of the turntable (Figure 3.4 and 3.3), in a distance of approximately 12.5 m from the 60-fan wall. A solid ramp with slope of roughly 45° was constructed from EPS and fastened to the downstream edge of the model to provide a smooth transition and reduce unwanted pressure drops and flow separation. The model was positioned in the chamber such that the plane of measurement, Line B (see Figure 3.5), was parallel to the flow direction. The experimental set-up is visualized in Figure 3.4.

3.2.3 Measurement Techniques

Two different measurement techniques were used. In order to capture the inflow conditions, with different roughness exposures and wind speeds Cobra Probe measurements were acquired. The investigation of the flow over the Bolund model was carried out with the help of the Particle Image Velocimetry (PIV) method.

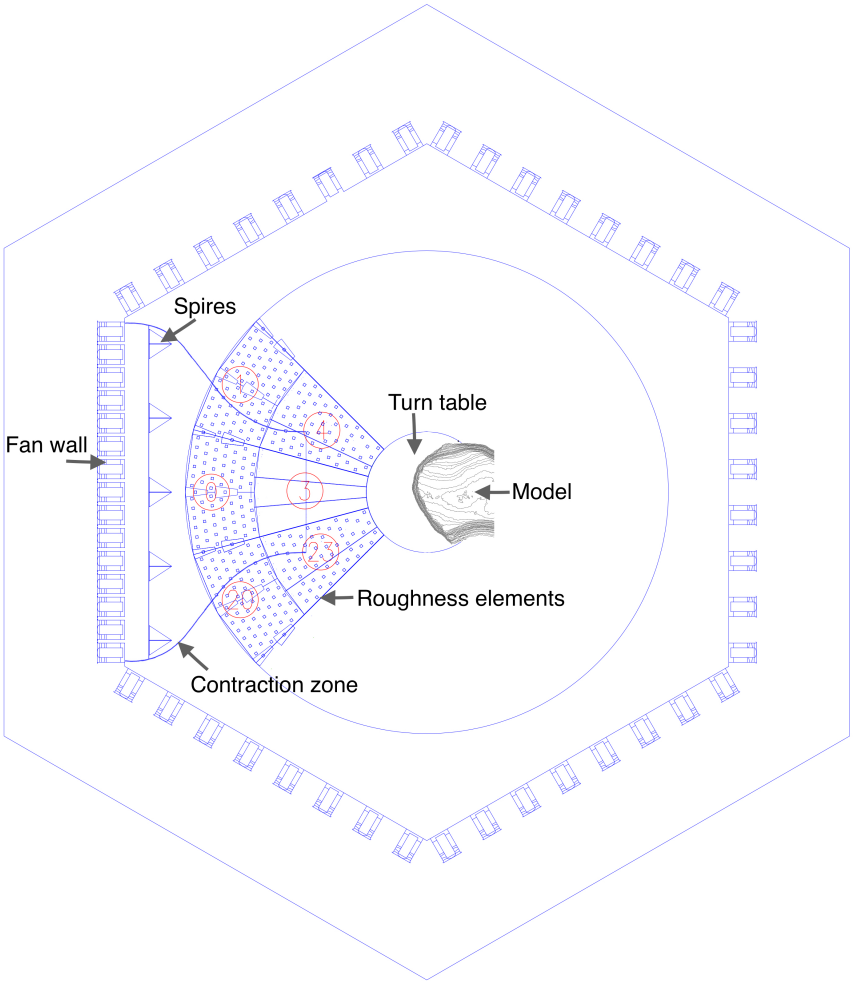

Figure 3.3: The layout of the WindEEE Dome. The experimental set-up viewed from above.

3.2.3.1 Cobra Probe measurements and inflow variations

Cobra Probe

The upstream profiles were measured with TFI Cobra Probes (CP), manufactured by Turbulent Flow Instrumentation Pty Ltd. The CP is a multi-hole pressure probe able to resolve 3-components of velocity (u, the component along the horizontal axis of the probe, v the horizontal component perpendicular to the probe, and w the vertical

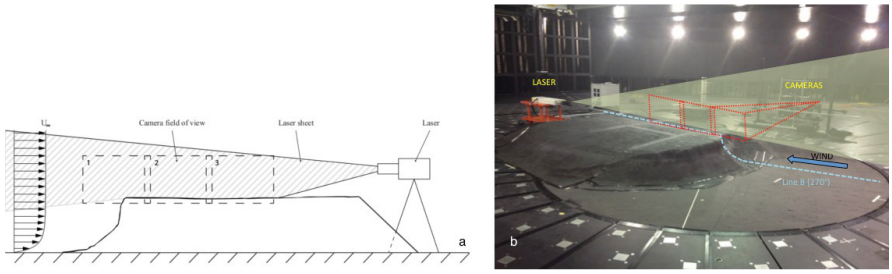

Figure 3.4: Experimental set-up for the WindEEE dome experiment. Schematic of the PIV multi-camera set-up (**a**) and an overall image of the experiment (**b**).

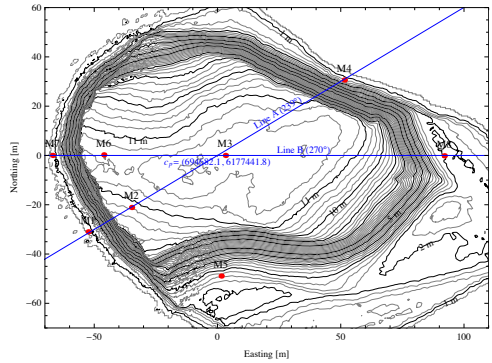

Figure 3.5: Contour plot of the Bolund peninsula. The blue lines indicate Line A and Line B. The red dots highlight the mast locations from the measurement campaign.

component), flow yaw and pitch angles and the instantaneous static pressure in real time. A vertical array of eight CPs was used, equally distributed over 60 cm or 15 m in full-scale. The probe array was mounted on a stationary floor rack positioned 2.5 m upstream of the model. All CP measurements were conducted with acquisition rate of 10000 Hz, output rate of 1250 Hz, and sampling time of 120 seconds. Further CP data processing steps are explained in appendix B, section 3.2. The CP measurement system delivers turbulence intensities with the definition $I_{uu} = \sqrt{u^2}/s = \sigma_u/s$ (same for I_{vv}, I_{ww}), with $s = \sqrt{u^2 + v^2 + w^2}$. From that σ_u, σ_v, σ_w were calculated for the determination of the TKE $k = (\sigma_u^2 + \sigma_v^2 + \sigma_w^2)/2$.

Inflow Variations

The inflow conditions were varied in order to address the question of Reynolds number dependence and to examine the dependence of the flow downstream of the escarpment

on different inflow details. Both aspects are investigated in a comprehensive and detailed study titled *Investigation on effect of Reynolds number and inflow parameters on mean and turbulent wind flow over complex topography*, which is attached in the appendix B and submitted to *Wind Energy Science*. A short summary of this study is presented in section 3.2.6. An overview of the different inflow profiles are summarized in the Table 3.1 and presented in the following:

The inflow speed was varied between 20%, 30% and 50% of full power (CP4-6 in Table 3.1) and in order to vary the shear of the inflow the speed of the third fan row was modified between 60%, 75% and 85% of full fan power, while the power of fan rows 1, 2 and 4 were kept constantly at 50% (CP1, CP2 and CP3 in Table 3.1). Figure 3.6, *top*, shows these variations and an increased shear with increased fan power is observed at maximal model height. Additionally we investigated the influence of the roughness elements of section 3 in front of the model (column 5 in Table 3.1), by comparing CP4/5, CP6/7 and CP8/9. The influence of the roughness elements in front of the escarpment is visualized in Figure 3.6, *bottom*. The mean and turbulent (σ_u) flow is clearly distinguishable at lower heights. If the elements are lowered, higher mean wind speeds and smaller turbulence intensities are observed at lower heights. This effect decreases with height and is barely seen at the maximal model height of 12 m. With increased fan power, the influence of the elements propagates to higher heights.

3.2.3.2 PIV

Particle Image Velocimetry (PIV) (Raffel et al. 2007) was used to measure the two-dimensional velocity field in a vertical plane above the model, along Line B, in the vicinity of the escarpment. The measurement region is extending roughly from Z = 11.4 m to 25 m and X = -70 m to X = -20 m in the full-scale Bolund coordinates, where the value Z = 0 corresponds to sea level and X=0 where line A and B meets, see figure 3.5. Three 12 megapixel cameras (IO Industries Flare 12M125-CL) were used, each with 105 mm f/2D Nikon AF DC-NIKKOR lenses, to capture images. The cameras were positioned in a row, in a distance of roughly 3.55 m from the model and parallel to the flow direction, at a height such that the bottom of the camera field of view was just below the island surface (Figure 3.4). The camera resolution was 4096 x 3072 pixels, and the corresponding field of view for each camera, based on the distance to the subject, was about 0.78 m wide by 0.58 m high. The cameras were positioned with an horizontal overlap to ensure spatial continuity of the flow measurements. Thus the combined coverage area was approximately 2 m wide by 0.55 m high. Each processing step is explained in the section 3.2.5. A Litron Nano PIV Series dual cavity Nd:YAG laser with wavelength 532 nm, energy 425 mJ/pulse and frequency of 18 Hz was used to illuminate the flow field. The laser was positioned directly behind the model, pointing upstream, aligned with Line B, with the laser head roughly 0.60 m off the ground, as shown in Figure 3.4. A cylindrical lens was positioned immediately in front of the laser head to convert the beam into a two-dimensional sheet. The laser was synchronized to the cameras and the frame grabber, thus the laser-firing rate of

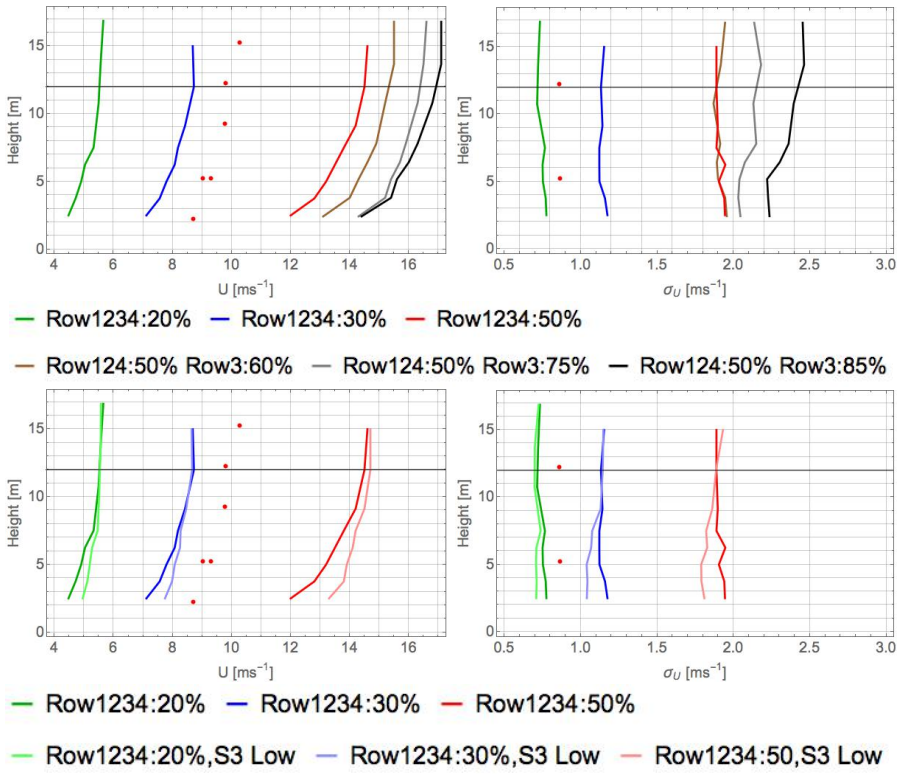

Figure 3.6: *Left:* Upstream mean and *Right:* turbulence profiles measured with a vertical array of Cobra Probes for different inflow conditions (see Table 3.1). *Top:* Variation of inflow speed and *Bottom:* Variation of roughness elements of section 3. The solid black horizontal line indicates the model height of 12m. The red dots display the real-world values.

9 Hz for each laser head corresponded to the identical 9 Hz capture rate for image pairs. IO Industries Coreview software was used to capture raw images. For each run, PIV data was typically recorded for three minutes, which provided 1600 image pairs. Images were recorded in TIFF format. An Ultratec CLF-4460 commercial fog generator, positioned in the dome's upper plenum, was used to seed the test chamber with non-toxic, water-based smoke.

3.2.4 Test Cases

3.2.4.1 Sharp / Round edge

Because the processing of the topographic information leads to a rounded appearance of the model escarpment edge in comparison with the actual, full-scale terrain (see chapter 2, page 2; Figure 1). Therefore the edge was modified by extending the horizontal top of the escarpment by 20 mm with modeling clay to make the edge sharper, almost a right angle (Figure 3.7). The maximum thickness of the clay is 15 mm. The corresponding runs are indicated by an x in column 8 in the Table 3.1.

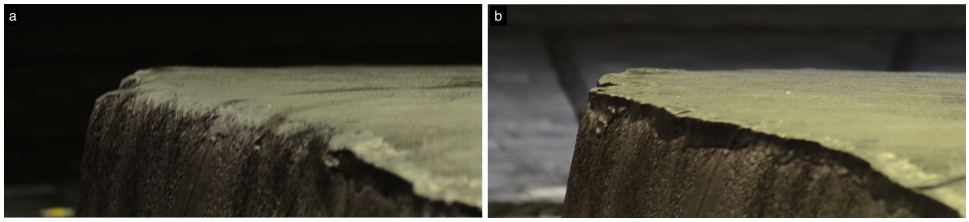

Figure 3.7: The two different topographies of the Bolund model edge. The round model edge (*a*) and the model modified with modeling clay to give a sharp edge (*b*).

3.2.4.2 Change of inflow direction

In order to measure the flow over the Bolund model for different inflow wind directions the turntable was turned with the Bolund model in place $\pm 10°$, while the laser sheet stayed aligned with Line B and therefore was also turned by $\pm 10°$. The turning of the turntable 10° clock-wise changed the inflow wind direction to 260°. The turning 10° counter-clockwise changed the incoming flow direction to 280°. In Table 3.1 is this set-up indicated in column 9 with the cw for clockwise and ccw for counterclockwise.

3.2.4.3 Experiment Overview

The flow field over the Bolund model was measured along Line B with the above mentioned PIV technique. Table 3.1 summarizes all set-up configurations that were realized. Firstly the table shows PIV run names (R1-R21) and combines them with different inflow conditions, measured by CPs (CP1-CP9). Column 3 shows the power of the rows 1, 2 and 4 of the 60-fan wall, which varies between 20% and 50% of full power. The power of the third row was varied between 20% and 85% of full power independently of the other rows to experiment with differently sheared inflow. The ”section 3” column indicates if the roughness elements were up or down. Hereafter the columns describe information for the PIV measurements. The x in the clay column indicates if the Bolund model edge was modified to a sharp edge by clay. Lastly the

ninth column points out if the sharp-edge cases were measured along the 270° line or if the turn-table was turned 10° clock-wise or counter clock-wise.

Table 3.1: Experiment overview; the columns from left to right: R1-R21 are the run names. CP1-CP9 are the measured inflow profiles. Fan power of row 1,2,4. Fan power of row 3. Roughness elements of section 3 are raised by 0 cm (down) or 7.5 cm (up). dt is the time between two pulses in ms. Exposure time of cameras in μs. Inflow direction deviation $\pm$ 10°.

Name	CP Run	Row 1,2,4	Row 3	Section 3	dt	Exposure	Clay	10° deviation
R1	CP1	50%	60%	up	-	250		
R2	CP2	50%	75%	up	-	250		
R3	CP3	50%	85%	up	-	250		
R4	-	50%	60%	down	200	275		
R5	-	50%	75%	down	200	275		
R6	-	50%	85%	down	200	275		
R7	CP4	20%	20%	up	450	400		
R8	CP5	20%	20%	down	450	400		
R9	CP6	30%	30%	up	300	300		
R10	CP7	30%	30%	down	300	300		
R11	CP9	50%	50%	down	150	250		
R12	CP7	30%	30%	down	300	300	x	straight
R13	CP7	30%	30%	down	300	300	x	cw
R14	CP7	30%	30%	down	300	300	x	ccw
R15	CP9	50%	50%	down	200	275	x	straight
R16	CP9	50%	50%	down	200	275	x	cw
R17	CP9	50%	50%	down	200	275	x	ccw
R18	-	50%	75%	down	200	275	x	straight
R19	-	50%	75%	down	200	275	x	cw
R20	-	50%	75%	down	200	275	x	ccw
R21	CP7	30%	30%	down	200	275	x	ccw

3.2.5 Processing of the PIV Images

In order to gain high quality flow fields, the raw image pairs acquired with core view (see Figure 3.8) were processed in the following steps:

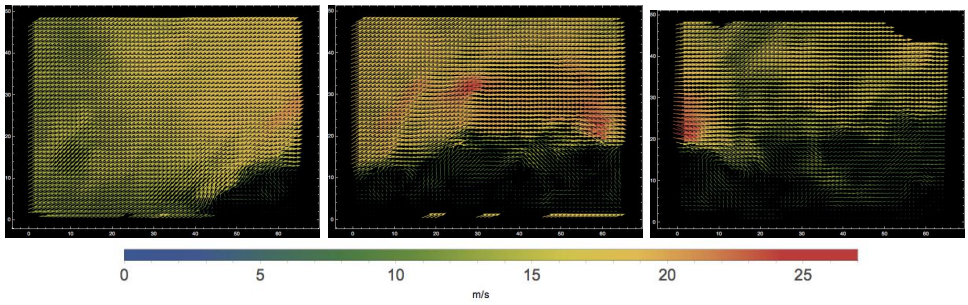

Figure 3.8: Instantaneous flow field of each camera frame.

1. During the first processing step a mask was produced for the Bolund model surface for each camera frame. Thus erroneous flow vectors through laser reflections along the surface model were avoided.

2. Prior to the PIV processing, the images were filtered because horizontal or vertical stripes were appearing occasionally, possibly caused by electromagnetic noise. The image intensity $I(x, y)$, where x and y are pixel positions, was Fourier transformed into $\hat{I}(k_x, k_y)$ where k_x and k_y are wave numbers in the two image plane directions. Then, $\hat{I}$ was set to zero for $k_x = 0$ or $k_y = 0$ and thereupon inversely Fourier transformed to get stripe-free images.

3. The image pairs were processed in the following step with DynamicStudio 4.0 (*Dantec*) and the adaptive PIV method. The images were analyzed with 64 $\times$ 64 windows using a 50% overlap. Typical vector removal rates were from 2% to 4%. For every camera frame 1600 image pairs were processed, which is equivalent to 3 min of PIV measurement time.

4. In order to combine the 3 camera frames, a camera calibration was necessary. For that the method described in Trucco and Verri 1998 was used, in which extrinsic and intrinsic parameters were determined. With the assumptions that the pixel aspect ratio $\alpha = 1$ and that the radial distortion is neglected $k_1 = 0$, a rotation matrix and a translation vector was calculated for each frame. With the help of this method the three frames were aligned and a clear overlap was identified to stitch the frames together.

5. The last step in the processing of the PIV images was the stitching/combination of the 3 frames. The results are presented in the beginning of the next chapter.

3.2.6 Investigation of the effect of Reynolds number and inflow parameters on mean and turbulent flow

The study of Kilpatrick et al. attached in appendix B investigates the mean and turbulent flow behavior in the presented experimental set-up over the Bolund model.

A range of Reynolds numbers, boundary-layer inflow-profiles, and upstream roughness values are examined in order to evaluate the influence of these parameters on the flow. Therefore three uniform fan profiles and one modified shear profile are tested and combined with the two different upstream roughness configurations, leading to a a total of eight unique sets of inflow conditions. Our results are presented in the form of normalized speed-up and TKE increment. They are compared to each other, to measurements from the Bolund field campaign and previous experimental work. The results show that the mean flow behavior was generally not affected by the Reynolds number, however a slight increase in speed-up over the escarpment was observed for cases with lower upstream roughness. The shape of the inflow wind shear profile also had a minor impact on the mean flow near the escarpment. More significant effects were observed in the turbulent flow behavior, where the turbulent kinetic energy (TKE) over the escarpment was found be a strong function of upstream roughness and a weak function of the Reynolds number. The local change in the upstream wind shear was found to have the most significant influence on the TKE magnitude, which more closely approximated the full-scale TKE data, and had not been previously observed in wind tunnel modeling of this topography.

CHAPTER 4

Results of WindEEE experiment

This chapter presents the analysis of the PIV results from the WindEEE experiment. In the following the influence of the modified model edge and of the inflow wind direction on the flow above Bolund is presented and analyzed.

4.1 Impact of escarpment edge modification

In order to analyze the influence of the modified model edge run 5 (without terrain modification) and run 18 (with modification, see Table 3.1) were compared. These two runs have fan row 1, 2 and 4 running at 50% of full power and row 3 at 75%. Also the roughness elements in section 3 immediately in front of the model are down.

The comparison revealed significant different flow fields with and without the edge modification (Figure 4.1). With the modified, sharp edge, a large recirculation zone is located behind the escarpment, which affects the mean wind, shear and turbulence. The recirculation zone, as well as the reattachment length, both of which are created by the sharp edge, resemble the flow over a forward-facing step to some degree (Largeau and Moriniere 2006). The occurrence of a permanent recirculation zone in the mean flow field is in contrast to Yeow et al. 2013 and Conan et al. 2016, who only find an intermittent recirculation zone in their wind-tunnel studies. The flow field of the round edge case shows a smoother flow downstream of the escarpment. The standard deviation of the u and v component of the flow is presented in Figure 4.2 [1]. Comparing the round and the sharp-edge cases highlights that directly downstream of the round edge a small and 0.2h (h being the step height) long area with high σ_u values up to 8 ms^{-1} is located. On the contrary, σ_u of the sharp-edge case displays a large, further downstream shifted and uplifted area with values as high as 8 ms^{-1}. In both cases is σ_v observed with the same patterns as σ_u, but with lower values.

[1] Here we use the usual wind tunnel convention, which denotes the vertical component v as opposed to the atmospheric convention where it is denoted w

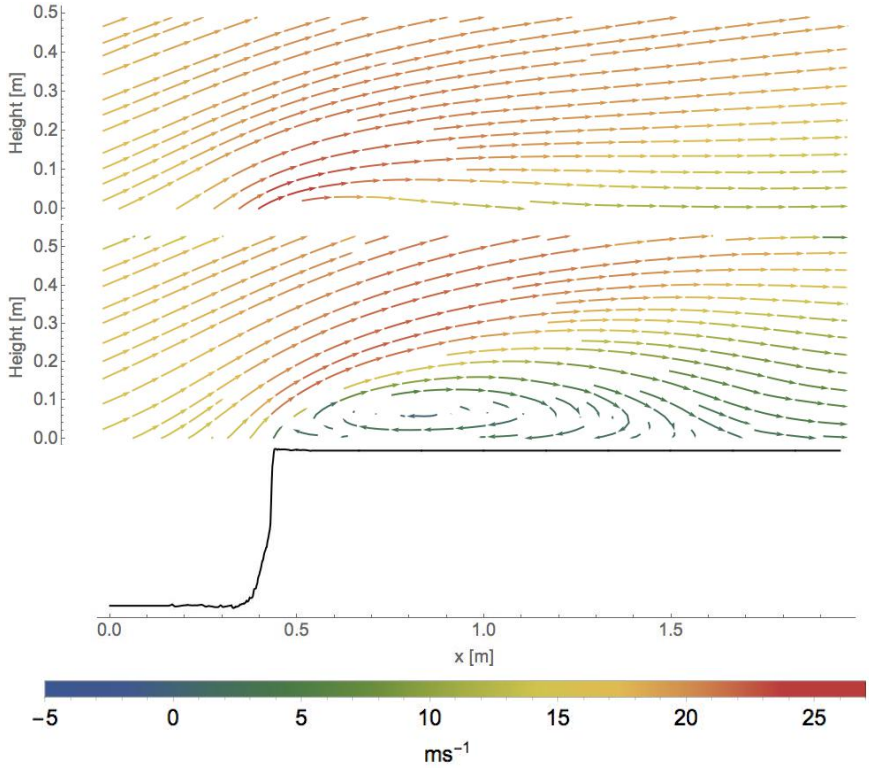

Figure 4.1: The mean flow field of the smooth (*top*) and sharp-edge (*bottom*) case. The mean is calculated using 1600 statistically independent image pairs. The Bolund contour line indicates the edge position.

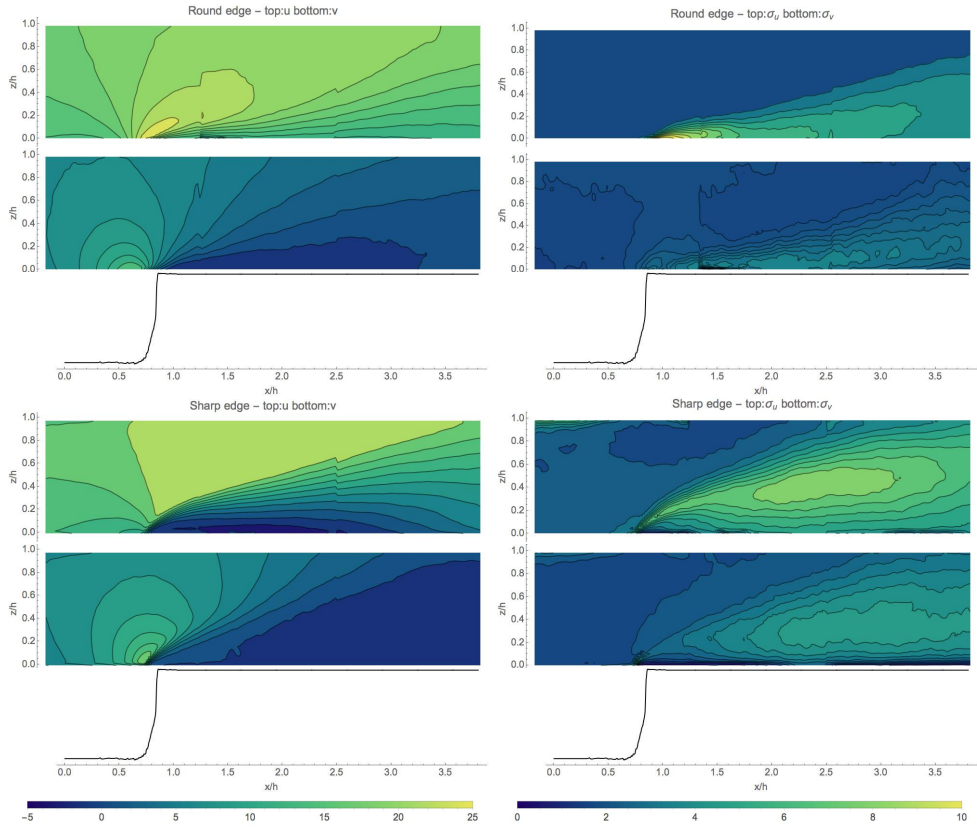

Figure 4.2: *Left:* The mean u and v component and the *Right:* Standard deviation of the u and v component of the flow field of the round and sharp-edge case. The fields are calculated using 1600 image pairs. The Bolund contour line indicates the edge position.

To put the findings into a wind energy perspective, we calculated the energy production of a wind turbine positioned close to the escarpment with and without the edge modification. We chose a Vestas V90 2MW Gridstreamer (*www.wasp.dk*) and assumed that the mean wind speed $\overline{U}$ at hub height in the inflow was between 5 and 10 m/s and that the mean wind distribution was a Weibull distribution with a shape parameter $k = 2$. Quite unrealistically, but to emphasize the differences in the flows with a sharp and a round edge, we assumed that the wind direction was constant and perpendicular to the escarpment. We used a model scale of 1/500. With an assumed wind turbine hub height of 90 m, which is equal to the rotor diameter, the model scale hub height is 0.18 m. The turbine is positioned three rotor diameters downstream of the escarpment, equivalent to 1.13 escarpment heights. We calculated the power output of the turbine using the power curve of V90 and a procedure integrating the

different winds over the rotor (Wagner et al. 2011), which involved the area-weighted average of the kinetic energy flux over the rotor. Both wind profiles were normalized with the wind speed at hub height of the round edge case, which assures that the external forcing was identical and resulted in the same wind speed distribution for the modified sharp-edge case.

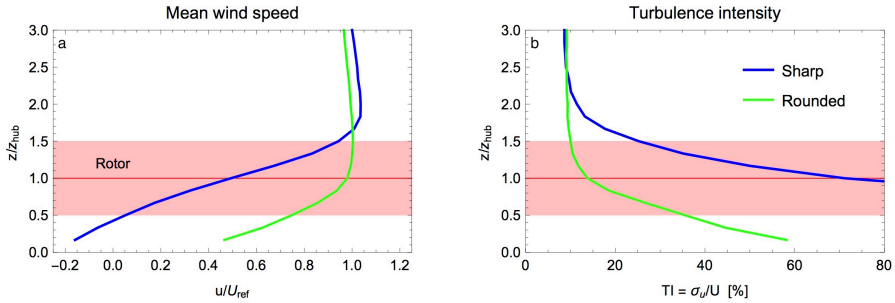

Figure 4.3: Profiles of normalized mean wind speed and turbulence intensity. Profiles are illustrated with sharp and round edges at a position 1.13 times the escarpment height downstream of the edge. The horizontal line indicates the hub height of a hypothetical wind turbine; the shaded area denotes the height swept by the rotor.

The results show that depending on the average wind speed at hub height for the round edge, the flow with the sharp edge gives an annual energy production (AEP) that is only 20% to 51% of the round-edge case (see Figure 4.3 and Table 4.1). Such a reduction would influence the economy of a wind-turbine project significantly.

In addition to very different AEP values, the modification of the edge could have dramatic consequences for the dynamic loads on the wind turbine. For assessment of the flow quality at a potential wind turbine site, the International Electrotechnical Commission (IEC) (IEC 2005) recommends that the turbulence intensity $I_u = \sigma_u/\overline{U}$, where σ_u is the standard deviation of horizontal wind, at the site should be less than 18% for this chosen turbine class. In addition, the shear exponent $\alpha = (z/\overline{U})(d\overline{U}/dz)$, where z is the height above the surface, should be less than 0.2 at hub height. For the case with the round edge, both parameters are within the limits of the IEC standard. However, in the sharp-edge case, the shear is far beyond the limit, which would cause strong fluctuating loads on the rotating wind turbine blades moving in and out of high and low wind speed air flow (Table 4.1). Furthermore, the turbulence is significantly larger and close to a level where wind turbines will cease to operate.

Table 4.1: *Left:* Calculated AEP as a function of mean wind speed for flow with a sharp versus a round escarpment edge. *Right:* Shear exponent α and turbulence intensity I_u at hub height for the two cases.

$\overline{U}$	AEP [MWh/yr]		Ratio [%]
[m/s]	Round	Sharp	Sharp/Round
5	3072	622	20
6	4804	1257	26
7	6510	2100	32
8	8048	3097	38
9	9353	4176	45
10	10396	5272	51

	Round	Sharp
α	0.17	2.15
I_u [%]	14	72

The described analysis is presented in a paper that is submitted to *Nature Energy*. The paper is currently under *review* and is presented in appendix B.

4.2 Verification against real scale data

Since the average flow field generated in the wind tunnel showed significant differences between the two terrains, it became important to investigate which of the two variations resembles the real world more closely. Therefore we use the wind profiles, measured by the WindScanner and which are presented in Lange et al., chapter 2, Fig.6. as a real world reference. To perform a comparison, the profile locations, corresponding to the full-scale WindScanner measurements, are determined in the wind tunnel flow field of the runs 5 and 18. In order to ensure the comparison of the same parameters, the line-of-sight velocity was calculated from the u and v component of the wind-tunnel flow field, by projecting the vector onto the line-of-sight based on the WindScanner location 20 m downstream of the escarpment. The real world profiles are normalized by the average free-stream line-of-sight velocity, measured at a height of 7 m above Bolund during the scanning campaign. The wind tunnel profiles are normalized by the velocity measured by the TFI Cobra Probes upstream the model at model height. Figure 4.4 shows the normalized time averaged wind speed profiles and the normalized standard deviation for all three cases (WindScanner, round edge, sharp edge). At first view, the profiles of the sharp-edge case show a qualitative better agreement with the real world, with negative wind speeds in the lower heights and an increasing turbulent layer, which is growing rapidly in height from the edge. Compared to the real world this turbulent layer is reaching up to higher heights in the wind-tunnel flow field. A closer look reveals that the round-edge mean and standard-deviation profile 5 are closer to the real world than in the sharp-edge case. In conclusion, it can be said that both model terrain variations do not reproduce the real-world flow-field directly. Moreover the real-world flow seems to fall in between the two situations. In the following the investigation of the recirculation zone behind the escarpment is in focus. The round-edge case does only show a very small recirculation zone in the mean flow field, therefore only the sharp-edge case will be considered in the following.

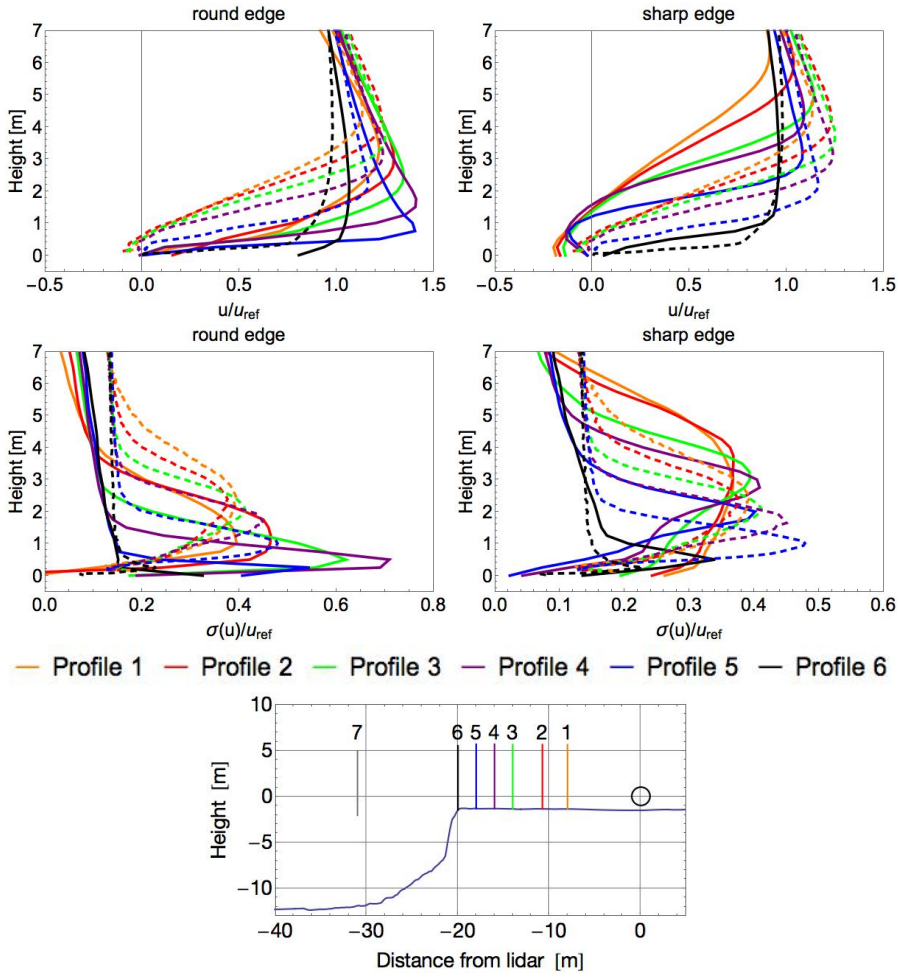

Figure 4.4: *Top:* Normalized mean wind speed and *Bottom:* Normalized standard deviation of seven 7-m tall vertical profiles downstream of the Bolund escarpment. Profiles from Lange et al. (chapter 2) (real world) are presented as the dashed lines, the wind tunnel round-edge and sharp-edge case are presented in solid lines.

4.3 Wake Dimensions and Direction Dependence

In the following the recirculation zone in the vicinity of the Bolund model escarpment is investigated. To characterize the recirculation zone of the wind tunnel flow, two parameters are investigated. The first one is the wake height, where the methods from Lange et al., chapter 2 are applied. The second parameter is the reattachment length, a dimension which is often used to characterize the flow over a forward-facing step (FFS).

4.3.1 Wake Height

The wake height is the height of the recirculation zone, that develops downstream of the Bolund escarpment. To determine the wake height, Method 1 and 2 from Lange et al., chapter 2 are applied on the average flow field shown in Figure 4.1.

1. The first approach determines the displacement thickness, δ_1, that is defined as the distance that the boundary layer is displaced to compensate for the reduction in flow rate on account of the wake formation, where $u(z)$ is the line-of-sight wind speed at height z, z_{top} is the top of the profile, and u_0 is the free stream velocity (Hinze 1975, pp. 593-597)

$$\delta_1 = \int_0^{z_{top}} \left(1 - \frac{u(z)}{u_0}\right) dz. \tag{4.1}$$

2. The second approach identifies the height of the maximum gradient of the line-of-sight wind speed, δ_2, of each vertical scan (Emeis et al. 2008, Sect. 2.2.2)

$$\delta_2 = \arg\max_z \left[\frac{du(z)}{dz}\right]. \tag{4.2}$$

As in the example of Lange at al., the wake height is determined from the flow fields for an inflow direction of 270° (run 18), as well as for deviated inflow directions of ±10° (runs 19 and 20). The results of both methods are combined with the real-world values presented in Lange et al. for each wind direction in Figure 4.5. It is clearly seen that the wake height in the wind tunnel flow field is higher than the real scale values, but it is also seen that the wake height grows with distance to the escarpment and that the wake height is changing with a wind direction deviating from 270°. Additionally, a higher wake height is observed, if the inflow direction is 260°, which is in agreement with Lange et al.. This unequal growth of the wake, depending on whether the wind-direction change is clock-wise or counter clock-wise, is also seen in the real world measurements.

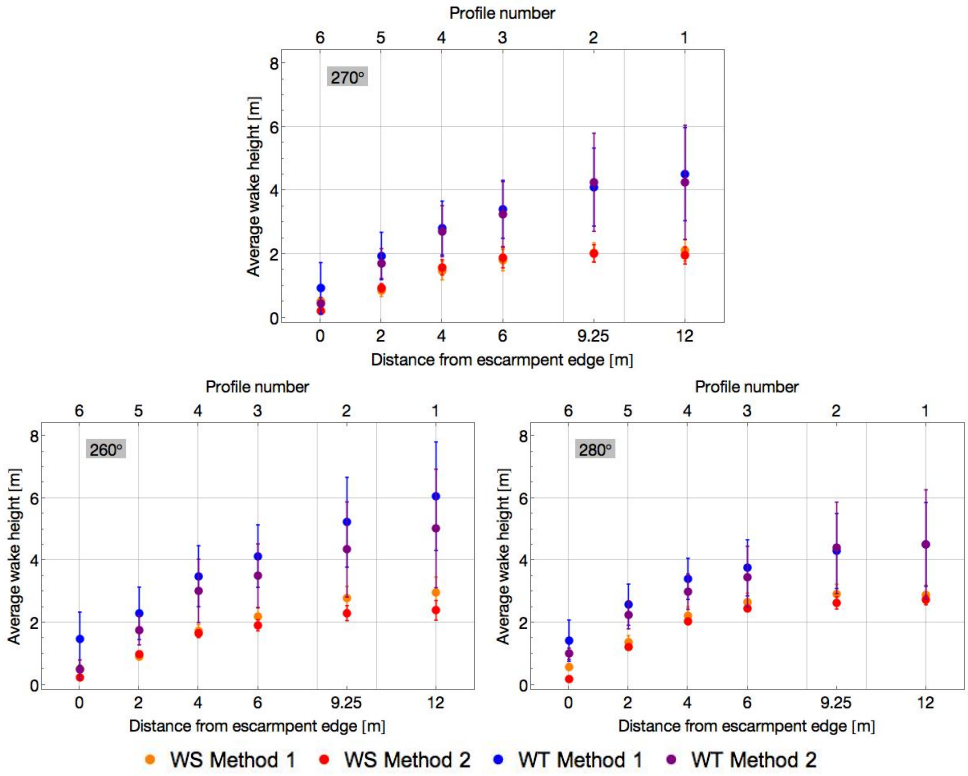

Figure 4.5: The mean wake height for three inflow wind directions 270°, 260°, 280° determined with two different methods and from the wind-tunnel flow-field (WT) and from the WindScanner measurement campaign (WS). The dots present the mean wake height and the error bars display the standard deviation.

4.4 Reattachment Length

The reattachment length is defined by Sherry et al. 2010 as the distance from the FFS edge to the position where the mean-flow streamline that divides forward and adverse surface flow. In purely two-dimensional flow the dividing streamline emanates from the edge of the escarpment. Calling the height of the step h, Sherry et al. 2010 determine a reattachment length of 2.9h and a reattachment height of 0.36h observing the flow over a 15mm FFS. The study of Largeau and Moriniere 2006 finds an average reattachment length of the flow over 3 different FFS (heights of 30 mm, 40 mm and 50 mm) of 4.5-5 h at 15 m/s and of 3.5-4 h at 40 m/s. It should be emphasized that those results are determined over a two-dimensional FFS, however Bolund is a three-dimensional model. Therefore the recirculation zone is influenced by a more complex

flow and and winds in and out of the measurement plane. Nevertheless in Figure 4.6 the identified recirculation bubble is presented for inflow angle of 260° (clock-wise), 270° and 280° (counter clock-wise). It is clearly observed that the length and height of the recirculation zone is inflow angle dependent. The reattachment length ranges from 2.2h at 280° over 3h at 270°, which is in close agreement with Sherry et al. 2010, up to 3.2h at 260°. A comparable study is presented by Rowcroft et al. 2015. They experiment with a FFS of h=0.05 m and a Reynolds number of 1×10^5 with regard to a varying yaw angle between 0°, 20°, 30° and 40°. They also find a varying reattachment length with deviating inflow angle. Moreover they observe a steadily increasing reattachment length with increasing yaw angle, starting with 2.8h at 0° up to 3.8 h at 40° showing a similar trend as 260° case, but contrary to the 280° case.

In order to show that the presented results are not an artifact of this specific set-up, the same analysis is shown for the run 11 (without the terrain modification) and run 15 (with modification, see Table 3.1) in appendix A. These runs have all fan rows running at 50% of full power. Also the roughness elements in section 3 immediately in front of the model are down. For the investigation of the inflow direction dependency run 16 (clock-wise) and run 17 (counter clock-wise) are used.

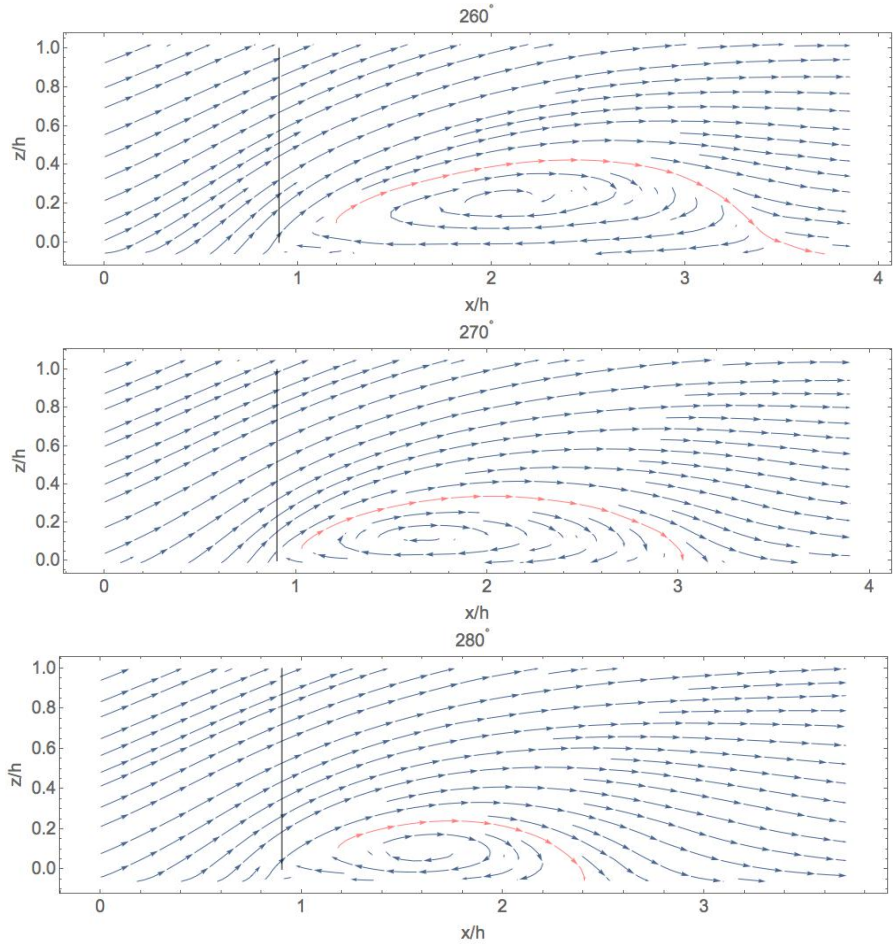

Figure 4.6: Mean flow fields for three different inflow angles (from top to bottom: 260°, 270° and 280°). The reattachment line is presented by the red line and the position of the edge is indicated by a black, vertical line.

CHAPTER 5

Conclusion

Within this study the flow behavior over a complex terrain was investigated with the help of different approaches.

High frequency atmospheric measurements with the WindScanner revealed the relationship between the wake height and the wind direction for the case of the Bolund peninsula. The wake increases in height with distance from the west-facing escarpment and shows highly turbulent structures. The highly resolved measurements allow for a precise determination of the wake height, which was calculated using three different methods. All three methods show a surprisingly sharp increase of the wake height with deviation of the wind direction from 270°. As the wind direction deviates from west by ±15°, the height grows between 10% and 70% depending on the distance from the edge with the strongest effect farthest from the edge. The experiment does not only introduce a new remote-sensing based wind profile measurement technique to provide unique data sets for validation of unsteady flow modeling over complex terrain for wind energy purposes. It also highlights that the usage of numerical models for onshore wind turbine siting needs to be carried out for different inflow wind directions. In order to achieve a more comprehensive picture of the recirculation zone by measuring all three wind components, the usage of three WindScanners would be necessary.

A large-scale wind laboratory investigation of the flow field over a large-scale model of the Bolund peninsula shows that the mean wind, wind shear and turbulence level are extremely sensitive to the exact details of the terrain. A modification of the escarpment of the Bolund model, to give a sharper edge, has dramatic consequences for a scaled, hypothetical wind turbine positioned close to the edge. The AEP for this situation is 20% to 51% of the round-edge case, while the turbulence level is increased by a factor of five. Our findings imply that detailed full-scale measurements are very important and that physical modeling can be an important tool for investigating terrain resolution effects and impacts of changing inflow profiles.

Demonstrated is that just a small change in the terrain, of approximately 2% of height, produces quantitative changes in the mean wind and turbulence levels and qualitative differences in wind profiles (Figure 4.3). In comparison, the most recent state-of-the-art studies with large eddy simulation used spatial resolutions of 0.31 m (close to the escarpment (Conan et al. 2016)) and 1 m (over the whole domain (Diebold et al. 2013)). In Diebold et al. 2013 the flow around Bolund was simulated at two different spatial resolutions. With a coarser 2-m resolution, the mean wind

error (the relative difference between simulated wind and real measured wind) was approximately twice as high as the value for the 1-m resolution simulation. These findings suggest that a further increase in the resolution, i.e. from 1 m downwards, could potentially bring the numerical simulations closer to real values, and thus, to a fairer representation of reality. Despite the higher resolution used by Conan et al. 2016, the values obtained for speed-up were overestimated close to the ground and close to the escarpment. This is comparable to the round-edge flow-field configuration. The flow field visible in the sharp-edge configuration has not yet been observed in numerical simulations of Bolund.

In order to refer back to the WindScanner experiment the wind-tunnel flow-field is measured for three different inflow directions of 260°, 270° and 280°. Additionally the wake height is calculated with two different methods using the example of chapter 2. The results reveal a similar behavior of a growing wake height with distance to the escarpment and an asymmetric dependence on whether the inflow angle is positive or negative. An additional approach to investigate the recirculation zone downstream of the escarpment is the comparison with the flow over a FFS. Here the reattachment length is observed at the three different wind directions and compared with values from the literature. Even though Bolund does not resemble an ideal two dimensional FFS the values of the reattachment length are comparable with the results from Largeau and Moriniere 2006 and Rowcroft et al. 2015. This investigation reveals also a change in recirculation zone size with changing inflow angle.

The WindEEE Dome experiment lead additionally to the investigation of the relative contributions of key upstream parameters to the flow behavior over the Bolund peninsula. Here the results are presented in the form of normalized speed-up and TKE increment. The mean flow behavior is observed to be marginal influenced by changes in the upstream conditions, but the turbulent flow field shows a significant TKE increase of over 200% at a height of 2 m above the model, when the shape of the inflow profile was changed from uniform to sheared. Through the ability of the WindEEE Dome facility to change the inflow shear profile, TKE increments could be produced that were closer to full-scale measurements than those that had been achieved previously in conventional wind tunnels, indicating a promising opportunity for future work in characterizing flow over topography.

These results indicate that more attention should be given to wind-turbine siting in complex terrain. It is important to consider different inflow wind direction when modeling wind-park layouts. The verification of the wind-tunnel flow fields reveals that the real-world flow lies between the round and the sharp-edge realization, which indicates clearly that only real-world measurements can give the best indication of mean and turbulent wind fields. Nevertheless wind-tunnel modeling can be a less cost intensive approach, as long as the used topography is described as detailed as possible.

A subsequent and interesting research problem, based on the findings from this thesis, would be the numerical modeling of the flow over the Bolund peninsula with different spacial resolutions and modified topographical details, e.g. round and sharp escarpment edges. As well as the numerical simulation of the flow over Bolund with

regard to different inflow wind directions. This could lead to a complex comparison study of the flow field from real world, wind tunnel and numerical simulations.

APPENDIX A

Here run 11 (without terrain modification) and run 15 (with modification, see Table 3.1) were compared. These two runs have all fan rows running at 50% of full power. Also the roughness elements in section 3 immediately in front of the model are down.

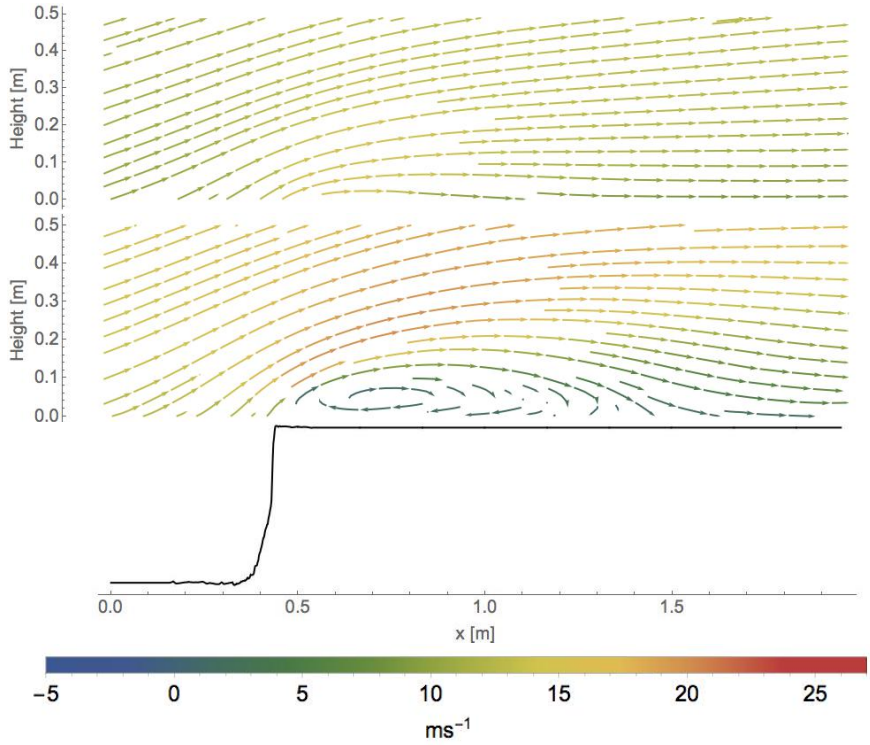

Figure A.1: The mean flow field of the smooth (*top*) and sharp-edge (*bottom*) case. The mean is calculated using 1600 statistically independent image pairs. The Bolund contour line indicates the edge position.

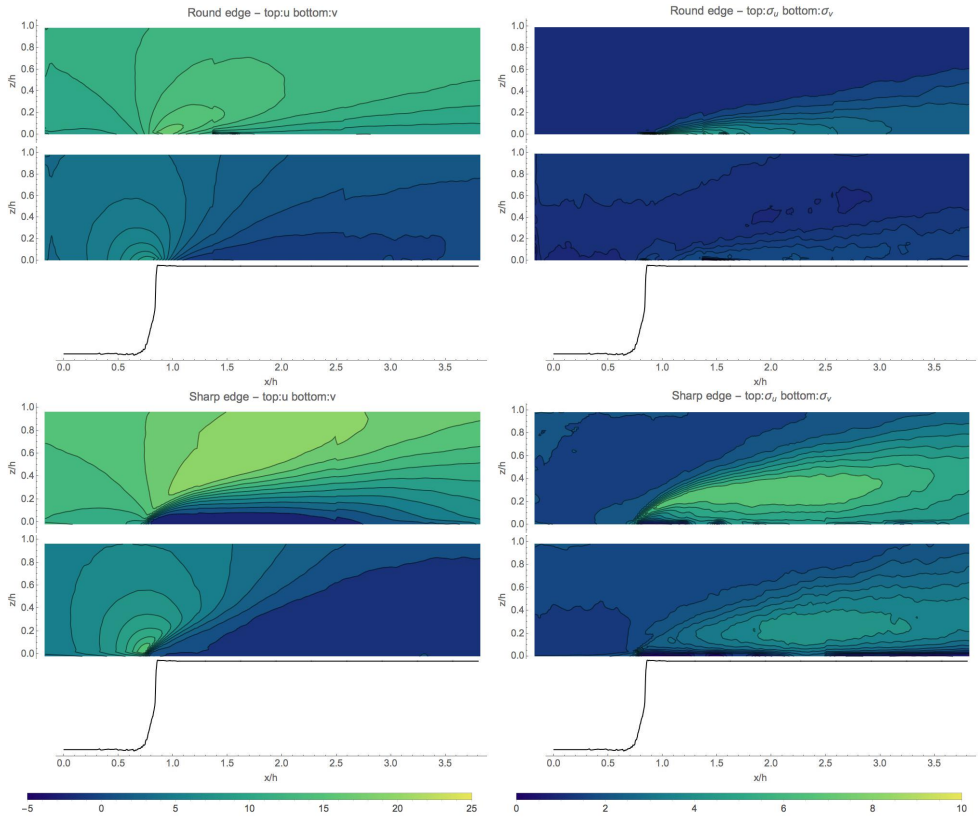

Figure A.2: *Left:* The mean u and v component and the *Right:* Standard deviation of the u and v component of the flow field of the round and sharp-edge case. The fields are calculated using 1600 image pairs. The Bolund contour line indicates the edge position.

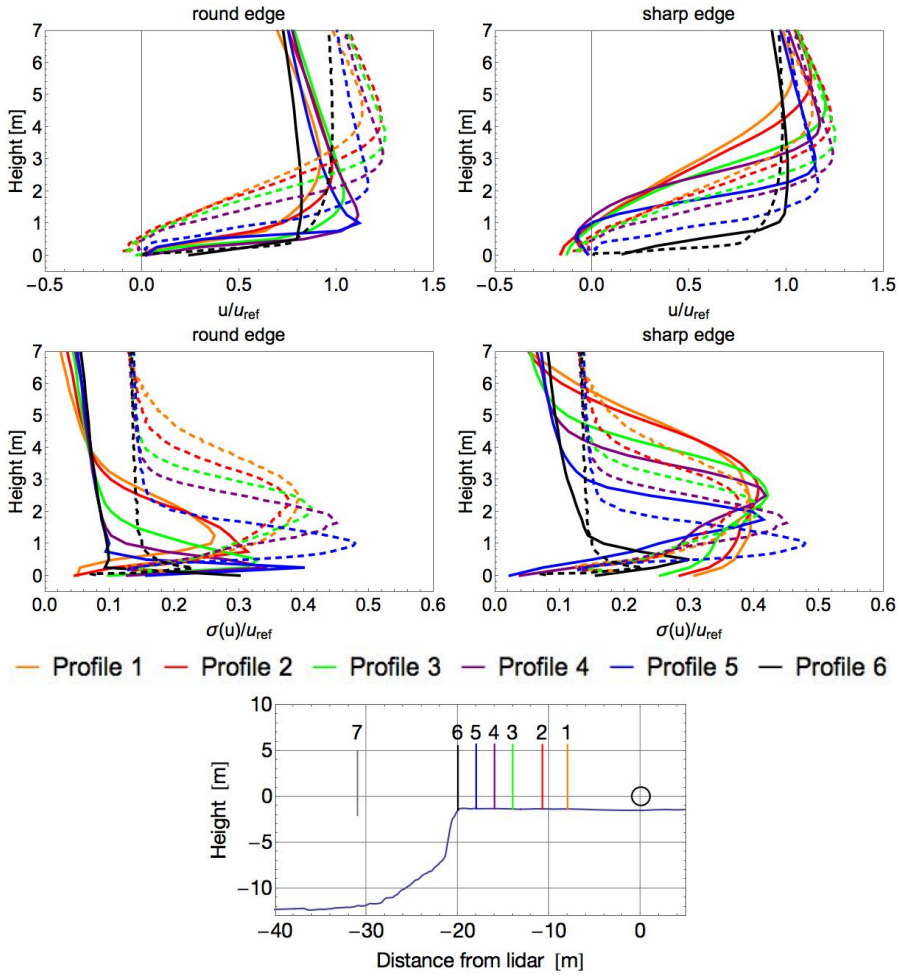

Figure A.3: *Top:* Normalized mean wind speed and *Bottom:* Normalized standard deviation of seven 7-m tall vertical profiles downstream of the Bolund escarpment. Profiles from Lange et al. (chapter 2) (real world) are presented as the dashed lines, the wind tunnel round-edge and sharp-edge case are presented in solid lines.

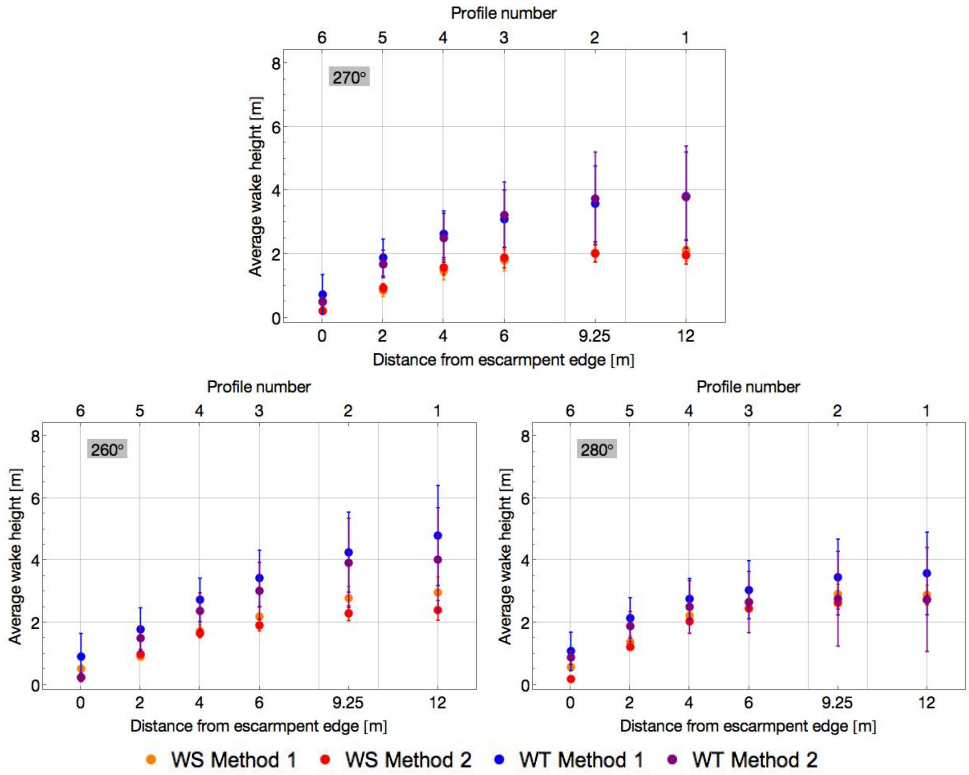

Figure A.4: The wake height for three inflow wind directions 270°, 260°, 280° determined with two different methods and from the wind-tunnel flow-field (WT) and from the WindScanner measurement campaign (WS). The dots present the mean wake height and the error bars display the standard deviation.

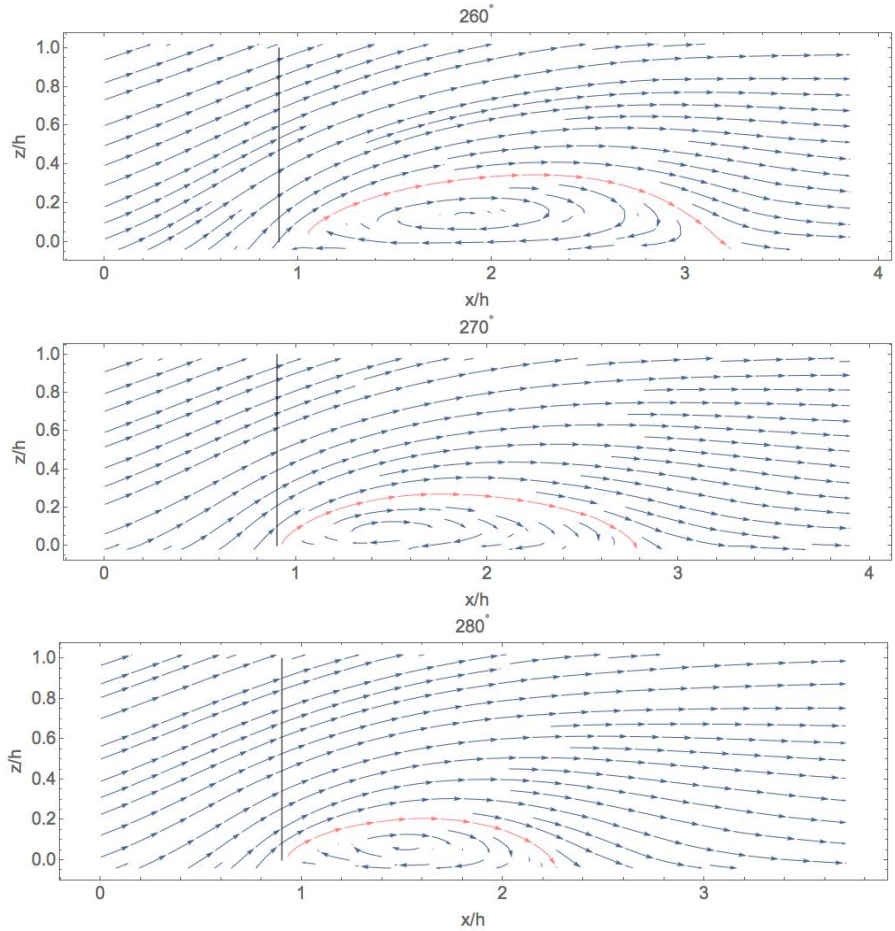

Figure A.5: Mean flow fields for three different inflow angles (from top to bottom: 260°, 270° and 280°) . The reattachment line is presented by the red line and the position of the edge is indicated by a black, vertical line.

APPENDIX B

Submitted to *Nature Energy*

For wind turbines in complex terrain, the devil is in the detail

Julia Lange[1], Jakob Mann[1], Jacob Berg[1], Dan Parvu[2], Ryan Kilpatrick[2], Adrian Costache[2], Jubayer Chowdhury[2], Kamran Siddiqui[2] & Horia Hangan[2]

[1] *DTU Wind Energy, Technical University of Denmark, Denmark*

[2] *WindEEE Research Institute, Western University, London, Ontario, Canada*

The cost of energy produced by onshore wind turbines is among the lowest forms of electricity generation; however, onshore wind turbines are often positioned in a complex terrain where the wind resources and wind conditions are quite uncertain, because of the surrounding topography or vegetation. In this study, we use a scale model in a three-dimensional wind-testing chamber to show how minor changes in the terrain can result in significant differences in the flow at turbine height. These differences affect not only the power performance but also the life-time and maintenance costs of wind turbines, and hence, the economy and feasibility of wind turbine projects.

According to the International Renewable Energy Agency (IRENA), onshore wind energy is currently one of the cheapest forms of electricity generation available[1], and the forecast for 2020 by the U.S. Energy Information Administration shows that wind energy will remain cheaper than most conventional power sources such as coal, gas, and all significant types of renewable energy, including hydro and solar photovoltaic[2]. By the end of 2014, 361 GW of onshore wind energy had been installed worldwide, constituting 20% of all renewable energy sources[3]. However, the

cost range of wind power generation ($\approx 0.03 - 0.16$ USD/kWh) is higher than that of fossil fuel ($\approx 0.04 - 0.14$ USD/kWh), and the local wind climate is a large contributor to this variation[1]. Many onshore wind turbines exploit the strong speed-up of the wind over steep ridges or escarpments. The flow in such situations is quite complex and associated with high levels of turbulence, making reliable energy and load predictions difficult. Uncertainty in the estimation of the wind energy potential and the level of wind shear and turbulence has obvious implications for the financial feasibility of wind energy projects: this uncertainty must be reduced to lower electricity costs.

Although full-scale experiments of wind flow around hills and escarpments have been performed with great success[4–6], experiments in controlled environments such as numerical simulations and wind tunnels provide the opportunity to study problems systematically in greater detail. One such problem addressed in this paper is the change in the wind pattern cause by very small changes in the terrain. Small geometric changes are known to affect wind energy production, for example, insects squashed on wind turbine blades can almost halve the power output[7]. In other fields such as sports aerodynamics[8] and bluff-body aerodynamics[9], tiny changes in the boundary conditions create very large modifications in the flow field, such as enlarged recirculation zones.

The sensitivity of the flow field to the terrain description has direct consequences for numerical modelling, which is the preferred tool in siting applications, and hence, the siting of wind turbines. Although the description of the terrain is often of a high resolution and quality because of modern laser-scanning techniques, the spatial resolution of numerical flow models is limited because of the limits on computational performance. More importantly, the terrain is often smoothed

to make it easier for the numerical solver to obtain a fully converged flow solution. This last point is not very well documented in the literature, and our results show that the problem may be more severe than initially anticipated. An undocumented method consists of smoothing the terrain by setting an upper bound for the terrain curvature in each point of the domain. Another method consists of averaging neighbouring points. In both methods, details of the terrain are incorrectly incorporated into the numerical models; therefore, as we show here, the actual complex flow pattern may not be observable in the model.

At present, many numerical tools are used to estimate local wind resources. One type is the Ellypsis3D flow solver[10], which is part of the commercial software tool WAsP[11]. The tool incorporates an automated grid-convergence algorithm, which estimates the difference in the mean wind speed between different resolutions[12]. When the difference between grids with yet higher resolution is below a critical value, it is often stated that grid convergence has been achieved. However, an implicit assumption, which is rarely mentioned, is that an asymptotic state has been reached. In this paper, we speculate that such a state may not actually exist in a complex terrain, unless the details of the terrain are fully accounted for.

Wind tunnels have been used to characterize flow around different terrain features for several decades, well before the advent of numerical models. A pioneering and complex study of the Askervein hill in the Outer Hebrides of Scotland investigated the role of surface roughness, model scale and measurement technique at three different model scales (1/800, 1/1200 and 1/2500[13] relative to full scale) and served as the basis of many subsequent wind tunnel studies. All these

studies investigated relevant issues regarding the wind-tunnel modelling of wind flows, i.e. horizontal length scale, scale ratio of roughness height, boundary-layer thickness[14] and influence of terrain, directionality, channelling and topographic features[15] over different complex terrains, but the model scales e.g. 1/6000[15], 1/2000[16], 1/5357 and 1/500[17] remained relatively small. Although these coarse models allow the study of even large domains, it is questionable how well the local scales at wind turbine rotor height are actually resolved. This last point is a crucial factor in our study.

In this paper, we present the results of an unique and first-in-class wind tunnel experiment at the Wind Engineering, Energy and Environment (WindEEE) Dome at the Western University, Canada: the world's first three-dimensional wind testing chamber[18]. We investigate the flow over a 1/25 scale model of the Bolund peninsula, Denmark. We find that the mean wind, wind shear (the increase in the mean wind speed with height) and turbulence level (the standard deviation of the wind fluctuations divided by the mean wind speed) are extremely sensitive to the exact details of the terrain. A modification of the edge of the Bolund peninsula model, which generates a sharper and more realistic model, results in a reduction of the estimated annual energy production (AEP) by at least 50% and an increase in the turbulence level by a factor of five.

The Bolund peninsula The Bolund peninsula in the Roskilde Fjord, Denmark is a well-known reference case for numerical and physical modelling[17,19–22]. Despite the fact that the Bolund peninsula is only 12 m high in reality, its isolated location and the absence of significant Coriolis and thermal effects provide the potential for up-scaling. In situations with neutral atmospheric strati-

fication and mean wind speeds larger than 8-10 m/s, i.e. above the cut-in wind speed of modern wind turbines, Bolund can be up-scaled by 10-30 times. The area thus resembles a full-scale table mountain such as those found in the US Midwest with wind turbines positioned close to the edges[6].

The WindEEE Dome This wind testing chamber is hexagonal, with a diameter of 25 m and return circuit of the same shape with a larger diameter of 45 m[18]. Using 106 individually controlled fans, a wide variety of wind systems such as tornadoes, down-bursts, gusts and currents, shear winds and boundary layers at large scales and Reynolds numbers can be modelled. In the multi-fan mode, the 4 rows $\times$ 15 columns = 60 fans on the north wall can be used to generate various flows such as boundary layer flows, horizontally sheared flows, vertically sheared flows and actively turbulent flows. Using a contraction zone with an inflow-outflow area ratio of 3:1 in front of this 60-fan wall, a channelled, accelerated, turbulent boundary-layer flow was created for this study.

Experimental set-up We constructed a 1/25 scale model of the often-studied Bolund peninsula[6,17,20–23] using a hot-wire and a CNC machine. A Styrofoam model with dimensions of 0.48 m height, 3 m width and 4 m length was placed with the head of the escarpment in the middle of the turntable (Figure 2), approximately 12.5 m from the wall. Because of the processing of the topographic information, the model appears rounded in comparison with the actual, full-scale terrain (see Lange et al.[20] page 2; Figure 1). We therefore modified the edge by extending the horizontal top of the escarpment by 20 mm with modelling clay to make the edge sharper, almost a right angle (Figure 1). The maximum thickness of the clay is 15 mm.

To perform high-resolution Particle Image Velocimetry (PIV) over such a large model, it was necessary to combine three cameras with overlapping views (Figure 2). For this experiment, we used a configuration allowing a field of view with an area of approx. 2 m x 0.5 m, one of the largest fields of view covered using PIV to date.

The Reynolds number based on the model height h is defined as $Re = \bar{U}h/\nu$, where $\nu = 1.478 \times 10^{-5}$ m^{2}s^{-1} is the kinematic viscosity of air at 20°C. The value of Reynolds number in this study is approximately 5×10^5, which is the largest documented in the literature for boundary-layer studies of the terrain to date. In addition, a dual-cavity Nd:YAG laser (532 nm, 425 mJ/pulse at 9 Hz) was used to illuminate the scene; using special optics, the laser beam was aimed at the experimental model and spread into a vertical sheet (Figure 2). An Ultratec CLF-4460 commercial fog generator was used to seed the test chamber with non-toxic, water-based smoke. The PIV results, mean velocity field and standard deviation were calculated based on 1600 image pairs.

Results and consequences for energy production and loads The flow fields with and without the edge modification are significantly different (Figure 3). With the modified, sharp edge, a large recirculation zone is located behind the escarpment, which affects the mean wind, shear and turbulence. The recirculation zone as well as the reattachment length, both of which are created by the sharp edge, resembles the flow over a forward-facing step[24].

To put the findings into a wind energy perspective, we calculated the energy production of

a wind turbine positioned close to the escarpment with and without the edge modification. We chose a Vestas V90 2MW Gridstreamer[11] and assumed that the mean wind speed $\overline{U}$ at hub height in the inflow was between 5 and 10 m/s and that the distribution was a Weibull distribution with a shape parameter $k = 2$. Quite unrealistically, but to emphasise the differences in the flows with a sharp and a rounded edge, we assumed that the wind direction distribution was 100% towards the escarpment. We used a model scale of 1/500. With an assumed wind turbine hub height of 90 m, which is equal to the rotor diameter, the model scale hub height is 0.18 m. The turbine is positioned three rotor diameters downstream of the escarpment, equivalent to 1.13 escarpment heights. We calculated the power output of the turbine using the power curve of V90 and a procedure integrating the different winds over the rotor [25], which involved the area-weighted average of the kinetic energy flux over the rotor. Both wind profiles were normalised with the wind speed at a hub height of the round edge case, which assures that the external forcing was identical and resulted in the same wind speed distribution for the modified sharp-edge case.

The results show that depending on the average wind speed at hub height for the round edge, the flow with the sharp edge gives an AEP that is only 20% to 51% of the round-edge case. Such a reduction would be devastating for the economy of a wind turbine project.

In addition to very different AEP values, the modification of the edge has dramatic consequences for the dynamic loads on the wind turbine. For assessment of the flow quality at a potential wind turbine site, the International Electrotechnical Commission (IEC)[26] recommends that the turbulence intensity $I_u = \sigma_u/\overline{U}$, where σ_u is the standard deviation of horizontal wind, at

the site should be less than 18%. In addition, the shear exponent $\alpha = (z/\overline{U})(d\overline{U}/dz)$, where z is the height above the surface, should be less than 0.2 at hub height. For the case with the round edge, both parameters are within the limits of the IEC standard. However, in the sharp-edge case, the shear is far beyond the limit, which would cause strong fluctuating loads on the rotating wind turbine blades moving in and out of high and low wind speed air flow (Table 1). Furthermore, the turbulence is significantly larger and close to a level where wind turbines will cease to operate.

Implications for numerical models used in wind turbine siting applications We demonstrate that just a small change in the terrain, of approximately 2% of height, produces quantitative changes in the mean wind and turbulence levels and qualitative differences in wind profiles (Figure 4). In comparison, the most recent state-of-the-art studies with large eddy simulation used spatial resolutions of 0.31 m (close to the escarpment[23]) and 1 m (over the whole domain[22]). In Diebold et al.[22] the flow around Bolund was simulated at two different spatial resolutions. With a coarser 2-m resolution, the mean wind error (the relative difference between simulated wind and real measured wind) was approximately twice as high as the value for the 1-m resolution simulation. Our findings in this paper suggest that a further increase in the resolution, i.e. from 1 m downwards, will bring the numerical simulations closer to real values, and thus, to a fair representation of reality. Despite the higher resolution used by Conan et al.[23], the values obtained for speed-up were too high close to the ground and close to the escarpment. This is comparable to the round-edge flow field configuration. The flow field visible in the sharp-edge configuration has not yet been observed in numerical simulations of Bolund.

Conclusion A large-scale wind laboratory investigation of the flow field over a large-scale model of the Bolund peninsula shows that the mean wind, wind shear and turbulence level are extremely sensitive to the exact details of the terrain. A modification of the escarpment of the Bolund model to give a sharper edge has dramatic consequences for a wind turbine positioned close to the edge. AEP for this situation is only 20% to 51% of the round-edge case, while the turbulence level is increased by a factor of five.

Our findings imply that detailed full-scale measurements are very important and that physical modelling can be an important tool for quantifying terrain effects. Furthermore, even if accurate terrain descriptions are available, it is unclear whether any flow model can predict the observed wind field to correctly estimate its impact on turbine energy production and mechanical loads and be able to forecast the financial feasibility of a project.

Methods

WindEEE Dome[27] configuration and experimental set-up The inflow was produced by the 60-fan wall, where rows 1, 2 and 4 were running at 50% and row 3 at 75% of full power. Spires and roughness elements acted as turbulence generators. Roughness elements were raised in and around the contraction zone by 7.5 cm; in the sector in front of the experiment model, no roughness elements were used. The upstream profiles were measured with TFI Cobra Probes and show that the turbulence intensity at 5 m to 13 m of 12% - 13% matches the results in Berg et al.[6] An array of 3 IO Industries Flare 12M125 high-speed CMOS cameras (12 megapixels) was placed 3.55 m away from the laser sheet with the lens axis perpendicular to the light sheet (Figure 2). The

cameras were equipped with Nikkor 50 mm f/1.8D lenses.

Fabrication of the model The topographic information used for the manufacturing of the model is available at `http://www.bolund.vindenergi.dtu.dk/Blind_Comparison`. The gridded 0.25-m resolution map is based on both ground-based and airborne laser terrain mapping. The triangulation of the laser scan data and the subsequent interpolation to the grid were estimated to remove 0.25 to 0.35 m of the edge, roughly corresponding to the added clay in the experiment. We used two machines in the fabrication of the model, a hot-wire (officially named FrogWire) for basic 2D cutting and a CNC router (officially named FrogMill) for detailed cutting using a 3/4 inch ball nose end mill. Both machines were supplied by Streamline Automation (http://www.3dcutting.com/). The model was cut from large blocks of expanded polystyrene and painted black with latex paint. The software used to translate the model geometry into machine code for FrogMill is named ArtCAM. This software was used to scale, position and slice the model into various pieces and generate the G-code instructions for FrogMill.

Processing of PIV data The image pairs were acquired with CoreView[28]. Prior to the PIV processing, the images were filtered because horizontal or vertical stripes were appearing occasionally, possibly caused by electromagnetic noise. The image intensity $I(x, y)$, where x and y are pixel positions, was Fourier transformed into $\hat{I}(k_x, k_y)$ where k_x and k_y are wave numbers in the two image plane directions. Then, $\hat{I}$ was set to zero for $k_x = 0$ or $k_y = 0$ and thereupon inversely Fourier transformed to get stripe-free images. The image pairs were processed in the following step with DynamicStudio 4.0[29]. Images were analysed with 32 x 32 windows using a 50% overlap. Typical vector removal rates were from 2% to 4%.

Calculation of AEP The height of Bolund is 12 m, whereas the height of a typical wind-farm escarpment would be 20 times larger. To assess the potential impact of the edge modification, we therefore scaled up the flow measured in WindEEE by a factor of $25 \times 20 = 500$. The position of the turbine (three rotor diameters from the edge) is commonly observed in real wind farm projects. We assumed that the Reynolds number was sufficiently high such that the flows in WindEEE at Bolund and at the hypothetical site 20 times larger than Bolund were all similar. The two terrain cases were run with identical forcing emulating two different landscapes with the same geostrophic forcing of the flow. The mean wind speed at hub height for the sharp edge is only 50.4% of the speed for the round edge. The cube root of the area-averaged third power over the rotor was calculated: the sharp edge was 62.7% of the round-edge flow. That value was combined with the power curve of the Vestas V90 2MW Gridstreamer obtained from the wind resource calculation program WAsP[11] to obtain AEP. The shear exponent was obtained from the mean wind profile by evaluating $(z/U)dU/dz$ at $z = z_{\mathrm{hub}}$. Inflow tilt angles were approximately 4° for both flow cases, which is far below the critical 10° limit given by IEC[26].

1. IRENA. Renewable power generation costs in 2014. Tech. Rep., International Renewable Energy Agency (2015). URL http://www.irena.org/documentdownloads/publications/irena_re_power_costs_2014_report.pdf.

2. EIA. Annual energy outlook 2015 with projection to 2040. Tech. Rep. DOE/EIA-0383(2015), U.S.Energy Information Administration (2015). URL http://www.eia.gov/forecasts/aeo/pdf/0383(2015).pdf.

3. IRENA. Renewable energy capacity statistics 2015. Tech. Rep., International Renewable Energy Agency (2015). URL http://www.irena.org/DocumentDownloads/Publications/IRENA_RE_Capacity_Statistics_2015.pdf.

4. Taylor, P. & Teunissen, H. The Askervein Hill project: Overview and background data. *Boundary-Layer Meteorol.* **39**, 15–39 (1987).

5. Taylor, P. A., Mason, P. J. & Bradley, E. F. Boundary-layer flow over low hills. *Boundary-Layer Meteorol.* **39**, 107 (1987).

6. Berg, J., Mann, J., Bechmann, A., Courtney, M. & Jørgensen, H. The Bolund Experiment, Part I: Flow Over a Steep, Three-Dimensional Hill. *Boundary-Layer Meteorol.* **141**, 219–243 (2011).

7. Corten, G. P. & Veldkamp, H. F. Aerodynamics: Insects can halve wind-turbine power. *Nature.* **412**, 41–42 (2001).

8. Norman, A. K., Kerrigan, E. C. & McKeon, B. J. The effect of small-amplitude time-dependent changes to the surface morphology of a sphere. *J Fluid Mech.* **675**, 268–296 (2011).

9. Choi, H., Jeon, W.-P. & Kim, J. Control of Flow Over a Bluff Body. *Annu Rev Fluid Mech.* **40**, 113–139 (2008).

10. Bechmann, A. & Sørensen, N. N. Hybrid RANS/LES method for wind flow over complex terrain. *Wind Energy.* **13**, 36–50 (2010).

11. www.wasp.dk .

12. Sørensen, N. N. *et al. How fine is fine enough when doing CFD terrain simulations* (European Wind Energy Association (EWEA), 2012).

13. Teunissen, H. W., Shokr, M. E., Bowen, A. J., Wood, C. J. & Green, D. W. R. The Askervein Hill Project: Wind-tunnel simulations at three length scales. *Boundary-Layer Meteorol.* **40**, 1–29 (1987).

14. Bowen, A. Modelling of strong wind flows over complex terrain at small geometric scales. *J Wind Eng Ind Aerodyn.* **91**, 1859–1871 (2003).

15. Chock, G. & Cochran, L. Modeling of topographic wind speed effects in Hawaii. *J Wind Eng Ind Aerodyn.* **93**, 623–638 (2005).

16. Shiau, B. S. & Tsai, B. J. Wind tunnel measurement of flow and dispersion of power plant emission on the coastal region with complex terrain. In *EACWE 5*, July (2009).

17. Conan, B. *Wind Resource Assessment in Complex Terrain by Wind Tunnel Modelling*. Ph.D. thesis, Karman Institute / Orléans University (2012).

18. Hangan, H. The Wind Engineering Energy and Environment (WindEEE) Dome at Western University, Canada. *Japan Association for Wind Engineering.* **39**, 350–351 (2014).

19. Bechmann, A., Sørensen, N. N., Berg, J., Mann, J. & Rethore, P.-E. The Bolund Experiment, Part II: Blind Comparison of Microscale Flow Models. *Boundary-Layer Meteorol.* **141**, 245 (2011).

20. Lange, J. *et al.* Variations of the Wake Height over the Bolund Escarpment Measured by a Scanning Lidar. *Boundary-Layer Meteorol.* **158** (2015). Doi: 10.1007/s10546-015-0107-8.

21. Yeow, T., Cuerva-Tejero, A. & Perez-Alvarez, J. Reproducing the Bolund experiment in wind tunnel. *Wind Energy.* **18**, 153–169 (2013).

22. Diebold, M., Higgins, C., Fang, J., Bechmann, A. & Parlange, M. Flow over Hills: A Large-Eddy Simulation of the Bolund Case. *Boundary-Layer Meteorol.* **148**, 177–194 (2013).

23. Conan, B. *et al.* Experimental and Numerical Modelling of Flow over Complex Terrain: The Bolund Hill. *Boundary-Layer Meteorol.* (2015). Doi: 10.1007/s10546-015-0082-0.

24. Largeau, J. F. & Moriniere, V. Wall pressure fluctuations and topology in separated flows over a forward-facing step. *Exp Fluids.* **42**, 21–40 (2006).

25. Wagner, R., Courtney, M., Gottschall, J. & Lindelöw-Marsden, P. Accounting for the speed shear in wind turbine power performance measurement. *Wind Energy.* **14**, 993–1004 (2011).

26. IEC. *IEC 61400-1. Wind turbines – design requirements*. International Electrotechnical Commission, 3 edn. (2005).

27. www.windeee.ca .

28. IO Industries Inc., London Ontario, Canada. CoreView.

29. Dantec Dynamics, Skovlunde, Denmark. Dynamic Studio 4.0.

Acknowledgements This work is supported by the Center for Computational Wind Turbine Aerodynamics and Atmospheric Turbulence funded by the Danish Council for Strategic Research, grant number 09-067216 and by the Canada Foundation for Innovation and Ontario Research Fund "Wind Engineering Energy and Environment (WindEEE) Dome" grant. The stay of Julia Lange at the Western University was funded by the Otto Mønsted Foundation, the Oticon Foundation and the Idella Foundation.

Competing Interests The authors declare that they have no competing financial interests.

Correspondence and requests for materials should be addressed to Julia Lange. (email: jull@dtu.dk).

Table 1: *Left:* Calculated AEP as a function of mean wind speed for flow with a sharp versus a round escarpment edge. *Right:* Shear exponent α and turbulence intensity I_u at hub height for the two cases.

$\overline{U}$	AEP [MWh/yr]		Ratio [$\%$]
[m/s]	Round	Sharp	Sharp/Round
5	3072	622	20
6	4804	1257	26
7	6510	2100	32
8	8048	3097	38
9	9353	4176	45
10	10396	5272	51

	Round	Sharp
α	0.17	2.15
I_u [%]	14	72

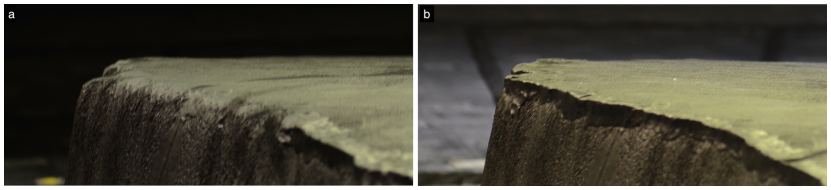

Figure 1: **The two different topographies of the Bolund model edge.** The round model edge (**a**) and the model modified with modelling clay to give a sharp edge (**b**).

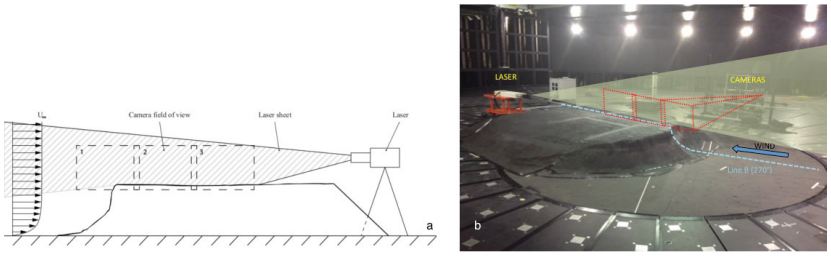

Figure 2: **Experimental set-up for the WindEEE dome experiment.** Schematic of the PIV multi-camera set-up (**a**) and an overall image of the experiment (**b**).

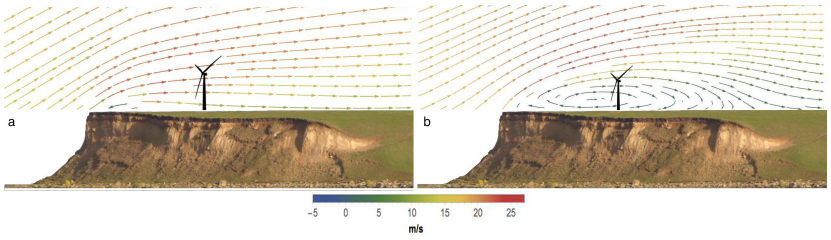

Figure 3: **The mean flow field over the two different Bolund model topographies.** Smooth flow over the round edge (**a**). The mean flow field over the modified sharp edge shows a recirculation zone behind the escarpment (**b**).

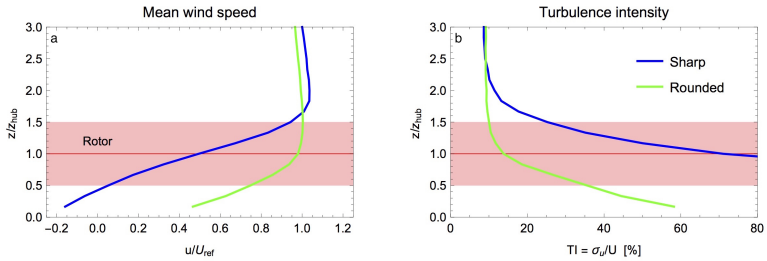

Figure 4: **Profiles of normalised mean wind speed and turbulence intensity.** Profiles are illustrated with sharp and round edges at a position 1.13 times the escarpment height downstream of the edge. The horizontal line indicates the hub height of a hypothetical wind turbine; the shaded area denotes the height swept by the rotor.

APPENDIX C

Submitted to *Wind Energy Science*

Investigation of the effect of Reynolds number and inflow parameters on mean and turbulent flow over complex topography

R. Kilpatrick[1,3], H. Hangan[1,2], K. Siddiqui[1,3], D. Parvu[1,2], J. Lange[4], J. Mann[4], and J. Berg[4]
[1]WindEEE Research Institute, University of Western Ontario, London, Ontario, N6M 0E2, Canada
[2]Department of Civil and Environmental Engineering, University of Western Ontario, London, Ontario, N6A 5B9, Canada
[3]Department of Mechanical and Materials Engineering, University of Western Ontario, London, Ontario, N6A 5B9, Canada
[4]DTU Wind Energy, Technical University of Denmark, Frederiksborgvej 399, DK-4000 Roskilde, Denmark

Correspondence to: R. Kilpatrick (rkilpatr@uwo.ca)

Abstract. A characterization of mean and turbulent flow behaviour over complex topography was conducted using a large-scale (1:25) model of Bolund Hill in the WindEEE Dome at Western University. The specific topographic feature considered was an escarpment. A total of eight unique inflow conditions were tested in order to isolate the impact of key parameters such as Reynolds number, inflow shear profile and upstream effective roughness, on flow behaviour over the escarpment.

The results show that the mean flow behaviour was generally not affected by the Reynolds number, however a slight increase in speed-up over the escarpment was observed for cases with lower upstream roughness. The shape of the inflow wind shear profile also had a minor impact on the mean flow near the escarpment. More significant effects were observed in the turbulent flow behaviour, where the turbulent kinetic energy (TKE) over the escarpment was found be a strong function of upstream roughness and a weak function of the Reynolds number. The local change in the upstream wind shear was found to have the most significant influence on the TKE magnitude, which more closely approximated the full-scale TKE data, and had not been previously observed in wind tunnel modelling of this topography.

1 Introduction

Wind turbines over the last few decades have emerged as a reliable and cost-competitive means of producing clean, renewable electricity. Although typically built on relatively flat terrain such as plains and farmland, wind farms are increasingly being placed in more rugged, or complex, terrain, marked by abrupt changes in elevation (Palma et al., 2008).

These sites often have strong wind resources, yet designing wind farms for these regions involves additional challenges due to the changes imposed by the terrain on the three-dimensional structure of the wind, such as speed-up regions, changes to the wind shear profile, large vertical wind velocities, and modification of turbulence characteristics (Walmsley and Taylor, 1996; Botta et al., 1998). As a result, the essential prediction of on-site wind conditions, often estimated from measurements at a limited number of mast locations, also becomes more challenging. The use of linearized models, the current industry standard for wind resource assessment and turbine micro-siting, proven to be very effective in gently sloping terrain, can produce inaccurate results when applied at sites with very complex terrain (Palma et al., 2008; Berg et al., 2011).

The use of more advanced modelling techniques such as Reynolds Averaged Navier Stokes (RANS), and Large Eddy Simulation (LES), have generally proven to be more accurate in complex topographic terrain (e.g. Rasouli and Hangan, 2013) compared to field measurements, and are making inroads with industry, although they come with the trade-off of higher computational cost (Ayotte, 2008; Ayotte et al., 2010). These advanced models generally require a higher degree of user input and experience and thus results can be significantly affected by changes to boundary conditions, turbulence closure models and other parameters, as shown for example in the wide spread of CFD results in the Bolund blind comparison exercise (Bechmann et al., 2011).

Thus, a better understanding of the wind regime in complex terrain, from a fundamental fluid dynamics perspective, is critical, given the opportunities for improved overall wind turbine performance including higher annual electricity production and reduced fatigue loading and associated maintenance costs (Peinke et al., 2004; Berg et al., 2011). This improved understanding of the flow behaviour can be used by modellers to select appropriate boundary conditions and turbulence models with greater confidence. One area that is not fully understood, and forms the subject of this study, is the sensitivity of the mean and turbulent response of the flow over complex topography to changes in the inflow conditions.

1.1 Wind tunnel modelling of flow over topography

In order to improve computational models, the model results need to be validated against actual flow conditions. Full-scale testing is ideal for this purpose, however due to the lack of control of inflow conditions, significant testing cost, time and effort required, wind tunnel modelling has served as a valuable tool for development and validation of both numerical and analytical models (Ayotte and Hughes, 2004). Provided that certain conditions are met, measurements taken of the flow across a scale model can provide very useful and repeatable representations of full scale conditions as well as benchmarking for the validation of numerical and analytical models. The controlled environment of the wind tunnel provides a means of isolating the effects of various parameters on the mean and turbulent flow behaviour, which is usually not possible in the field.

There are several examples of wind-tunnel experiments conducted on flow over scale models of real topography for the purpose of wind resource assessment and wind turbine siting. These include isolated hill cases such as Askervein Hill (Taylor and Teunissen, 1987), Kettles Hill (Salmon et al., 1988), and more recently Bolund Hill (Berg et al., 2011), as well as highly topographically complex regions with multiple hills and valleys (Chock and Cochran, 2005; Rasouli et al., 2009; McAuliffe and Larose, 2012).

1.2 Bolund experiment

The Bolund experiment arose from the need for additional model validation of flow in a complex terrain, extending the Askervein Hill Project of the early 1980s by offering steeper terrain and thus a greater challenge for numerical models to resolve. Bolund Hill is a peninsula located near Roskilde, Denmark, and is characterized by a long upstream open fjord fetch, a steep escarpment and a long flat section on top of the island. The Bolund topography is geometrically similar to a

typical wind turbine site in complex terrain, albeit at smaller scale, and is well-suited as a test site given its well-defined, undisturbed inflow conditions, neutral atmospheric stratification and relative absence of thermal and Coriolis effects (Berg et al., 2011). Although Bolund is a small hill, approximately 12 m high by 75 m wide and 130 m long, similarity laws allow for upscaling of 10 – 30 times under neutral atmospheric stratification.

Studies of the wind flow over Bolund Hill include the original field campaign (Berg et al., 2011); follow-up Lidar measurements of the escarpment wake (Lange et al., 2016); computational and physical modelling of the hill as a part of the blind comparison test (Bechmann et al., 2011); wind tunnel modelling (Yeow et al., 2015); LES modelling (Diebold et al., 2013); and wind-tunnel and LES modelling (Conan et al., 2016). During the field campaign, measurements were taken via 35 anemometers on 10 masts, positioned along two main incoming flow directions referred to as, Line A (239°) and Line B (270°). These were the benchmark measurements against which the results of subsequent modelling efforts have been compared. A detailed diagram of the Bolund topography, with mast positions and flow directions, appears in Berg et al. (2011).

1.3 Present study: Characterization of mean and turbulent flow over Bolund across a range of input conditions

The present study is focused on the characterization of the flow over Bolund Hill, along Line B, in the vicinity of the escarpment, using two physical scale models (1:100 and 1:25), at Reynolds numbers (based on model hill height and wind speed at hill height) ranging from 4×10^4 to 5×10^5. The main objectives of this study were to isolate and analyse the dependence of the mean and turbulent flow behaviour over the escarpment on various parameters including Reynolds number, inflow wind shear profile, and upstream roughness. The 1:25 scale experiments were conducted at the Wind Engineering, Energy, and Environment Research Institute (WindEEE), while the 1:100 scale experiments were conducted at the Boundary Layer Wind Tunnel Laboratory (BLWTL). Both facilities are located at Western University. The two sets of results were then compared with the full-scale measurements, and with results from previous studies on Bolund Hill. Particle Image Velocimetry (PIV) and Cobra Probes were used for flow velocity measurements at key locations on the scaled models.

2 Experimental Setup

2.1 WindEEE experimental setup

2.1.1 WindEEE facility

The WindEEE dome is a unique wind research facility designed to simulate a wide variety of wind flow patterns including rotational (axisymmetric) and boundary-layer flows at larger laboratory scales. A general description of the facility is provided in Hangan (2014). The hexagonal test chamber (25 m diagonal length), is enclosed in a return air chamber of 40 m diagonal length. The WindEEE test chamber contains 106 fa**Word did not find any entries for your table of contents.**ns,

whose wind speed and direction can be varied independently to produce the desired flow conditions. The facility can be operated in two distinct modes: multi-fan wind tunnel or axisymmetric mode. The present experiment was conducted exclusively under the former configuration, with only the fans along one wall of the hexagon mounted in an array format i.e. four rows of 15 fans each, for a total of 60 fans. Each of these fans are 0.8 m in diameter and operate at approximately 25 m/s at nominal power of 30 kW. Each fan is equipped with variable speed drive and can be individually controlled to create a customized flow pattern. A contraction section was positioned immediately downstream of the 60-fan wall to improve flow uniformity and increase flow speed across the 5 metre diameter test section (turntable) in the centre of the chamber. A trip and a series of spires were employed upstream to enhance turbulence intensity.

In addition to individual fan control, the WindEEE facility also provides the ability to set roughness element position and height, allowing physical simulation of a wide range of incoming Atmospheric Boundary Layer (ABL) flow profiles. There are over 1500 roughness elements in the test chamber, each with maximum height of 30 cm. The present experiment employed only the roughness element sections in the vicinity of the contraction, upstream of the turntable. Two different roughness element configurations, both with uniform element height of roughly 7.5 cm, were used for the WindEEE experiment, hereinafter referred to as RC1 and RC2. For RC1, all of the roughness elements upstream of the turntable were raised, whereas for RC2, one block of about 80 elements immediately upstream of the turntable was lowered to the floor, resulting in a lower effective roughness value than that for RC1.

2.1.2 Bolund scale model

The 1:25 scale model of Bolund Hill was produced by CNC milling of several large blocks of Expanded Polystyrene (EPS) according to topographical data of the island. These blocks were then glued together and painted black with latex paint. The overall size of the model was roughly 4.5 m across, 0.5 m high, and 3.5 m long. A solid ramp with slope of roughly 45° was constructed from EPS and fastened to the downstream edge of the model to provide a smooth transition and reduce unwanted flow separation. The model was positioned in the chamber such that the escarpment edge was roughly 12.4 m from the 60-fan wall, and the plane of measurement (Line B) was parallel to the flow direction. A photograph of the experimental setup is presented in Figure 1a. The $X = 0$ position in the longitudinal direction is indicated by the centre-point of the model, C_p, also the intersection of Line A and Line B, as per the full-scale co-ordinate system, shown in Figure 1a.

2.1.3 PIV measurement

Particle Image Velocimetry (PIV) was used to measure the two-dimensional velocity field in a vertical plane above the model, along line B, in the vicinity of the escarpment. The measurement region encompassed a rectangular area extending roughly from $Z = 11.4$ m to 25 m and $X = -70$ m to $X = -20$ m in the full-scale Bolund co-ordinates, where the value $Z = 0$ corresponds to sea level. Throughout this work uppercase Z denotes absolute height above sea level while lowercase z denotes height relative to the hill surface. Three 12 megapixel cameras (IO Industries Flare 12M125-CL), each with 105 mm f/2D Nikon AF DC-NIKKOR lenses, were used to capture images. The cameras were positioned in a row parallel to the flow

direction, facing the model at a distance of roughly 3.55 metres from the camera lens to the measurement plane, at a height such that the bottom of the camera frame of view was just below the hill surface. Camera resolution was 4096 x 3072 pixels, and the corresponding measurement field of view for each camera in the current setup was about 0.78 m wide by 0.58 m high. The horizontal positions of the cameras were set in a way to form overlap among the adjacent fields of view to ensure spatial continuity of flow measurements. The overlap between cameras 1 and 2 was 0.167 m, and between cameras 2 and 3 was 0.088 m, with camera 1 being the most upstream. Thus the combined measurement area was roughly 2.09 m wide by 0.58 m high.

A Litron Nano Piv Series dual cavity Nd:YAG laser with the energy of 425 mJ/pulse operating at the wavelength of 532 nm was used to illuminate the flow field. The laser was positioned directly behind the model, pointing upstream, coincident with Line B, with the laser head roughly 0.60 m off the ground, as shown in Figure 1. A 50° cylindrical lens was positioned immediately in front of the laser head to convert the beam into a two-dimensional sheet. The laser was synchronized to the cameras and the frame grabber. In this study, the pulse repetition rate for each laser cavity was set at 9 Hz resulting in the image acquisition rate of 18 frames per second by each camera or 9 Hz for each image pair. The images were acquired via Coreview software (IO Industries) as 8-bit grayscale images in the TIFF format. PIV data were recorded for 5 minutes per test case, providing roughly 2700 image pairs. An Ultratec CLF-4460 commercial fog generator, positioned in the dome's upper plenum, was used to seed the test chamber with non-toxic, water-based smoke that served as the tracer.

2.1.4 Cobra Probe measurement

Cobra Probes, manufactured by Turbulent Flow Instrumentation Pty Ltd., are dynamic multi-hole pressure probes for measuring all three components of mean and fluctuating velocities and static pressure. In the present experiment, Cobra Probe measurements were taken at an upstream reference location, as well as a few positions along the hill. A vertical array of eight Cobra Probes was used, with spacing between probes ranging from roughly 5 cm near the bottom of the array to 15 cm near the top. The total vertical measurement distance was about 60 cm, or 15 m in full-scale. The upstream reference position was located 4.44 m upstream of C_p in the model scale, or X = -111 m in the full-scale. Although initially intended for the Cobra probe position to coincide with the full-scale upstream reference mast M0, located at X = -180.8 m, this was not possible in the current setup due to the proximity of the model to the contraction opening. However, the current location was deemed to be sufficient as a reference location given that it was far enough from the fan wall to assume fully mixed flow and far enough from the model to avoid significant slow-down effects. Along the hill, Cobra Probe measurements were taken at the escarpment edge (X = -54.7 m), at M6 (X = -46.1 m) and at M3 (X = 3.2 m), where values in parenthesis are full-scale co-ordinates. Due to time constraints, Cobra Probe measurements at these positions were not taken for each of the PIV test case configurations. The probe array was mounted either on a stationary floor rack, or fixed to the overhead rail system, and moved to various positions along line B. All Cobra Probe measurements were conducted at acquisition rate of 10,000 Hz, output to file rate of 1250 Hz, and sampling time of 120 seconds.

2.2 BLWTL experimental setup

The model used for the BLWTL experiments was a 1:100 scale model of Bolund Hill, using the same topographical data as the WindEEE model. The BLWTL model was similarly cut from EPS, in two sections, and fastened together. The model was then fixed to the turntable at the centre of the test section and rotated such that the principal flow direction coincided with Line B (270° wind direction). Figure 1b shows a photograph of the experimental setup with wind direction and mast positions indicated. BLWTL Tunnel 1 is an open circuit type with a length of 33 m and has the cross-section of 2.4 m (width) × 2.15 m (height) at the test section. In the present setup, three triangular spires, as well as a bar trip were positioned at the far upstream end of the tunnel, however no active roughness elements were used, in order to simulate upstream conditions with ABL profile over a smooth surface. The measurements were conducted at a wind speed of 4.6 m/s that corresponds to a Reynolds number of approximately 3.6×10^4, based on the maximum height of the hill (0.117 m in model-scale) as the characteristic length scale.

Cobra Probe measurements were conducted along vertical profiles at model-scale positions equivalent to the full-scale co-ordinates of M0, M7, M6, M3 and M8, as well as at the escarpment (X = -54.7 m in full-scale). The vertical velocity profile was obtained by using two Cobra Probes mounted to the wind tunnel traverse system and the vertical position was incremented after each sample, by 12.7 mm in model-scale, or 1.27 m in full-scale, near the floor, and 50–100 mm (5–10 m full-scale) higher up. The vertical extent of the measurements was about 1.2 m from the floor (equivalent to 120 m in full-scale). PIV measurements were conducted as well, but are not presented here due to a number of issues with data quality.

3 Data processing

3.1 PIV data processing

PIV instantaneous velocity fields were obtained by cross-correlating the interrogation regions in the first image of the image pair with the corresponding search regions in the second image. An in-house algorithm implemented in image processing software Heurisko® developed by AEON Verlag & Studio GmbH & Co. KG was used for the PIV data processing. The search window and interrogation window sizes were set as 128 and 64 pixels, respectively, while grid size was 16 pixels. Spurious vectors were identified and corrected using a local median test developed by Siddiqui et al. (2001). Subsequently, mean fields were calculated by averaging the respective velocity component (streamwise, u, and vertical, w, in the present case) at each grid point over the sampling time. The turbulent velocity fields were computed by subtracting the mean velocity from the instantaneous velocity at each grid point in a given velocity field. These two steps were performed using an in-house code in MATLAB.

PIV statistics were calculated in a manner analogous to Yeow et al. (2015) to enable direct comparison. Mean flow speed, S, was calculated using the two mean wind components U and W from the PIV measurement plane (see Figure 1) as per:

$$S = (U^2 + W^2)^{1/2} \quad (1)$$

Results shown throughout this work are often expressed as a normalized speed-up ratio $S(x,z)/S_0(z)$, where $S_0(z)$ is the upstream reference speed at the same height. Since the upstream reference measurements were taken with Cobra Probes at a limited number of heights, extrapolation to all of PIV grid heights was performed using the logarithmic law (Manwell et al., 2009):

$$U(z)/U(z_r) = \ln\left(\frac{z}{z_0}\right) / \ln\left(\frac{z_r}{z_0}\right) \quad (2)$$

where z_r is the reference height. Mean turbulent kinetic energy (TKE), $\bar{k}$ was calculated according to:

$$\bar{k} = \left(\overline{u'^2} + \overline{w'^2}\right)/2 \quad (3)$$

where lowercase u' and w' represent the fluctuating velocity vectors. The change in TKE, or TKE increment $\Delta\bar{k}$ was obtained by subtracting the upstream reference TKE $\bar{k}_{05}$ at a fixed height of Z = 5 m in full-scale (0.2 m in model-scale) from the measured TKE at each PIV grid position and normalizing by the square of the upstream reference speed, again consistent with Yeow et al. (2015) as per:

$$\Delta\bar{k} = \left[k(x,z) - \bar{k}_{05}\right]/{S_0}^2(z) \quad (4)$$

Despite efforts to properly align the three cameras, some minor discrepancies were observed in the velocity data recorded by each camera. For mean wind speeds, error between camera frames typically ranged from about 2–4%, with slightly more error in the highly turbulent region close to the escarpment and just above the model surface. To improve the clarity of presentation, a frame stitching algorithm using was implemented to smooth the data within the overlap region between camera frames. At each point in the overlapping region, a weighted average of the data at the two overlapping nodes was taken, such that data points closer to one camera or another were weighted more heavily towards that camera's values. The weightings varied linearly from 0.5 for each camera at the centre of the overlap region (equal weighting), to 1 and 0 on one side, and 0 and 1 on the other.

3.2 Cobra Probe data processing

Cobra Probe output data is generated by the companion TFI Device Control software, and consists of a time history of *u*, *v* and *w* wind speed components, as well as a summary output of the mean wind speeds, Reynolds stresses and pressures. Generally only the mean data from the summary files were used, with spot checks performed against the time history data to ensure consistency. The Cobra Probe results presented in this work generally use two-component calculations, where the spanwise wind speed component *v* is neglected, as per Eq. 1 and Eq. 3, which allows for direct comparison with the PIV results, which is analogous to the approach adopted by Yeow et al. (2015) for hot-wire measurements. However, when comparing the WindEEE and BLWTL inflow profiles, measured with Cobra Probes, against the full-scale data from upstream mast M0, all three wind velocity components from the Cobra Probe data were used.

4 Inflow profiles

4.1 WindEEE inflow profiles

4.1.1 Fan configuration

For the present set of experiments, the 60 fans were operated using four different configurations, which were selected in attempt to match the full-scale incoming wind profile, as well as to produce a range of Reynolds numbers (see Table 1):

a) All fans running at 20% of the maximum fan RPM
b) All fans running at 30% of the maximum fan RPM
c) All fans running at 50% of the maximum fan RPM
d) Fans in row 1, 2, and 4 running at 50%, fans in row 3 at 75%, of the maximum fan RPM. For reference, fan row 1 is at floor level

The notation for each test case was set based on the upstream wind speed and the upstream surface roughness. That is, each of the four fan configurations are identified by the mean streamwise incoming wind speed at the model escarpment height in m/s (i.e. U5, U8, U14, U15) and the two upstream roughness configurations as RC1 and RC2, where, RC1 corresponds to the higher upstream roughness. For example, case U5RC1 correspond to the test case conducted at the inflow condition of 5 m/s wind flowing over higher roughness. These combinations yielded eight unique flow configurations representing the WindEEE PIV test cases described throughout this work, as listed in Table 1.

4.1.2 Calculation of Reynolds number, friction velocity and surface roughness

The inflow parameters for the WindEEE experiment in Table 1 were determined from the upstream reference Cobra Probe data. Reynolds number was calculated according to:

$$Re = \frac{U_h h}{\nu} \tag{5}$$

where the characteristic length h is the hill height, U_h is the inflow streamwise velocity at h, and ν is the kinematic viscosity of air at 20°C i.e. 1.50×10^{-5} m/s^2. The Reynolds numbers in Table 1 use the model hill height h = 0.468 m. For the test cases with the same fan configuration but different roughness configuration, Reynolds number was almost identical.

For the present study, which focuses mainly on how upstream conditions affect flow behaviour over the escarpment, the means by which the upstream parameters are calculated are important, as there is often some variability depending on the method of calculation. For example, friction velocity u_* can be determined using several different methods, which often show considerable differences between them (Weber 1999). To compare the variability of the resulting normalized upstream profiles for the WindEEE experiment, the friction velocity was calculated using four different methods. For method 1, friction velocity was calculated according to Eq. 6, as per Weber (1999) using only the longitudinal component of the Reynolds stress vector, which is the same method used by Berg et al. (2011) to calculate friction velocity using data from the upstream reference mast M0 in the Bolund field campaign.

$$u_* = (-\overline{uw})^{1/2} \quad (6)$$

Method 2 adds the spanwise Reynolds stress component (Ly 1993, Weber 1999), and always produces a higher value of u_* than Method 1. It is similar to the method used in Bechmann et al. (2011) and is given by:

$$u_* = [(\overline{u'w'})^2 + (\overline{v'w'})^2]^{1/4} \quad (7)$$

For Methods 1 and 2, a single reference value u_{*05} was taken as the friction velocity at a reference height of Z = 5 m in full-scale (0.2 m in model-scale), consistent with the approach used by Bechmann et al. (2011) and Yeow et al. (2015). For method 3, upstream effective roughness z_0 and friction velocity u_*were determined by fitting the streamwise velocity profile data within the logarithmic region to the standard logarithmic wind profile for neutral stability conditions (Manwell et al., 2009):

$$U(z) = \frac{u_*}{\kappa} \ln\left(\frac{z}{z_0}\right) \quad (8)$$

where z is the vertical height from the ground, $U(z)$ is the streamwise wind speed at that height, and the von Karman constant κ was considered to be 0.41. Method 4 may be considered a combination of Methods 1 and 3, and follows the approach of Akomah et al. (2011), who describe a region of constant shear stress corresponding to the equilibrium sub-layer where TKE production and dissipation balance. The values of friction velocity computed using each of the four methods are presented in Table 1. The difference between the highest and lowest estimate was relatively high, ranging from about 15% to 50% depending on the test case. Friction velocity is still calculated using Eq. 6, however unlike in Method 1 where a single data point was used, Method 3 uses the mean of the values within the constant shear stress region, which were identified from the plots of height vs. $|\overline{u'w'}|$ as the first three data points closest to the floor for each test run. The z_0 values were obtained using Method 3, and are presented in full-scale units in Table 1. The values show a clear distinction between the RC1 cases ($z_0 \sim 10^{-3}$ m) and RC2 cases ($z_0 \sim 10^{-6}$ m). The full-scale roughness measured at mast M0 was $z_0 = 3\times10^{-4}$ (Berg et al., 2011), so the U15RC1 case shows the closest match.

4.1.3 Comparison between inflow profiles

Cobra Probe measurements of upstream reference mean flow speed S_0 and TKE $\overline{k_0}$, normalized by the u_* values estimated using method 1, are shown in Figure 2a, along with the full-scale measurements at M0 (Berg et al., 2011). A clear separation is observed between the profiles with higher roughness (RC1) and those with lower roughness (RC2), with the RC2 group having higher normalized mean wind speed as well as TKE. Comparison of the upstream mean speeds for the test cases with the full-scale data shows that all model-scale values are lower than the full-scale wind speeds, with the exception of U5RC2, whereas the normalized TKE profiles are all higher than the full-scale profiles, illustrating the inherent difficulty in matching both the mean wind speed and TKE profiles with the full-scale values. The shape of the TKE profiles is in contrast to the wind-tunnel experiment conducted by Yeow et al. (2015) whose normalized TKE inflow profiles were lower than the full-scale values, and decreased with height. Most of the WindEEE normalized TKE profiles are relatively vertical between z = 5

m and z = 12 m which is consistent with the full-scale data, although having only two full-scale data points available from the reference mast M0 in the field campaign, none of which were above a height of 12 m (i.e. just above escarpment height), is a limiting factor in determining whether a good match to the full-scale conditions has been achieved.

The results for Method 2 (not shown) are similar to Method 1, with all profiles shifted slightly to the left, given the slightly higher values of u_*. There is also less separation between the RC1 and RC2 groups. Inflow profiles determined using Method 3 are somewhat different, with the RC1 profiles showing a better match to the full-scale data for mean speed, although still higher for TKE, but significantly higher values for the RC2 group, for both mean speed and TKE, due to the higher values of u_*. Profiles using Method 4 are quite similar to those of Method 1, with profiles collapsing slightly more within the RC1 and RC2 groups.

4.2 BLWTL inflow profiles

Table 2 shows the main test parameters for the BLWTL Cobra Probe measurements. Friction velocity was calculated as per the four methods outlined above, and z_0 was estimated using Method 3. Figure 2b shows inflow profiles from the BLWTL Cobra Probe data, measured at the upstream reference location of X = -1.82 m in model scale (X = -182 m in full-scale). Mean speed and TKE were normalized by friction velocity calculated using the four methods identified above. The results show that the profiles for Methods 1–3 are quite close to each other, and higher than the full-scale data points, while Method 4, with higher u_*, produced profiles shifted slightly to the left, and matched particularly well with the full-scale data. The reduction in normalized TKE with height was consistent with the inflow profiles measured by Yeow et al. (2015), but different from the WindEEE and full scale TKE profiles, which were relatively constant with height over the measurement region.

5 Results and Discussion

The results are divided into two main sections: analysis of the mean flow behaviour, and analysis of the turbulent flow behaviour. Most of the results presented were obtained from the WindEEE PIV data, while some additional data is presented from the WindEEE Cobra Probe profiles, as well as the BLWTL Cobra Probe measurements as necessary.

5.1 Mean flow behaviour

The streamlines of the mean flow field are shown in Figure 3 for upstream velocities of U5, U8, U14 and U15 at higher roughness configuration (RC1). Mean streamlines for the RC2 cases (not shown) were nearly identical. None of the streamlines for the mean flow showed any clear evidence of recirculation. Even upon close inspection of the mean flow field in the vicinity of the escarpment, it is difficult to ascertain whether the negative values of streamwise velocity observed in the separated flow region are indicative of recirculation or due to other factors such as near-wall effects. The small region between -55.25 m < X < -55 m and 11.75 m < Z < 12 m appears to show some vectors of low magnitude pointing

horizontally in the reverse streamwise direction, however the higher uncertainty in this region, due to very high velocity gradients, prohibits drawing a firm conclusion.

Contour plots of speed-up ratio for U14RC1 (Figure 4a) and U15RC1 (Figure 4b) clearly illustrate the speed-up region near the escarpment, and the re-establishment of the boundary layer on top of the hill. The U5 and U8 contour plots (not shown) were very similar to the U14 case, analogous to the similarity observed in the streamline plots between the three cases. While speed-up is generally similar between the U14RC1 and U15RC1 cases, slightly higher values are observed for U15RC1 in the vicinity of the escarpment, and this case also shows a more elongated, oblong shape of the speed-up region at the escarpment edge. Reynolds number for the two flows did not differ by a great amount (4.57×10^5 for U14RC1 vs. 5.21×10^5 for U15RC1), i.e. much less than the difference in Reynolds number between the U5RC1 and U14RC1 cases, indicating that the difference in normalized mean flow behaviour can be most likely attributed to the higher upstream shear for the U15 case.

5.2 Mean flow comparison to previous experiments

In addition to the full-scale measurements, results from previous physical modelling of the Bolund Hill, are available in the literature for comparison to the present results. These include wind tunnel and water channel experiments from the blind comparison (Bechmann et al., 2011), wind tunnel PIV and 3-component hotwire (3CHW) tests conducted by Yeow et al. (2015) at 1:115 scale at two Reynolds numbers (4.15×10^4 and 8.21×10^4), and wind-tunnel PIV modelling conducted by Conan et al. (2016) at 1:500 scale and $Re = 2.1\times10^4$. Benchmarking the WindEEE Cobra Probe and PIV, and BLWTL Cobra Probe results from the present experiment against these datasets provides some validation of the present experimental procedure, and also serves as an initial point of discussion on the differences between conducting the same experiment at three scales, i.e. wind tunnel ($Re \sim10^4$), WindEEE ($Re \sim10^5$) and full-scale ($4.25\times10^6 < Re < 1.02\times10^7$).

Figure 5 shows horizontal profiles of the wind speed-up at two locations corresponding to the full-scale mast measurement positions at heights of z = 2 m (Figure 5a) and z = 5 m (Figure 5b) above hill surface level. Results from the WindEEE PIV data and those of previous experiments mentioned above are presented for comparison. The topography and the mast locations are shown in Figure 5c for reference. Figure 6 shows the comparison for vertical profiles at three horizontal locations along the hill. The U14RC1 and U15RC1 cases were selected from the eight WindEEE PIV cases as representative cases to avoid clutter; the differences between all of the WindEEE cases are discussed further below. From the horizontal profiles, agreement is generally quite good between all datasets at z = 5m, whereas significant variability is observed at z = 2 m, which is within the highly turbulent shear layer observed in the TKE contour plots (see Figure 10), referred to also by Yeow et al. (2015) and observed in the scanning Lidar data (Lange et al., 2016). Similarly for the vertical profiles, better agreement is observed at position M7 upstream of the escarpment (Figure 6a), with greater variability seen at the other two positions (Figure 6b, c), with higher variability at z < 5 m.

5.3 Influence of Reynolds number, upstream roughness, inflow profile and model resolution on mean flow

The WindEEE experiments were conducted by changing one variable at a time, allowing for the influence of a particular modifier to the flow to be isolated and the resultant flow behaviour analysed. In this section, the isolated effects of Reynolds number, upstream roughness, shape of the inflow profile, and scale model & measurement resolution, on the mean flow behaviour are discussed.

5.3.1 Reynolds number and upstream wind profile effects on the mean flow

The horizontal profiles of the wind speed-up for four Reynolds numbers at full-scale heights of z = 5 m and z = 2 m above the island surface level are shown at two upstream roughness cases; higher roughness RC1 in Figure 7a and lower roughness RC2, in Figure 7b. Full-scale data are also plotted for reference. The results show almost identical trends of the normalized mean flow for three uniform fan speed cases (U5, U8 and U14), for both RC1 and RC2. This indicates an absence of Reynolds number effect on the mean flow over a Reynolds number range of 1.7×10^5 to 4.6×10^5. The U15 case, however, with modified inflow shear profile, displays different behaviour than the uniform fan speed cases. The U15RC1 peak speed-up is higher at the escarpment compared to the other RC1 cases, then changes to become relatively lower further downstream. For the U15RC2 case, speed-up is generally equal or slightly lower than the other RC2 cases at z = 5 m (Figure 7c), and lower along horizontal locations at z = 2 m (Figure 7d).

In Figure 8, a similar comparison is made along the vertical profiles at M6. Results show a trend similar to that observed for the horizontal profiles, i.e. little difference among the mean flow profiles at three uniform fan speed cases, with the RC2 profiles collapsing more closely. Again the U15RC1 case (Figure 8a) shows different behaviour, with higher speed-up than the other cases, and also shows a better match to the full-scale data points. For RC2 (Figure 8b), the U15 case generally collapses with the others, with the only difference being the relatively lower speed-up for $z < 4$ m which is again closer to the full scale behaviour.

5.3.2 Upstream roughness effects on the mean flow

The comparison of speed-up profiles at the same Reynolds number but different roughness configuration provides an insight into the effect of upstream surface roughness, z_0, on the mean flow behaviour over the escarpment. Such analysis can be obtained by comparing the profiles in Figure 7 and Figure 8 for two roughness cases. It is observed at that in general, the speed-up profiles for the same Reynolds number at the two different roughness heights were similar, despite relatively significant difference between z_0 values, which was about three orders of magnitude larger for RCI compared to RC2. The difference in peak speed-up for two roughness configurations at z = 2 m was about 6% 8% and 5% for U5, U8 and U14, respectively. For the uniform fan speed cases, a lower upstream z_0 was found to generate a higher peak speed-up at the escarpment, with diminishing effect moving downstream. A different trend was observed for the U15 cases, where a slight reduction in peak speed-up of about 3% was observed at the escarpment for the RC2 case, with the difference between the

two roughness cases slightly growing moving downstream. At M6, the lower roughness cases showed a slightly better match to the full-scale data (see Figure 8).

5.3.3 Effect of measurement and model resolution on the mean flow

The Cobra Probe measurements were taken under identical fan speed and roughness element configurations as the PIV cases, although not simultaneously, and therefore from the mean flow perspective, they provide useful independent evidence for Reynolds number dependence. A comparison of speed-up ratio between PIV and Cobra Probe measurements, for the three uniform fan speed cases, for both roughness configurations, along the same vertical profile at M6, is shown in Figure 9. The results show very good matching between the two methods of measurements, with some systematic bias error resulting in slightly lower speed-up for Cobra Probe measurements, perhaps due to PIV calibration. Notwithstanding, very little evidence of Reynolds number dependence is observed between the Cobra Probe profiles, confirming the trends observed earlier in the PIV data.

Now turning to the discussion on the effect of model resolution on the mean flow, it is generally accepted by wind tunnel modellers that for bluff bodies submerged in deep boundary layers, Reynolds number effects are negligible for $Re > (2–3)\times10^4$, particularly for flows without steady vortical regions (Lim et al., 2007). Given that the BLWTL tests were conducted at Reynolds number above this threshold (3.6×10^4), as were the two tests conducted by Yeow et al. (2015), at 4.15×10^4 and 8.21×10^4, one would expect to see Reynolds number independence preserved between normalized speed-up profiles at the BLWTL scale (1:100) and the WindEEE scale (1:25), measured using the same instrument, with similar upstream conditions. Such comparison can be made using results in Figure 6, which illustrates the speed-up profiles from Cobra Probe measurements at BLWTL and WindEEE. Some discrepancies are observed, particularly at M6 at $z < 5$ m, where WindEEE measurements were found to be higher, and closer to the full-scale measurements. Assuming that the Reynolds number threshold (Lim et al., 2007) is applicable under present conditions, it can be concluded that the discrepancies between Cobra Probe results observed at two different model resolutions, are not due to the Reynolds number but rather are caused by other factors related to model and measurement resolution such as proximity of the measurement instrument to the surface, size of the instrument relative to the model and surface roughness of the model.

5.4 Turbulent flow behaviour

The results for the turbulent flow are presented in a similar manner as for the mean flow behaviour in Section 5.1. To obtain a better insight into the overall turbulent flow behaviour, contour plots of the change in TKE $\Delta\bar{k}$ over the same area as in the earlier speed-up plots, are shown in Figure 10a and Figure 10b for U14RC1 and U15RC1, respectively. A high-turbulent intensity region is observed at the escarpment, which dissipates moving downstream. Several significant differences are observed between the two cases, with U15RC1 having a larger high-intensity TKE region near the escarpment, and a longer

and higher wake region. The TKE increment also begins further upstream of the escarpment. The U5 and U8 TKE contour plots (not shown) were similar to the U14 case, but with slightly lower values of $\Delta\bar{k}$ throughout.

5.5 Turbulent flow comparison with previous experiments

A comparison of horizontal profiles of WindEEE TKE increment against previous experimental results, at z = 5 m and z = 2 m above surface level is presented in Figure 11. The two WindEEE PIV profiles stand out from the others as they feature a shallow hump between M6 and M3 at z = 5 m, and a sharp spike between the escarpment and M6 at z = 2 m. Both features are much more pronounced for the U15RC1 case compared to U14RC1. The Cobra Probes were not able to capture the TKE spike to the same extent, also observed in the vertical profile at M6 (see Figure 12). As was the case for speed-up ratio, the U15RC1 case was observed to better approximate the full-scale values of $\Delta\bar{k}$ than the others.

5.6 Influence of Reynolds number, upstream roughness, inflow profile and model resolution on turbulent flow

5.6.1 Reynolds number and upstream wind profile effects on the turbulent flow

Figure 13(a,b) and Figure 13(c,d) show horizontal profiles of $\Delta\bar{k}$ for the four wind speed cases at RC1 and RC2, respectively. The two U15 profiles stand out from the other cases, and the discrepancy is much more significant than it was for the speed-up ratio – the peak TKE increment for U15RC1 was about 200% higher than that for U14RC1. As noted earlier, the only difference between the U14 and U15 cases was the increase in the operating speed of fans in the third row by 50% compared to all other fans. This produced a slightly higher Reynolds number at the hill height for the U15 cases than for U14, but the Reynolds number difference is only about one third of the difference between the U8 and U14 cases. Thus the difference in profile shapes at heights of z = 2 m and z = 5 m above the island appears to be attributable mainly to the induction of the strong shearing effect between fan rows 2 and 3, despite the fan row interface being about two metres off the tunnel floor in model scale, or 50 m in full-scale, more than four times the hill height. There do not appear to be any indications of this behaviour from the inflow profiles, at least not from the normalized mean wind speed and TKE profiles, where the U15RC1 inflow profile is generally similar to the others in the RC1 group, regardless of which method was used to determine u_*. While analyzing the WindEEE inflow profiles up to a height of about 100 m in full-scale would have provided a better picture of the difference in inflow conditions between the U14 and U15 cases, the comparison with upstream data from the field campaign at mast M0 at these heights not being available would preclude the interpretation of this better fit between the U15 case and full scale. Nevertheless, the results highlight the important fact that a relatively small change to the inflow wind shear profile, even well above the model height, can significantly alter the turbulent flow behaviour near the hill surface.

Among the three uniform fan speed profiles, there is little difference at z = 5 m, however, at z = 2 m, peak TKE for the U14 case between the escarpment and M6 is higher than the other two cases, for both RC1 and RC2, indicating a possible Reynolds number dependence in this region. Vertical profiles of change in TKE at M6 were also plotted (see Figure 14) for

the RC1 and RC2 cases. The profiles for the uniform fan speed cases again tended to collapse, with the exception of the U14 cases, below z = 2 m, where a slight increase in TKE was observed. Consistently higher TKE is observed for the U15RC1 case, and again the U15 results are closer to the full scale data.

5.6.2 Upstream roughness effects on the turbulent flow

The influence of upstream roughness can be seen in Figure 14 at M6. For the uniform fan speed cases, configuration RC2, with lower z_0, appeared to cause a moderate increase in TKE compared to RC1 at z < 5 m, while little difference in TKE was observed between the U15 cases. A comparison of horizontal profiles of RC1 and RC2 cases (not shown) showed higher TKE increment for the RC2 cases at all positions downstream of about X = -50 m, particularly at z = 2 m. The difference in peak TKE increment at different roughness configurations was about 13%, 28%, 27% at U5, U8 and U14, respectively, with the RC2 value being higher for these cases. The U15 case showed negligible difference for the two roughness cases with a weak trend of a decrease in TKE increment with the roughness. Thus, a change in the upstream roughness was observed to have an effect on the TKE for the uniform fan speed cases, while the case with modified shear profile appeared to be more resilient to changes in the roughness.

5.6.3 Effect of model and measurement resolution on the turbulent flow

A comparison of TKE increment between WindEEE PIV and WindEEE Cobra Probe measurements, for the same Reynolds number, and for the same vertical profile at M6 is presented in Figure 15. Strong similarity is observed between the two types of measurements, down to about z = 3 m, at which point some divergence is observed, with the Cobra Probes being unable to capture the spike in TKE to the same extent as the PIV measurements, which may be partially due to the reverse flow at this location. Although Reynolds number effects may contribute to the higher TKE for the U14 PIV profile at z < 3 m, Reynolds number independence appears to be preserved completely among the three Cobra Probe profiles all the way down. This observation once again raises the question of why the measurements of the 1:25 scale model at WindEEE are higher than those over the 1:100 BLWTL model, and why they are closer to the full-scale measurements, as seen in Figure 12b at M6. The resolution of the model, and the ability to measure closer to the surface level thus appears to be one contributing factor. A separate study by Lange et al. recently submitted for publication investigates the effect of sharpening the escarpment edge. Preliminary analysis shows that this has a large effect on the flow behaviour in the region close to the top of the hill.

6 Conclusions

An experimental investigation to characterize the mean and turbulent flow behaviour over a steep escarpment, represented by the topography of Bolund Hill, was conducted at two distinct scales (1:100 and 1:25) by means of wind tunnel testing using Particle Image Velocimetry (PIV) and Cobra Probes. A range of Reynolds numbers, boundary layer inflow profiles, and

upstream roughness values were examined. At the WindEEE research facility, three uniform fan profiles and one modified shear profile were tested at two different upstream roughness configurations, for a total of eight unique sets of inflow conditions. These results, presented in the form of normalized speed-up and TKE increment, were compared to each other and to measurements from the field campaign and previous experimental work, to attempt to establish the relative contributions of the key upstream parameters to flow behaviour over the hill.

Mean flow behaviour was found to be generally resilient to changes in upstream conditions, with negligible Reynolds number dependence observed between the uniform fan speed cases, across a Reynolds number range of 1.7×10^5 to 4.6×10^5, for both Cobra Probe and PIV measurements. Slight modification of the speed-up behaviour was observed for the shear profile case, but this did not appear to be related to the Reynolds number. Lower upstream roughness was observed to cause a marginal increase in peak speed-up at the escarpment for the uniform fan speed cases, whereas for the shear case, lower roughness caused a slight reduction in speed-up, particularly near the surface. Slightly higher values of speed-up were observed for the 1:25 scale model compared to the 1:100 model, which are attributed to factors such as proximity of the instrument to the model surface, or model surface roughness.

From the turbulent flow field data represented in the form of TKE increment, a weak Reynolds number dependence was observed whereby TKE increased with an increase in the Reynolds number, but only in the highly turbulent shear layer near the escarpment. Lower upstream roughness also served to moderately increase peak TKE among the uniform fan speed cases. A much more significant TKE increase was observed for the shear profile case, where peak normalized TKE at a height of 2 m above the hill increased by over 200% compared to the uniform fan speed case at a similar Reynolds number. Through modification of the inflow shear profile, the WindEEE facility was able to produce TKE increments that were closer to full-scale measurements, and higher than those that had been achieved previously in conventional wind tunnels, indicating a promising trend for future work in characterizing flow over topography.

For the wind developer, these results reinforce the need for very careful and detailed assessment of wind turbine inflow conditions in complex topography, as even very small changes to the inflow profile used in the modelling process can cause highly significant changes at turbine height, particularly in the turbulent flow behaviour.

References

Akomah, A., Hangan H., and Naughton, J.: Very high Reynolds number boundary layers over 3D sparse roughness and obstacles: the mean flow, Experiments in Fluids, 51, 743–752, doi: 10.1007/s00348-011-1086-2, 2011.

Ayotte, K. W. and Hughes, D. E.: Observations of boundary-layer wind-tunnel flow over isolated ridges of varying steepness and roughness, Boundary-Layer Meteorology, 112, 525–556, doi: 10.1023/B:BOUN.0000030663.13477.51, 2004.

Ayotte, K. W.: Computational modelling for wind energy assessment, Journal of Wind Engineering and Industrial Aerodynamics, 96, 1571–1590, doi: 10.1016/j.jweia.2008.02.002, 2008.

Ayotte K. W., Sullivan P. P., and Patton E. G.: LES and wind tunnel modelling over hills varying steepness and roughness, Fifth International Symposium on Computational Wind Engineering (CWE2010), Chapel Hill, North Carolina, USA, May 23–27, 2010.

Bechmann A., Sørensen, N. N., Berg J., Mann J., and Réthoré, P.-E.: The Bolund experiment, part II: blind comparison of microscale flow models. Boundary-Layer Meteorology, 141:245–271, doi: 10.1007/s10546-011-9637-x, 2011.

Berg, J., Mann, J., Bechmann, A. Courtney, M.S., and Jørgenson, H.E.: The Bolund experiment, part I: flow over a steep, three-dimensional hill. Boundary-Layer Meteorology, 141:219–243, doi: 10.1007/s10546-011-9636-y, 2011.

Botta, G., Cavaliere, M., Viani, S., and Pospíšil, S.: Effects of hostile terrains on wind turbine performances and loads: The Acqua Spruzza experience, Journal of Wind Engineering and Industrial Aerodynamics, 74–76, 419–431, doi: 10.1016/S0167-6105(98)00038-5, 1998.

Chock, G. and Cochran, L.: Modeling of wind speed effects in Hawaii, Journal of Wind Engineering and Industrial Aerodynamics, 93, 623–638, doi: 10.1016/j.jweia.2005.06.002, 2005.

Conan, B., Chaudhari, A., Aubrun, S., van Beeck, J., Hämäläinen, J., and Hellsten, A.: Experimental and numerical modelling of flow over complex terrain: the Bolund Hill. Boundary-Layer Meteorology, 158, 183–208, doi: 10.1007/s10546-015-0082-0, 2016.

Hangan, H.: The Wind Engineering Energy and Environment (WindEEE) dome at Western University, Canada. Wind Engineers, JAWE, 39, 4(141), doi: 10.5359/jawe.39.350, 2014.

Lange, J., Mann J., Angelou, N., Berg, J., Sjoholm, M., and Mikkelsen, T.: Variations of the wake height over the Bolund escarpment measured by a scanning Lidar, Boundary-Layer Meteorology, 159, 147–159, doi: 10.1007/s10546-015-0107-8, 2016.

Lim, H. C., Castro, I. P., and Hoxey, R. P.: Bluff bodies in deep turbulent boundary layers: Reynolds-number issues. Journal of Fluid Mechanics, 571, 97–118, doi: 10.1017/S0022112006003223, 2007.

Ly, L.N.: Effect of the angle between wind stress and wind velocity vectors on the aerodynamic drag coefficient at the air-sea interface, Journal of Physical Oceanography, 23, 159–163, doi: 10.1175/1520-0485(1993)023<0159:EOTABW>2.0.CO;2, 1993.

Manwell, J. F., McGowan, J. G., and Rogers, A. L.: Wind energy explained, 2nd Ed. Wiley: 2009.

McAuliffe B.R. and Larose G.L.: Reynolds-number and surface-modeling sensitivities for experimental simulation of flow over complex topography. Journal of Wind Engineering and Industrial Aerodynamics, 104–106: 603–613, doi: 10.1016/j.jweia/2012.03.016, 2012.

Palma, J. M. L. M., Castro, F. A., Ribeiro, L. F., Rodrigues, A. H., and Pinto, A. P.: Linear and nonlinear models in wind resource assessment and wind turbine micro-siting in complex terrain, Journal of Wind Engineering and Industrial Aerodynamics, 96, 2308–2326, doi: 10.1016/j.jweia.2008.03.012, 2008.

Peinke, J., Barth, S., Böttcher, F., Heinemann, D., and Lange, B.: Turbulence, a challenging problem for wind energy, Physica A 338, 187-193, doi: 10.1016/j.physa.2004.02.040, 2004.

Rasouli, A., and Hangan, H.: Micro-scale CFD simulation for wind mapping over complex topographic terrains, Journal of Solar Energy Engineering, 135(4), 041005, 18 pages, doi: 10.1115/1.4024124, 2013.

Rasouli, A., Hangan, H., and Siddiqui, K.: PIV measurements for complex topographic terrain, Journal of Wind Engineering and Industrial Aerodynamics, 97, 242–254, doi: 10.1016/j.jweia.2009.06.010, 2009.

Salmon, J. R., Teunissen, H. W., Mickle, R. E., and Taylor, P. A.: The Kettles Hill project: field observations, wind-tunnel simulations and numerical model predictions for flow over a low hill', Boundary-Layer Meteorology, 43, 309–343, doi: 10.1007/BF00121711, 1988.

Siddiqui, K., Loewen, M. R., Richardson, C., Asher, W. E., and Jessup, A. T.: Simultaneous particle image velocimetry and infrared imagery of microscale breaking waves, Physics of Fluids, 13, 1891–903, doi: 10.1063/1.1375144, 2001.

Taylor, P. A. and Teunissen, H. W.: The Askervein Hill project: overview and background data, Boundary-Layer Meteorology, 39, 15–39, doi: 10.1007/BF00121863, 1987.

Walmsley, J. L. and Taylor P. A.: Boundary-layer flow over topography: impacts of the Askervein study, Boundary-Layer Meteorology, 78, 291–320, doi: 10.1007/BF00120939, 1996.

Weber, R. O.: Remarks on the definition and estimation of friction velocity, Boundary Layer Meteorology 93, 197–209, doi: 10.1023/A:1002043826623, 1999.

Yeow T.S., Cuerva-Tejero, A., and Perez-Alvarez J.: Reproducing the Bolund experiment in wind tunnel, Wind Energy, 18, 153–169, doi: 10.1002/we.1688, 2015.

Table 1. Inflow parameters for WindEEE PIV test cases

Case ID	Fan configuration	u_h (m/s)	Re	z_0 (m)	u_{*05} (m/s) Method 1	u_{*05} (m/s) Method 2	u_* (m/s) Method 3	u_* (m/s) Method 4
U5RC1	All fans 20%	5.42	1.70×10^5	1.84×10^{-3}	0.314	0.326	0.254	0.333
U5RC2	All fans 20%	5.49	1.72×10^5	1.96×10^{-6}	0.229	0.252	0.145	0.231
U8RC1	All fans 30%	8.70	2.72×10^5	1.98×10^{-3}	0.488	0.489	0.409	0.505
U8RC2	All fans 30%	8.57	2.68×10^5	4.12×10^{-7}	0.373	0.415	0.203	0.355
U14RC1	All fans 50%	14.60	4.57×10^5	2.72×10^{-3}	0.856	0.869	0.723	0.848
U14RC2	All fans 50%	14.69	4.60×10^5	2.29×10^{-6}	0.668	0.361	0.392	0.640
U15RC1	Fan rows 1,2,4: 50% Fan row 3: 75%	15.60	5.21×10^5	2.87×10^{-4}	0.992	1.070	0.650	0.970
U15RC2	Fan rows 1,2,4: 50% Fan row 3: 75%	~15.60	~5.21×10^5	Not measured*				

Roughness lengths shown in full-scale.
*The upstream profile for case U15RC2 was not measured due to an oversight, and as a result the U15RC2 PIV results had to be normalized against the U15RC1 upstream Cobra Probe data.

Table 2. Inflow parameters for BLWTL experiment

Case ID	u_h (m/s)	Re	z_0 (m)	u_{*05} (m/s) Method 1	u_{*05} (m/s) Method 2	u_* (m/s) Method 3	u_* (m/s) Method 4
BLWTL	4.65	3.63×10^4	1.266×10^{-4}	0.1643	0.1651	0.1640	0.1858

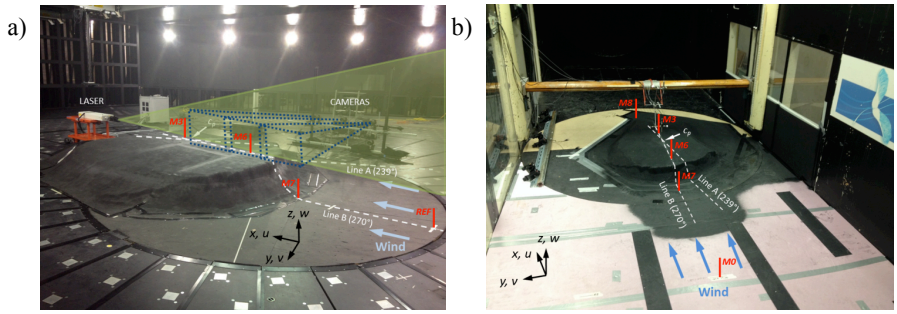

Figure 1. Experimental setup for a) WindEEE b) BLWTL.

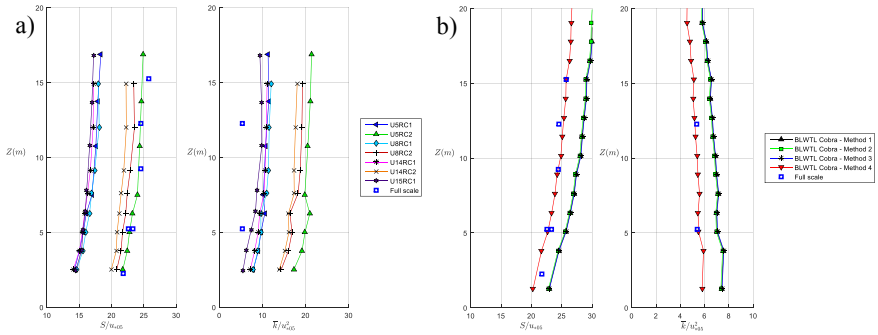

Figure 2. a) WindEEE upstream profiles of upstream reference mean flow speed and TKE normalized by friction velocity obtained using Method 1, and b) BLWTL upstream profiles of upstream reference mean flow speed and TKE, normalized by friction velocity obtained using four different methods. S and $\bar{k}$ calculated using all three components of wind speed from Cobra Probe measurements. Z co-ordinates shown in full-scale.

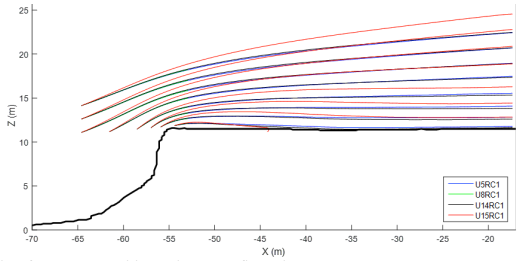

Figure 3. Mean streamline plots for test cases with roughness configuration RC1.

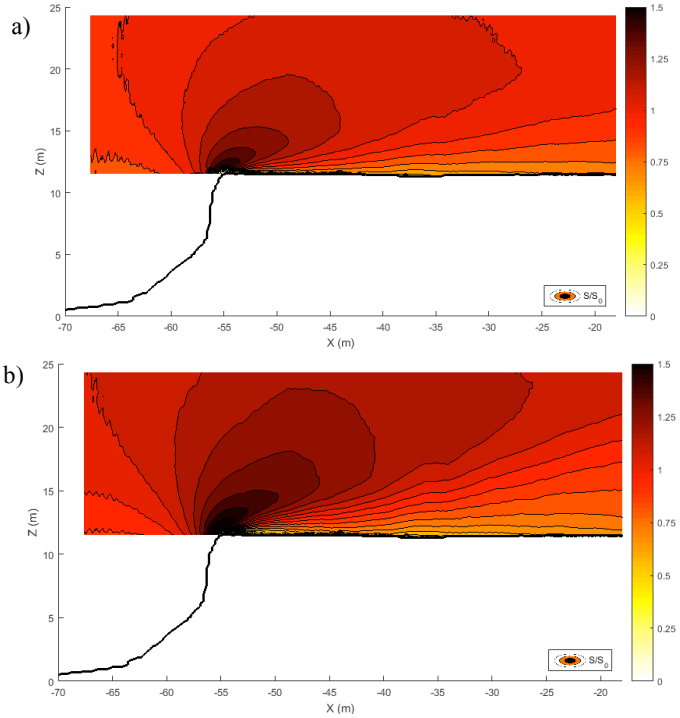

Figure 4. Speed-up ratio contour plot for a) U14RC1 and b) U15RC1.

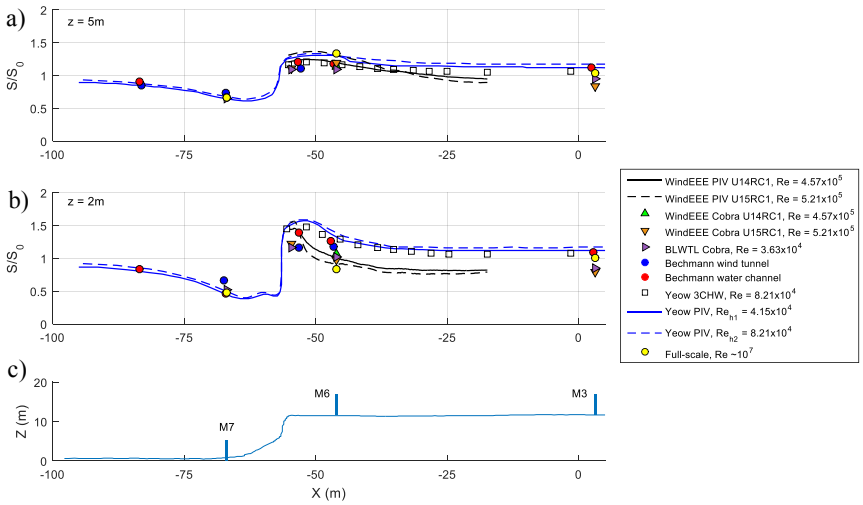

Figure 5. WindEEE and BLWTL speed-up ratio along horizontal profiles at a) z = 5 m and b) z = 2 m above surface level for PIV and Cobra Probe measurements with comparison to full-scale and to previous physical experiments.

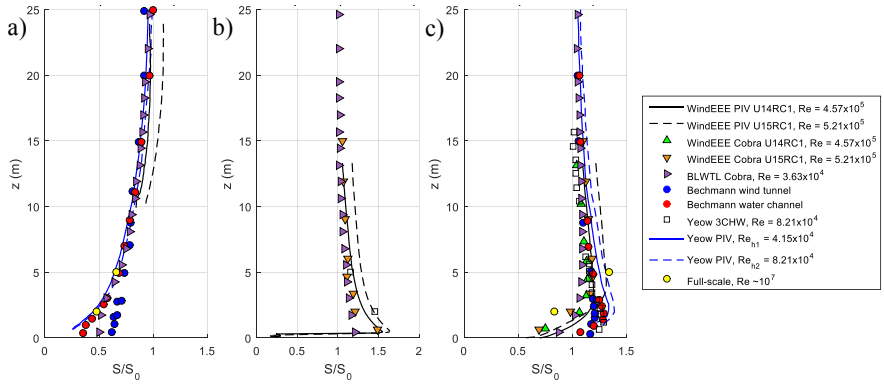

Figure 6. Comparison of WindEEE and BLWTL speed-up ratio along vertical profiles at a) M7 (X = -66.9 m), b) escarpment (X = -54.7 m) and c) M6 (X = -46.1 m) with comparison to full-scale and to previous physical experiments.

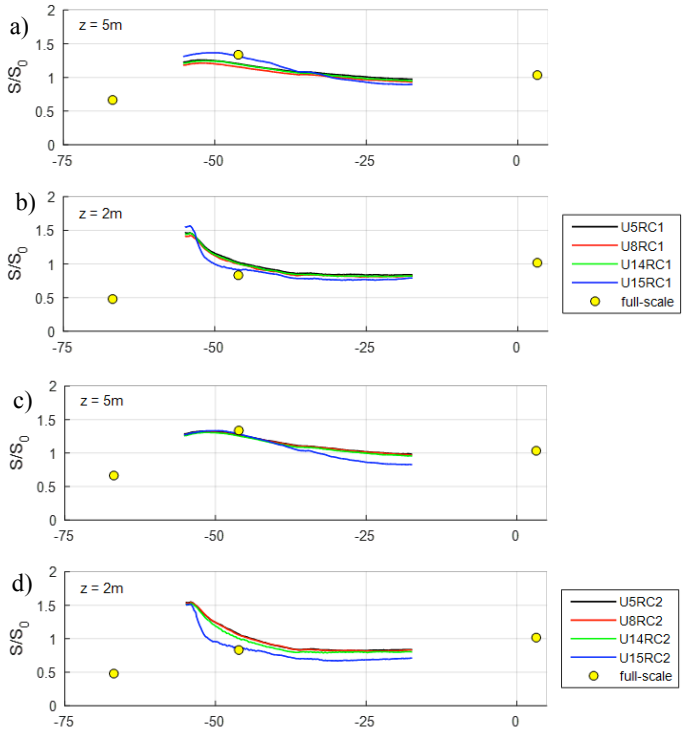

Figure 7. Horizontal profiles of speed-up ratio for a) RC1 cases, z = 5 m, b) RC1 cases, z = 2 m, c) RC2 cases, z = 5 m and d) RC2 cases, z = 2 m.

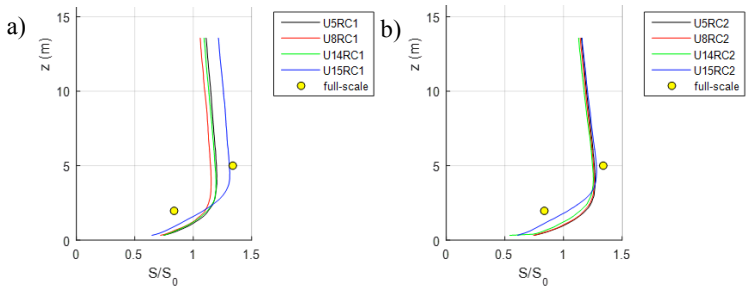

Figure 8. Vertical profiles of speed-up ratio at M6 for a) RC1 cases (left) and RC2 cases (right).

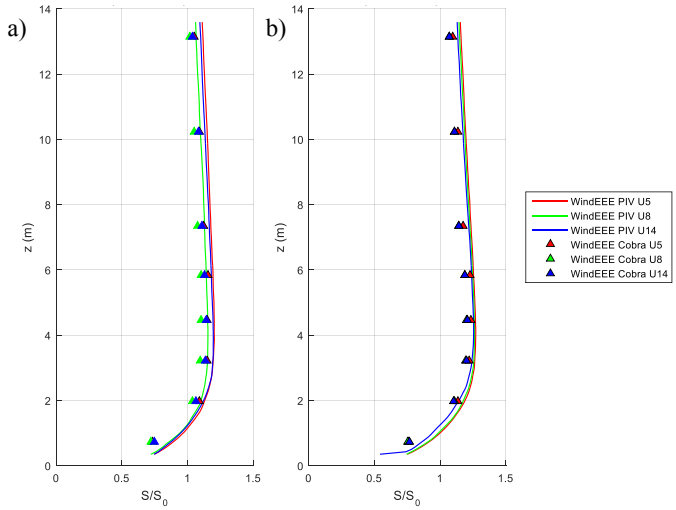

Figure 9. WindEEE PIV and Cobra Probe vertical profiles of speed-up ratio at M6, for RC1 (left) and RC2 (right).

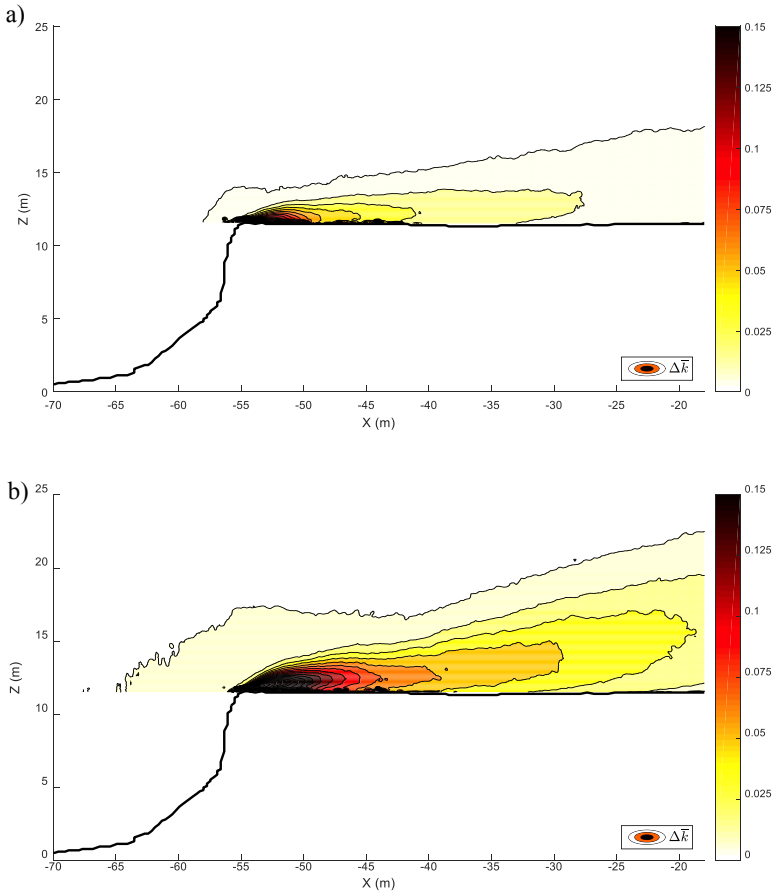

Figure 10. Mean TKE increment contour plot for a) U14RC1, and b) U15RC1.

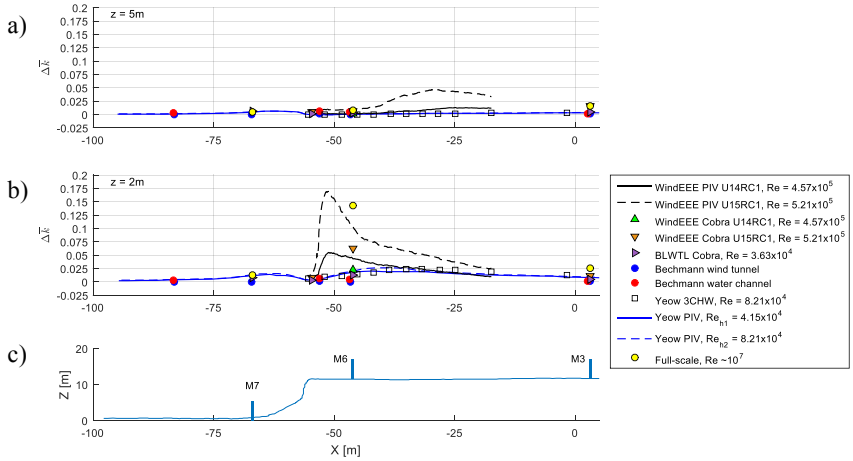

Figure 11. WindEEE and BLWTL TKE increment along horizontal profiles at a) z = 5m and b) z = 2m above surface level for PIV and Cobra Probe measurements with comparison to full-scale and to previous physical experiments.

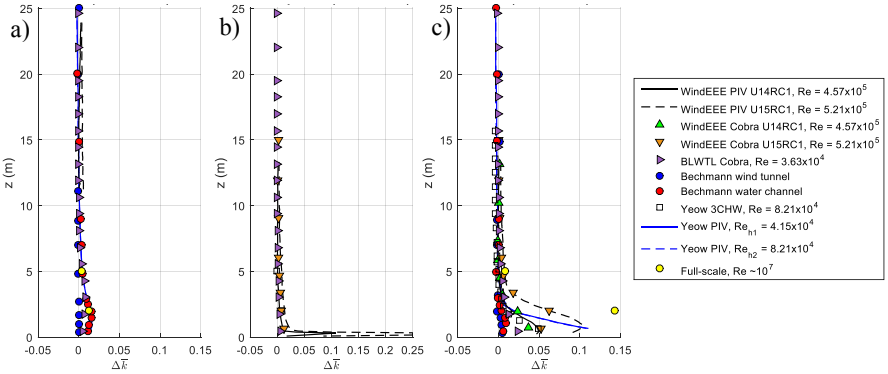

Figure 12. Comparison of WindEEE and BLWTL TKE increment along vertical profiles at a) M7 (X = -66.9 m), b) escarpment (X = -54.7 m) and c) M6 (X = -46.1 m) with comparison to full-scale and to previous physical experiments.

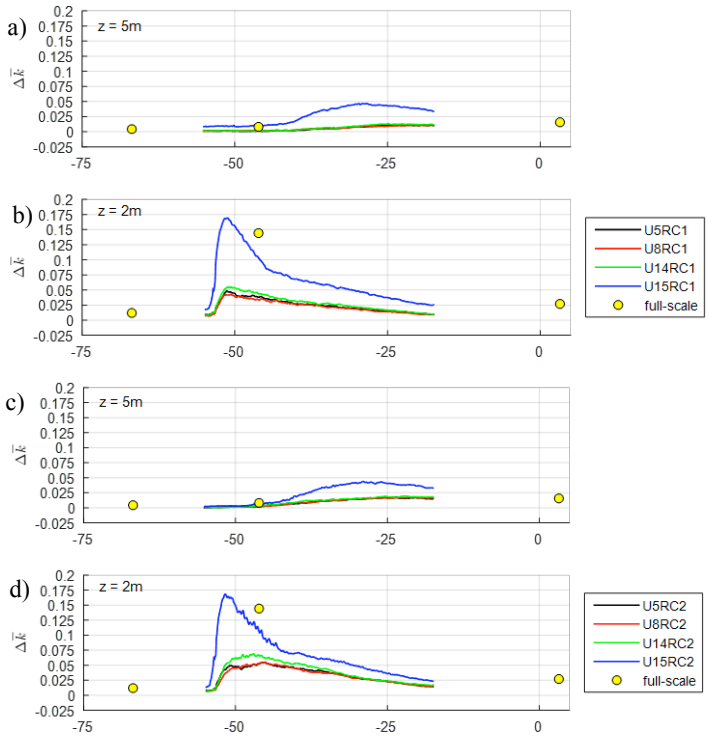

Figure 13. Change in TKE horizontal profiles for a) RC1 cases at z = 5 m. and b) RC1 cases at z = 2 m, c) RC2 cases at z = 5 m, and d) RC2 cases at z = 2m.

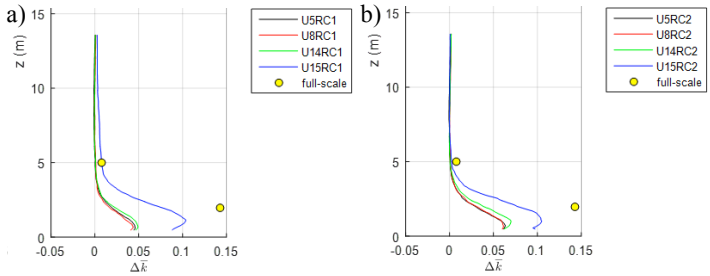

Figure 14. Vertical profiles of TKE increment at M6 for a) RC1 cases and b) RC2 cases.

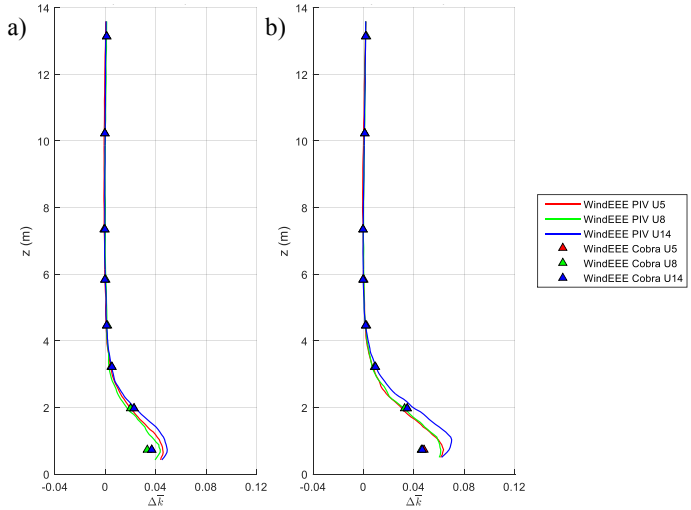

Figure 15. WindEEE PIV and Cobra Probe vertical profiles of TKE increment at M6, for a) RC1 and b) RC2 cases.

Bibliography

Baskaran, V., Smits, A.J., and Joubert, P.N. (1987). "A turbulent flow over a curved hill Part 1. Growth of an internal boundary layer". In: *J Fluid Mech* 182, pp. 47–83. DOI: http://dx.doi.org/10.1017/S0022112087002246.

Bechmann, A., Berg, J., Courtney, M.S., Jørgensen, H.E., Mann, J., and Sørensen, N.N. (2009). *The Bolund Experiment : Overview and Background Risø-R-Report*. Tech. rep. July. Roskilde: Risø-DTU, National Laboratory for Sustainable Energy, p. 51.

Berg, J., Mann, J., Bechmann, A., Courtney, M.S., and Jørgensen, H.E. (2011). "The Bolund Experiment, Part I: Flow Over a Steep, Three-Dimensional Hill". In: *Boundary-Layer Meteorol* 141.2, pp. 219–243. DOI: DOI:10.1007/s10546-011-9636-y.

Bowen, A.J. (1979). "Some Effects of Escarpments on the Atmospheric Boundary Layer". PhD Dissertation. University of Canterbury, p. 322. URL: http://hdl.handle.net/10092/5640.

Bowen, A.J. and Lindley, D. (1977). "A wind-tunnel investigation of the wind speed and turbulence characteristics close to the ground over various escarpment shapes". In: *Boundary-Layer Meteorol* 12.3, pp. 259–271. DOI: 10.1007/BF00121466.

Castro, F. A., Palma, J.M.L.M., and Lopes, A.S. (2003). "Simulation of the Askervein Flow. Part 1: Reynolds Averaged Navier–Stokes Equations (k-ϵ Turbulence Model)". In: *Boundary-Layer Meteorol* 107.3, pp. 501–530. DOI: 10.1023/A:1022818327584.

Chow F.K. and Street, R.L. (2009). "Evaluation of Turbulence Closure Models for Large-Eddy Simulation over Complex Terrain: Flow over Askervein Hill". In: *J Appl Meteorol Clim* 48.5, pp. 1050–1065. DOI: http://dx.doi.org/10.1175/2008JAMC1862.1.

Conan, B. (2012). "Wind Resource Assessment in Complex Terrain by Wind Tunnel Modelling". PhD thesis. Karman Institute / Orléans University, p. 182. ISBN: 978-2-87516-056-0. URL: https://tel.archives-ouvertes.fr/tel-00843645/.

Conan, B., Chaudhari, A., Aubrun, S., Beeck, J.v, Hämäläinen, J., and Hellsten, A. (2016). "Experimental and Numerical Modelling of Flow over Complex Terrain: The Bolund Hill". In: *Boundary-Layer Meteorol.* 158.2, pp. 183–208. DOI: 10.1007/s10546-015-0082-0.

DantecDynamics. *Dantec*. Skovlunde, Denmark. URL: http://www.dantecdynamics.com/dynamicstudio.

Dellwik, E., Mann, J., and Bingöl, F. (2010). "Flow tilt angles near forest edges - Part 2: Lidar anemometry". In: *Biogeosciences* 7.5, pp. 1759–1768. DOI: 10.5194/bg-7-1759-2010.

Diebold, M., Higgins, C., Fang, J., Bechmann, A., and Parlange, M.B. (2013). "Flow over Hills: A Large-Eddy Simulation of the Bolund Case". In: *Boundary-Layer Meteorol* 148.1, pp. 177–194. DOI: 10.1007/s10546-013-9807-0.

EIA (2015). *Annual energy outlook 2015 with projections to 2040*. Tech. rep. U.S.Energy Information Administration, pp. 1–244. URL: http://www.eia.gov/forecasts/aeo/.

Emeis, S., Frank, H.P., and Fiedler, F. (1995). "Modification of air flow over an escarpment. Results from the Hjardemål experiment". In: *Boundary-Layer Meteorol* 74.1-2, pp. 131–161. DOI: 10.1007/BF00715714.

Emeis, S., Schäfer, K., and Münkel, C. (2008). "Surface-based remote sensing of the mixing-layer height – a review". In: *Meteorol Z* 17.5, pp. 621–630. DOI: 10.1127/0941-2948/2008/0312.

Hangan, H. (2014). "The Wind Engineering Energy and Environment (WindEEE) Dome at Western University, Canada". In: *Japan Assoc. Wind Eng.* 39.4, pp. 350–351. DOI: http://doi.org/10.5359/jawe.39.350.

Hinze, J.O. (1975). *Turbulence*. Ed. by B.J Clark. 2nd ed. McGraw-Hill Book company. ISBN: 0070290377.

Hunt, J.C.R., Leibovich, S., and Richards, K.J. (1988). "Turbulent shear flows over low hills". In: *Q J R Meteorol Soc* 114, pp. 1435–1470. DOI: 10.1002/qj.49711448405.

IEC (2005). *IEC 61400-1. Wind turbines – design requirements. International Electrotechnical Com- mission, 3 edn.* Tech. rep.

IRENAa (2015). *Renewable Energy Capacity Statistics 2015*. Tech. rep. International Renewable Energy Agency. URL: http://www.irena.org/DocumentDownloads/Publications/IRENA_RE_Capacity_Statistics_2015.pdf.

IRENAb (2015). *Renewable Power Generation Costs in 2014*. Tech. rep. International Renewable Energy Agency. URL: http://www.irena.org/documentdownloads/publications/irena_re_power_costs_2014_report.pdf.

Jackson, P.S. and Hunt, J.C.R. (1975). "Turbulent flow over a low hill". In: *Q J R Meteorol Soc* 101, pp. 929–955. DOI: 10.1002/qj.49710143015.

Jensen, N.O. and Peterson, E.W. (1978). "On the escarpment wind profile". In: *Q J R Meteorol Soc* 104.441, pp. 719–728. DOI: 10.1002/qj.49710444113.

Kiya, M. and Sasaki, K. (1983). "Structure of a turbulent separation bubble." In: *J Fluid Mech* 137, pp. 83–113. DOI: 10.1017/S002211208300230X.

Lange, J., Mann, J., Angelou, N., Berg, J., Sjöholm, M., and Mikkelsen, T. (2016). "Variations of the Wake Height over the Bolund Escarpment Measured by a Scanning Lidar". In: *Boundary-Layer Meteorol* 159.1, pp. 147–159. DOI: 10.1007/s10546-015-0107-8.

Largeau, J.F. and Moriniere, V. (2006). "Wall pressure fluctuations and topology in separated flows over a forward-facing step". In: *Exp Fluids* 42.1, pp. 21–40. DOI: 10.1007/s00348-006-0215-9.

Prospathopoulos, J.M., Politis, E.S., and Chaviaropoulos, P.K. (2012). "Application of a 3D RANS solver on the complex hill of Bolund and assessment of the wind flow predictions". In: *J Wind Eng Ind Aerodyn* 107-108, pp. 149–159. DOI: 10.1016/j.jweia.2012.04.011.

Raffel, M., Willert, C.E., Wereley, S., and Kompenhans, J. (2007). *Particle Image Velocimetry, A Practical Guide*. Springer-Verlag Berlin Heidelberg, p. 448. ISBN: 978-3-540-72307-3. DOI: 10.1007/978-3-540-72308-0.

Rowcroft, J., Burton, D., Blackburn, H.M., and Sheridan, J. (2015). "Siting wind turbines near cliffs-the effect of wind direction". In: *Wind Energy*. DOI: 10.1002/we.1931.

Sacré, C. (1979). "An experimental study of the airflow over a hill in the atmospheric boundary layer". In: *Boundary-Layer Meteorol* 17.3, pp. 381–401. DOI: 10.1007/BF00117926.

Sherry, M., Lo Jacono, D., and Sheridan, J. (2010). "An experimental investigation of the recirculation zone formed downstream of a forward facing step". In: *J Wind Eng Ind Aerodyn* 98.12, pp. 888–894. DOI: 10.1016/j.jweia.2010.09.003.

Silva Lopes, A., Palma, J.M.L.M., and Castro, F.A. (2007). "Simulation of the Askervein flow. Part 2: Large-eddy simulations". In: *Boundary-Layer Meteorol* 125.1, pp. 85–108. DOI: 10.1007/s10546-007-9195-4.

Taylor, P.A., Mason, P.J., and Bradley, E.F. (1987). "Boundary-layer flow over low hills". In: *Boundary-Layer Meteorol* 39.1987, pp. 107–132. DOI: 10.1007/BF00121870.

Teunissen, H.W., Shokr, M.E., Bowen, A.J., Wood, C.J., and Green, D.W.R. (1987). "The Askervein Hill Project: Wind-tunnel simulations at three length scales". In: *Boundary-Layer Meteorol* 40.1-2, pp. 1–29. DOI: 10.1007/BF00140067.

Trucco, E. and Verri, A. (1998). *Introductory techniques for 3-D Computer Vision*. Prentice Hall, p. 343. ISBN: 0-13-261108-2.

Wagner, R., Courtney, M., Gottschall, J., and Lindelöw-Marsden, P. (2011). "Accounting for the speed shear in wind turbine power performance measurement". In: *Wind Energy* 14, pp. 993–1004. DOI: 10.1002/we.509.

Walmsley, J.L. and Taylor, P.A. (1996). "Boundary-layer flow over topography: Impacts of the Askervein study". In: *Boundary-Layer Meteorol* 78.3-4, pp. 291–320. DOI: 10.1007/BF00120939.

WAsP. *www.wasp.dk*.

Yeow, T.S, Cuerva-Tejero, A., and Perez-Alvarez, J. (2013). "Reproducing the Bolund experiment in wind tunnel". In: *Wind Energy* 18.1, pp. 153–169. DOI: 10.1002/we.1688.

{2.7182818284}ϑφερτυθιοπσδφγηξκλ